UNIVERSITY OF OTTAWA

A mass spectrometry and XPS investigation of the catalytic decomposition of Formic Acid

by

JOHN SELWYN

A THESIS

SUBMITTED TO THE FACULTY OF GRADUATE STUDIES

IN PARTIAL FULFILMENT OF THE REQUIREMENTS FOR THE

DEGREE OF Master of Science

Department of Chemistry

Ottawa, Ontario

April, 2012

UNIVERSITY OF OTTAWA

FACULTY OF GRADUATE STUDIES

The undersigned certify that they have read, and recommend to the Faculty of Graduate Studies for acceptance, a thesis entitled " A mass spectrometry and XPS investigation of the catalytic decomposition of Formic Acid " submitted by John Selwyn in partial fulfilment of the requirements of the degree of Master of Science.

_____

Supervisor, [FULL NAME AND DEPARTMENT]

_____

[FULL NAME AND DEPARTMENT]

_____

[FULL NAME AND DEPARTMENT]

_____

[FULL NAME AND DEPARTMENT]

_____

Date

Abstract

This thesis examines the catalytic characteristics of two materials with respect to the decomposition of Formic Acid. The decomposition of formic acid proceeds via two principal reaction pathways: dehydration and dehydrogenation. Dehydrogenation is a valuable reaction producing Hydrogen suitable for use in fuel cells whereas the dehydration pathway produces carbon monoxide, a poison for many fuel cell materials. One of the surface species, the formate ion, is also implicated in other important chemical reactions, most notably the water gas shift and the decomposition of methanol.

The author seeks to document various intermediate surface species associated with the two reaction pathways with hope to use this information to future tailoring of catalysts for greater selectivity.

Acknowledgements

I would like to thanks Javier Giorgi for all of the guidance and encouragement that he has given me. Javier has been an enduring and patient mentor as well as an inspiration to me in my choice of surface science.

I would like to thank Matthew Brown and Richard Green for their help at the ALS and in being remarkable role models.

I would like to thanks Sander Mommers and the Mayer lab for their help in the building and repair of lab equipment and for their guidance analysis.

I would like to thanks my lab-mates, especially Julie O'Brien and David Mandia for making it fun and always being there with an answer to my questions.

I would like to thank Jim Elder for all of the philosophical discussions with respect to the meaning of life and the value of science.

Table of Contents

List of Tables

List of Figures and Illustrations

Chapter 1

Chapter 2

Chapter 3

Chapter 4

Chapter 5

Chapter 6

List of Symbols, Abbreviations and Nomenclature

Symbol	Definition
ALS	Advance Light Source
AES	Auger Electron Spectroscopy
AMU	Atomic Mass Unit
Auger	Auger spectroscopy
BE	Binding Energy
ETH	Eidgenossische Technische Hochschule
FWHM	Full Width Half Maxima
KE	Kinetic Energy
PSI	Pounds per Square Inch
QMS	Quadruple Mass Spectrometer
RGA	Residual Gas Analyser
RSF	Relative Sensitivity Factor
TPD	Temperature Programmed Desorption
UHV	Ultra High Vacuum
WGS	Water Gas Shift
XPS	X-ray Photoelectron Spectroscopy
YSZ	Yttria Stabilized Zirconia

Chapter One: Introduction:

The economic and quality of life gains over the past 150 years are largely dependent on the use of fossil fuels. Apart from being cheap and accessible sources of energy, fossil fuels have a very high energy density which we measure in energy per unit mass or energy per unit volume. A high energy density is important because it facilitates use, storage and transport of the fuel. Liquid fossil fuels have provided the "optimal" set of properties for many years and for a period of time, their combustion products were thought to be innocuous, simply being dispersed into the atmosphere. With increasing evidence of global warming and fossil fuel combustion induced climate change we see that is not the case. Concerns regarding the health of the planet and limitations of fuel availability have led us to search for other energy alternatives.

Before we look for alternatives, let us consider our energy needs. Energy is not just for transport, heating and cooking. Energy is also used extensively to produce food to feed the earth's human population. Food production accounts for approximately 30 percent of the global energy consumption ([1]). Given that much of the growth in the worlds food supply is also dependent on fossil fuel based fertilizers and with the world's population now exceeding 7 billion ([2]), it is not just our economic prosperity that is reliant on fossil fuels. Projections indicate that we will need more liquid fuels (Figure 1.1) in at a time when we find increased difficulty in reaching new sources of fossil fuels and with the realisation of their harmful effects on the environment, a new and sustainable approach to providing energy for the planet is required.

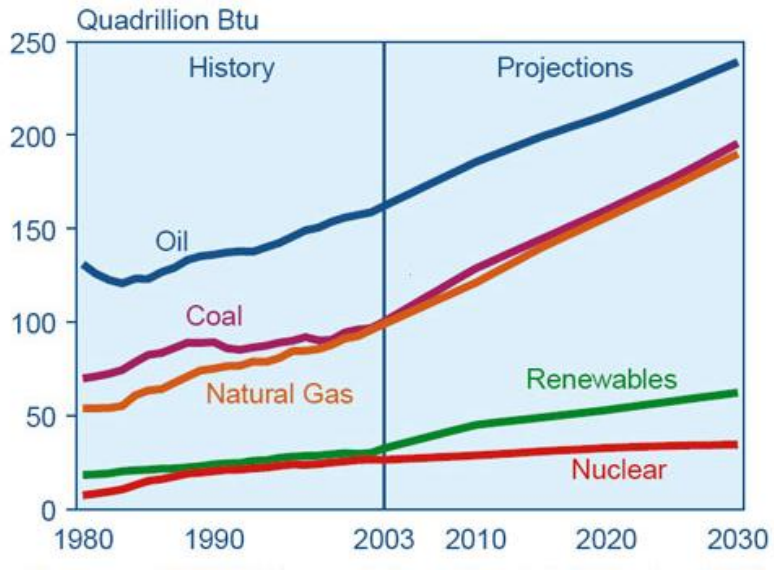

Figure 1.1 World energy use by fuel type, 1980 – 2030 [1]

We look to the following four points in evaluating potential alternatives for energy storage and use.

1. Humanity must shift its emphasis from fossil fuels to renewable energy.
2. The planet receives vastly more energy from the sun than it currently consumes but simply put it is in the wrong place at the wrong time.
3. We must find a way of storing energy, especially renewable energy, so that it can be transported and released where and when it is needed.
4. We must find solutions that take advantage of the infrastructure that humanity has created.

Therefore in short we need additional sources of energy, ideally in the form of liquid fuels that are renewable and carbon neutral.

The largest source of sustainable energy by many orders of magnitude is solar energy. While solar energy is ubiquitous, it also has a very low intensity peaking at 340 Wm^{-2}.

Photo voltaic cells can convert the solar radiation to electrical energy which can in turn be used to split water to provide a source of hydrogen which is the simplest and cleanest fuel. However both electricity and hydrogen gas are difficult to store. The energy available from the sun would be immensely more useful if it could be concentrated and stored as chemical energy similar to that found in fossil fuels.

1.1 Formic Acid

One of the more interesting candidates for a sustainably generated liquid hydrocarbon is formic acid (HCOOH). Formic acid is a pungent, colourless and somewhat viscous liquid with a melting point of 8.3°C, and a boiling point of 101°C.

Globally, 720,000 tons of formic acid are produced annually through industrial processes. Formic acid is currently a feedstock for industry and it is used in agriculture as a preservative and antibacterial agent [3]. The industrial process involves the conversion of methanol and carbon monoxide to methyl formate which is subsequently hydrolysed to form formic acid (equation 1 and 2).

Equation 1 $CH_3OH + CO(g) \rightleftharpoons HCO_2CH_3$

Equation 2 $HCO_2CH_3 + H_2O \rightleftharpoons HCO_2H + CH_3OH$

The high temperature and pressure of the reaction and caustic reagents involved make this process well suited to industrial production of formic acid but not suitable for many non-industrial energy storage applications.

1.2 Hydrogen storage via formic acid

Being the simplest of the carboxylic acids, formic acid is attractive as a method of hydrogen storage, having 4.3% hydrogen by weight and being a fluid at room

temperature. More impressive is the hydrogen storage per unit volume of 53g/l which is more than double that of compressed hydrogen gas at 350 bar.

1.3 History of Formic acid

Early work on the catalytic decomposition of formic acid by Sabatier[4] reaches back a century. An excellent review of the subject was written by Mars[5] that documented the potential reactions, reaction pathways and catalytic trends.

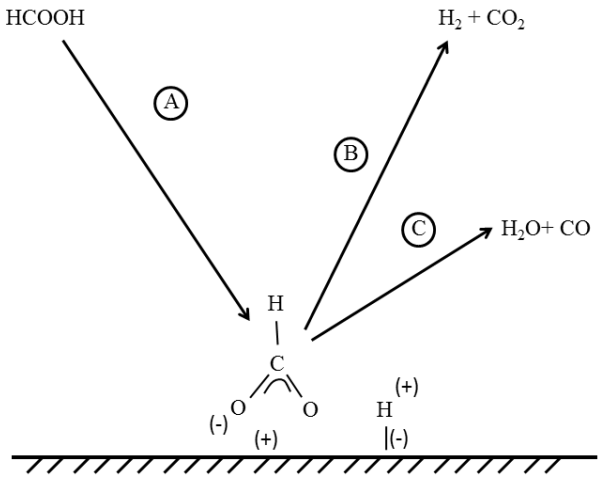

Figure 1.2 Proposed surface catalyzed decomposition of formic acid, A dissociative adsorption of formate anion, B Dehydrogenation reaction, C Dehydration reaction

Mars highlights the creation of an adsorbed formate ion as an intermediate in both of the decomposition reactions and the instability of the intermediate controlling the rates of the two decomposition reactions (see Figure 1.2). Mars also proposes a third decomposition pathway with formaldehyde as a product but suggests that it is insignificant.

1.4 On demand Hydrogen via formic acid

On demand decomposition of formic acid selectively through reaction 3 would create an exceedingly useful source of hydrogen gas. It is easy to envision formic acid combined with small fuel cells to consume the H_2 as a replacement for batteries and generators.

Formic acid alone does decompose at room temperature however the rate of the reaction is exceedingly slow[6]. The principal barrier to the reaction is its high activation energy ($107.4 kJmol^{-1}$)[6]. For this reason, heterogeneous catalysis offers the potential to lower the activation energy, increase the rate of decomposition and unlock the potential of using formic acid as a source of hydrogen on demand. As the carbon monoxide created in the dehydration reaction binds strongly to many surfaces and can be toxic to catalysts associated with PEM fuel cells[7]. It is therefore imperative that a means to be highly selective in which decomposition path is activated.

1.5 Energy storage and release with formic acid

The small size of the hydrogen molecule, the difficulty to compress or liquefy hydrogen and its explosive nature and colourless flame make storage and transport difficult and costly. If a means could be found to both create and decompose formic acid on demand then it could be used in to many applications for large and small scale energy storage, transportation and use. Ideally a catalyst could be found that would facilitate both the creation of formic acid from hydrogen and carbon dioxide and the decomposition of formic acid into hydrogen and carbon dioxide (equation 3 & 6).

Equation 3 $HCOOH_{(l)} \rightleftharpoons H_2 + CO_{2(g)}$

$\Delta H = 32$ kJ/mol, $\Delta S = 415.42\ JK^{-1}mol^{-1}$ at 300K, $\Delta G = -92.6$kJ/mol

As reported in the 81st edition of the CRC handbook, the standard thermodynamic properties of formic acid are as follows:

$\Delta_f H^{\ominus}$ = -425 kJ mol $^{-1}$(liq)

$\Delta_f G^{\ominus}$ = -361.4 kJ mol $^{-1}$ (liq)

$S^{\ominus}$ = 129.0 J mol $^{-1}$ K^{-1}

However to use formic acid for energy storage we are more interested in the reactions involving the cycling of formic acid into either hydrogen and carbon dioxide or water and carbon monoxide.

The two principal reaction pathways for formic acid decomposition are dehydration and dehydrogenation.

The dehydrogenation (see equation 3) involves the decomposition to hydrogen and carbon dioxide. Although endothermic its positive entropy (S) of 415.42 JK^{-1}mol^{-1} allows it to have a Gibbs free energy (ΔG) of -92.6kJ/mol at 300K.

Formic acid can also decompose to form water and carbon monoxide in a dehydration reaction (see equation 4). This reaction is more strongly endothermic and has a smaller entropy leading to a ΔG of only -4.3 kJ/mol at 300K.

Equation 4 $HCOOH_{(l)} \rightleftharpoons CO_{(g)} + H_2O_{(v)}$

ΔH = 73.1 kJ/mol ΔS = 257.5 JK^{-1}mol^{-1} at 300K, ΔG= -4.3kJ/mol

The decomposition reaction becomes favourable ($\Delta G<0$) for the dehydration at temperatures above 283K as compared to above 77K for the dehydrogenation reaction. Therefore low temperatures should help favour dehydrogenation over dehydration.

As important for our discussions regarding energy storage is the enthalpy for water splitting (reaction 5) and formation of formic acid from CO_2 and H_2 (reaction 6).

Equation 5 $H_2O \rightleftharpoons H_2 + ½ O2_{(g)}$ $\Delta H_f = 285.8$ kJ/mol

Equation 6 $H_2 + CO_{2(g)} \rightleftharpoons$ HCOOH $\Delta H = -32$kJ/mol

Here we see a large amount of energy ($\Delta H = 285.8$ kJ/mol) is required for the splitting of liquid water and a small amount is liberated during the formation of formic acid. The overall energy cycle as diagrammed in Figure 1.3 highlights the four steps in the cycle that can be thought of as:

1. Energy storage $\Delta H_f = 285.8$ kJ/mol
2. Hydrogen storage $\Delta H = -32$ kJ/mol
3. Hydrogen release $\Delta H = 32$ kJ/mol
4. Energy release $\Delta H_f = -285.8$ kJ/mol

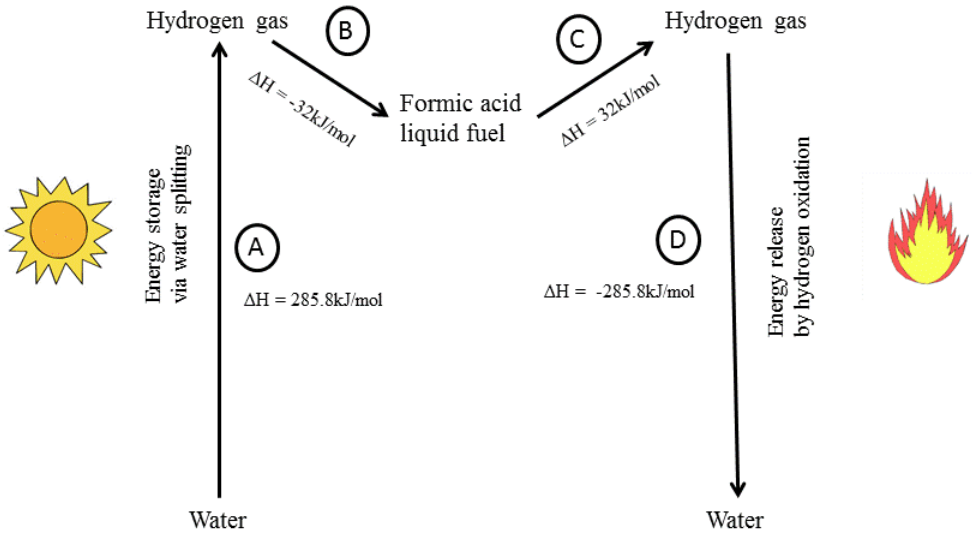

Figure 1.3 Energy storage and release cycle. A) water splitting, B) hydrogen storage in formic acid, C) hydrogen release through formic acid decomposition, D) Energy release through oxidation of hydrogen.

Taken together, water splitting and formic acid creation can be seen as a means to store large amounts of energy into what could be considered as a carbon neutral renewable liquid hydrocarbon. Each of the four steps in the energy storage and release cycle as envisioned is being studied. Step A, water splitting, especially water splitting utilizing solar energy are being explored by Nocera and others[8]. Step D ranges from simple from combustion through to modern fuel cell research aimed at facilitating a hydrogen economy. Of particular interest is the storage and release of hydrogen associated with steps B & C.

1.6 Formic acid reactions

Apart from reactions 1 & 2 there are a number of other reactions that we need to be aware of when considering formic acid. Arguably the most famous is the water gas shift (equation 7).

Equation 7 $CO_{(g)} + H_2O_{(v)} \rightleftharpoons CO_{2(g)} + H_{2(g)}$ Water Gas Shift (WGS)

This reaction acts as a path between the products of reaction 3 and 4. If our goal is a supply of pure hydrogen, a catalyst must have very good selectivity and must not facilitate the WGS to convert the hydrogen and carbon dioxide products back to carbon monoxide and water. At first glance it might seem as though the WGS reaction would limit the ability to produce pure hydrogen but research [9][10] has shown that an intermediary in the WGS reaction is in fact the formate or carbonate ion. Senanayake seeking to understand the water gas shift reaction with a view to hydrogen production has identified the creation of the formate intermediate species as the rate determining step in the reaction[11]. Fuller understanding of the WGS reaction and its intermediates is of potential benefit as it offer a potential path to the creation of hydrogen from carbon monoxide and water. The reaction on CeO_2 was described as proceeding by formic acid adsorption onto the surface creating a formate ion through dissociation of the proton[11].

Equation 8 $HCOOH \rightleftharpoons HCOO^-_{ads} + H^+_{ads}$

Once created the formate ion can follow two pathways,

Equation 9 $HCOO\text{-}_{ads} \rightleftharpoons H^+_{ads} + CO_{2(g)}$

followed by

Equation 10 $2H^{+}_{ads} + 2\ e^{-} \rightleftharpoons H_{2(g)}$

Equation 11 $HCOO_{ads} \rightleftharpoons OH_{ads} + CO_{(g)}$

followed by

Equation 12 $H_{ads} + OH_{ads} \rightleftharpoons H_2O_{(v)}$

In addition, other potentially unwanted reactions include the creation of coke and formaldehyde (eq 13 and 14).

Equation 13 $2H_{2(g)} + CO_{2(g)} \rightleftharpoons 2C + 2H_2O$ Coke formation

Equation 14 $2HCOOH_{(g)} \rightleftharpoons CH_2O_{(g)} + CO_{2(g)} + H_2O_{(g)}$ Formaldehyde

1.7 Formaldehyde

Given the various potential species associated with formic acid decomposition it is unlikely that formaldehyde will be seen due to its tendency to disproportionate into formate and methoxy anions according to the Cannizzaro reaction (see Figure 1.4). The Cannizzaro reaction involves two adsorbed formaldehyde molecules transforming into a formate and a methoxy by the trading of a proton. The reaction mechanism consists of a nucleophilic attack by a surface oxygen on the carbonyl carbon allowing the transfer of a proton to the neighbouring formaldehyde thus creating the methoxy and formate products. This creates a formate anion on the originating molecule and creates a methoxy on the neighbouring surface adsorption site[12].

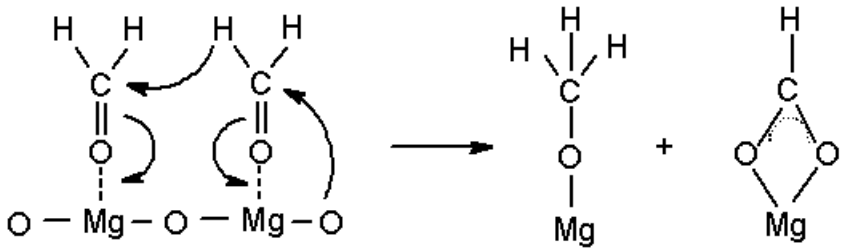

Cannizzaro reaction Methoxy Formate

Figure 1.4 Cannizzaro reaction

1.8 Potential catalytic materials

In addition to looking at the potential reactions one should also look at the properties of potential catalysts. Although pure metals can act as catalysts, often metal oxides are more successful as they can provide polar surfaces with complex coordination environments that aid in the formation of intermediates necessary to catalyse the reaction. A literature search indicates that a number of transition metals facilitate decomposition of formic acid with Ni and Cu being prime examples. Metal oxides are less well studied but offer potential for improved catalytic performance especially with respect to selectivity.

Yttria Stabilized Zirconia (YSZ) as a support has been shown to promote the activity of metal catalysts[5]. It has been suggested that the surface shell reduction stimulates the production of hydroxyl groups that facilitate the water-gas shift reaction. If this is found to be the case then partially reducible oxides such as ceria and zirconia should also effect change in the selectivity of catalysts in formic acid decomposition.

1.9 Catalytic activity

The rate of a reaction is governed by energy barriers that stand in the way of the reactants becoming products. These energy barriers are described by an energy value known as the activation energy. In a simple sense, catalysts work by lowering the activation energy or barrier to the reaction. For a heterogeneous catalyst, the reactants must coordinate on the surface of catalyst, react, and then leave the surface. The rate of the reaction is then limited by the amount of catalyst and its activity. The reaction cycle or activity is measured by the turn over number, the higher the number the faster the cycling. As the temperature is raised, higher kinetic energies lead to higher turnover numbers. Often catalysts that are highly active facilitate more than one reaction. In many cases there are a number of competing reactions that can occur. Catalytic selectivity is a description of how much a catalyst favours or selects one reaction over competing reactions. Ideally a catalyst would be 100% selective to the desired reaction. On metals it is reported that formic acid dehydrogenation occurs almost exclusively. Metal oxides are also catalytically active, however their surface chemistry is more complicated. Formic acid is considered a Brønsted acid (facility to donate a proton) and has been shown to undergo heterolytic dissociation on MgO and other basic materials[12].

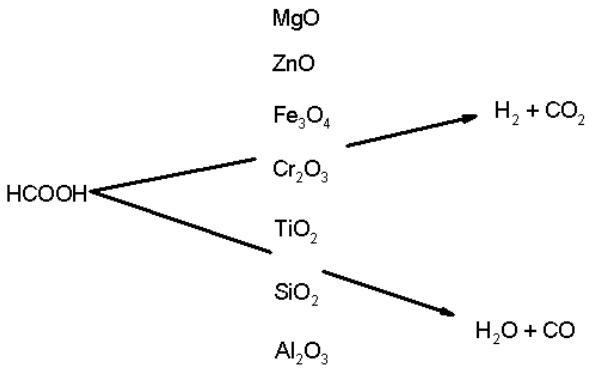

Figure 1.5 Oxide catalytic selectivity. Trends in selectivity for formic acid decomposition via dehydrogenation or dehydration. [13]

Some oxide catalysts are known to promote dehydrogenation (TiO_2, SiO_2, Al_2O_3), others dehydration (MgO, ZnO) and still others both reactions (Cr_2O_3 and Fe_2O_3) (Figure 1.5)[5]. NiO was absent from these studies but one would expect that it would fall somewhere between iron and zinc in its activity and favour dehydrogenation.

1.10 Light off temperature

The conversion-temperature plot is often called the light-off curve. In general conversion-temperature curves have an S shape for any irreversible reaction. The kinetic energy of the reactants must be sufficient to overcome the activation energy. The sudden increase at the bottom of the S is due to the exponential dependence of the rate constant on the temperature. The top of the S featuring a slowdown in the reaction is due to the depletion of the reactants.

One attribute to characterising catalysts is the light off temperature or the temperature at which the reaction starts to proceed. For example, an automotive catalytic converter is ineffective at catalyzing the oxidation of un-burnt fuel until it reaches a minimum temperature, typically around 250°C. This minimum temperature is known as its light-off temperature. Therefore a successful catalyst for formic acid decomposition would show high activity, highly favour dehydrogenation (selectivity), and have a low light off temperature.

1.11 References for Chapter 1

[1] H. Gruenspecht, "International Energy Outlook 2011," *Center for Strategic and International Studies*, 2010.

[2] "World bank, Data, Population, total," *The World Bank*, 2011. [Online]. Available: http://data.worldbank.org/indicator/SP.POP.TOTL/countries?display=graph. [Accessed: 27-Apr-2012].

[3] W. P. Hammes and P. S. Tichaczek, "The potential of lactic acid bacteria for the production of safe and wholesome food.," *Zeitschrift für Lebensmittel-Untersuchung und -Forschung*, vol. 198, no. 3, pp. 193-201, Mar. 1994.

[4] P. M. Sabatier, "The catalytic formation of ether salts of formin acid from formic ether.," *Comptes rendus hebdomadaires des seances de l'academie des sciences*, vol. 154, pp. 175-177, 1912.

[5] P. Mars, P Scholten, J Zwietering, "The Catalytic decomposition of formic acid," *Advances in Catalysis*, vol. 14, no. I, pp. 35-113, 1963.

[6] W. Clark, "The Decomposition of Formic Acid at Low Temperatures, *Journal of the American Chemical Society*, vol. 73, no. 10, pp. 4638-4640, 1951.

[7] N. P. Lebedeva, "Carbon dioxide poisoning on proton-exchange-membrane fuel cell anodes," *Science And Technology*, no. October 2004, pp. 6-7, 2005.

[8] D. G. Nocera, "Chemistry of personalized solar energy.," *Inorganic chemistry*, vol. 48, no. 21, pp. 10001-17, Nov. 2009.

[9] G. Jacobs, P. Patterson, U. Graham, a Crawford, and B. Davis, "Low temperature water gas shift: the link between the catalysis of WGS and formic acid decomposition over Pt/ceria," *International Journal of Hydrogen Energy*, vol. 30, no. 11, pp. 1265-1276, Sep. 2005.

[10] S. A. C. C. R. G. Mellor J.R., Coville N.J., "Raney copper catalysts for the water-gas shift reaction II. Initial catalyst optimisation," *Science*, vol. 164, pp. 185-195, 1997.

[11] S. D. Senanayake and D. R. Mullins, "Redox Pathways for HCOOH Decomposition over CeO_2 Surfaces," pp. 9744-9752, 2008.

[12] X. D. Peng and M. A. Barteau, "Acid-base reactions on model MgO surfaces," *Catalysis Letters*, vol. 12, pp. 245-253, 1992.

[13] P. Mars, P Scholten, J Zwietering, "The Catalytic decomposition of formic acid," *Advances in Catalysis*, vol. 14, no. I, pp. 35-113, 1963.

Chapter Two: Analysis techniques

The chemistry of surfaces is of special interest with regards to heterogeneous catalysis in two ways: one that the reactions are confined to interactions at or very near the surface of the catalyst and two; the chemistry of the surface, its oxidation state, its coordination chemistry, dangling bonds and their termination chemistry are all different than that of the bulk of the material.

A cube 1 cm on a side has approximately 10^{23} atoms, the surface of the cube has only 10^{15} atoms and yet it is those surface atoms that are most involved in the catalytic reactions. Techniques must be used that can differentiate between the surface and bulk chemistry or that are sensitive to only the surface chemistry.

2.1 X-Ray Photoelectron Emission

When a surface is bathed in high energy photons they interact with the electrons of atoms near the surface exciting them to higher energy levels. If the incoming photons impart more energy ($h\nu$) than the work function of the atom, the electron can be ejected from the surface into the vacuum or free space with some measurable kinetic energy (KE) (Figure 2.1).

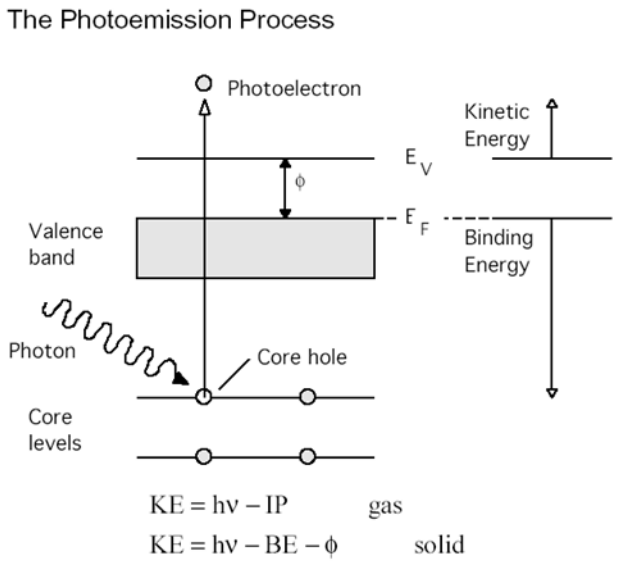

Figure 2.1 The photoemission process

In an isolated atom, the energy required to remove an electron is equal to the energy required to remove an electron from its highest valence level. This is known as the ionization energy or potential (IP). In a bulk material there is a shifting of levels into bands which allow electrons to reside at a slightly different level. The energy required to remove an electron from an isolated atom is its ionization energy; in a bulk, it is known as the work function (φ)[1].

2.2 Auger Electron Emission

If an electron is knocked out of an inner (high energy) electron orbital it naturally leaves a vacancy. The vacancy can be filled with an outer shell electron transitioning to fill the inner orbital (see Figure 2.2). This produces a unique energy surplus specific to the two orbitals involved (E_a– E_b). The surplus energy can then cause the ejection of a second electron. The ejected electron will have a unique kinetic energy based on the initial surplus energy and the binding energy of the second electron (E_c). As three electrons are

involved, the process is normally described by the orbitals involved. An initial electron ejected from the K orbital, having the vacancy filled by an electron from the L orbital and subsequently ejecting an electron from the L orbital will be referred to as the KLL auger peak for a specific element.

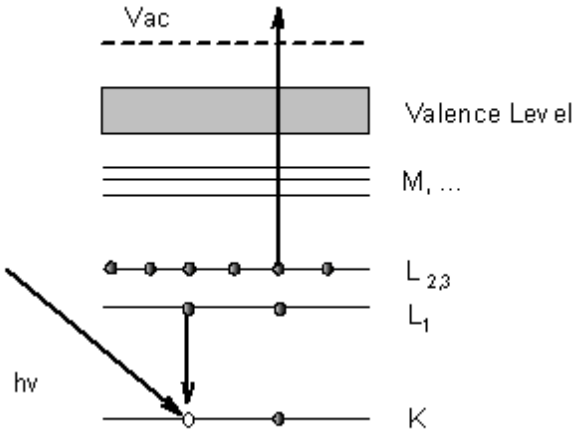

Auger Electron KE = $E_A - E_B -$ $E_C -$ Φ

Energy gained by core-hole annhilation

Energy needed to overcome BE of Auger electron

Figure 2.2 Auger electron emission, E_A is the binding energy of the K level electron, E_B the binding energy of the L_1 level electron, E_C the binding energy of the L_2 level electron, for the Auger KLL emission.

Unlike photo emission electrons, the kinetic energy of Auger electrons in not dependent on the incoming photon wavelength. Changing the incoming photon wavelength will shift the kinetic energy of photo emission electrons but not Auger electrons.

2.3 Surface effect

X-ray photons interact weakly with solid matter penetrating several μm into the surface however escaping electrons are much more restricted on average traveling less than 2 nm colliding with other matter. Statistically the vast majority of electrons ejected come from within approximately 1 nm of the surface[2]. Therefore it is not the penetration of the X-Rays but the escape of the electrons that make this a useful surface science technique.

The surface sensitivity can be estimated by considering the distance travelled by the electron. The mean free path (λ) of electrons is the average distance they travel between collisions. In a material that approximates an ideal gas, the mean free path can be calculated if one knows the mean velocity of the particle and the collision frequency ($\lambda = c/z$). The collision frequency can in turn be calculated from the collision cross section of the material. Electrons interact strongly with matter at energies ranging from 20 eV to 500 eV resulting in mean free paths of 0.5 nm to 1.0 nm. Graphing the mean free paths for various elements over a range of electron energies produces a curve, known generally as the "universal curve"[3] (see Figure 2.3).

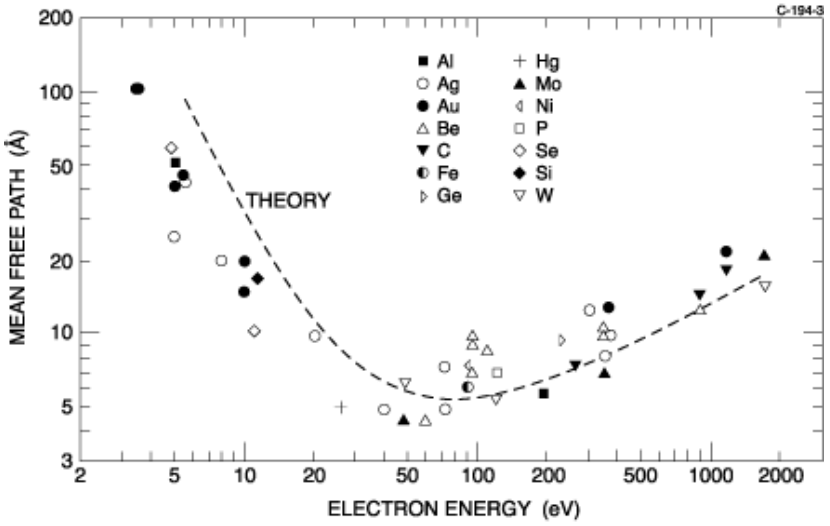

Figure 2.3 Universal curve for mean free path of electrons. [1]

The inelastic mean free path decreases with increasing energy below 50 eV and increases with energies over 100 eV. At higher kinetic energies the speed of the electron is higher and so the interaction with atomic electrons is reduced resulting in a larger mean free path above 100 eV. At low electron energies, the number of available sites for scattering is small. As the energy is increased, more sites become available resulting in more interactions and hence shorter mean free paths.

In the range of eV that are produced by the X-Ray source it can then be expected that for most elements the mean free path would be somewhere between 1 nm and 2 nm[4]. This corresponds to only a few atomic layers in a material such as MgO.

2.4 X-Ray Photoelectron Spectroscopy

XPS is a surface sensitive technique that allows both qualitative and quantitative analysis of the surface of a material. Conceptually the analysis technique is quite simple. The surface is illuminated with an x-ray photons of a known energy/frequency using x-ray source (see Figure 2.5). As atoms on the surface absorb the energy they can re-emit the energy or convert it to some other form. One way for the energised atom to lose the excess energy and return to the ground state is to emit an electron. The ejected electron will have a kinetic energy equal to the energy of a photon ($h\nu$) from the X-ray beam less the binding energy of the electron to the atom (work function (Φ) in a solid) see Figure 2.1.

Therefore an X-Ray Photoelectron spectrograph is simply a graph of the number of electrons emitted as a function of the electron's kinetic energy. Knowing the incoming

photon energy it is then a simple matter to plot the electron counts as a function of bonding energy.

Much information regarding the surface atoms can be extracted from the resulting spectra. The binding of an electron to its host atom is very sensitive to not only atomic parameters such as the atomic number of the atom and the electron orbital but also to the atoms environment, its oxidation state, its bonds to other atoms, its neighbouring atoms, charging and even energetic waves in the environment such as phonons and plasmons. As an example, common carbon 1s binding energy values are listed in Table 2.1.

Functional Group		Binding Energy (eV)
Hydrocarbon	C-H, C-C	285
Amine	C-N	286
Alcohol	C-O-H	286.5
Carbonyl	C=O	288
Amide	N-C=O	288.2
Acid	O-C=O	289
Urea	NCON	289
Formate	COOH	288.6 – 289.2
Carbonate		290.3
Carbon tri-fluoride		293-294

Table 2.1 Typical C1s binding energies for organic molecules ([1])

2.5 X-Ray Photoelectron Spectrometer

To perform XPS, one needs both an X-Ray source and a photoelectron spectrometer. An idealized X-ray photoelectron spectrometer consists of three key parts, a vacuum chamber, a narrow pass filter for electrons and a sensitive electron detector. A standard laboratory setup is schematically represented in Figure 2.4. The x-rays illuminating the sample have an element specific probability of ejecting an electron via the photoelectric effect. The kinetic energy of the escaping electron is determined by the energy of the photon, its initial element's orbital binding energy, any interaction with other atoms prior to reaching the detector and the work function of the material.

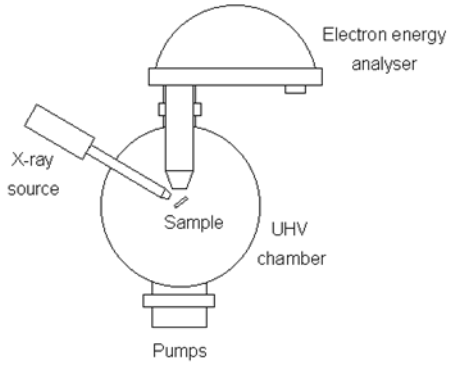

Figure 2.4 Schematic of an x-ray photoelectron spectrometer. The x-ray source illuminates the sample with photons of a specific energy (1486.6 eV for Al anode) which in turn eject core electrons via the photoelectric effect. The hemispheric energy analyser allows only electrons of a specific energy to pass through to the detector. The energies allowed to pass are scanned to form an XPS spectrum.

As emitted electrons also interact with gas phase molecules, typical XPS experiments require a pressure of less than 10^{-7} mbar to ensure a sufficient proportion of the electrons emitted from the surface reach the detector. At pressures greater than 10^{-7} mbar, electrons produced from the surface will be absorbed or scattered before then can be measured. One way to overcome this problem is to use a more powerful x-ray source, such as synchrotron radiation. The greater the intensity of the X-Ray source, the more sensitive the technique. The higher flux of synchrotron x-ray photons results in a higher signal to noise ratio, allowing for higher sensitivity (lower element concentration) to be detected, and for experiments to be performed at higher pressures. Ambient pressure XPS generally indicates pressures up to several Torr. It is expected that ambient pressure XPS provides a better approximation to real world surface chemistry than the normal UHV XPS systems can provide.

2.5.1 Electron detection.

With XPS the electrons' kinetic energy is measured with a hemispheric analyser. The analyser uses two concentric charged surfaces to bend incoming electrons. Electron with too high or too low a kinetic energy will be captured by one or the other surface. If an electron has just the right kinetic energy it will pass between the two charged surfaces and reach the detector. As only a narrow range of kinetic energies can pass through the hemispheric analyser, it is known as a narrow pass filter. The kinetic energy range of the electrons that succeed in navigating the hemispheric analyser is known as the pass energy. As the potential on the surfaces is changed, so will the kinetic energy of the detected electrons allowing for the scanning of a range of kinetic energies. The energy of the electrons allowed to pass is scanned over a desired range to produce an XPS spectrum.

2.6 X-Ray source.

2.6.1 Tube type x-ray source

There are a range of X-Ray sources although the most common are the Al Kα and Mg Kα. The most common X-ray source found in lab use utilizes an electron beam to irradiate a metal target knocking out core electrons (Figure 2.5).

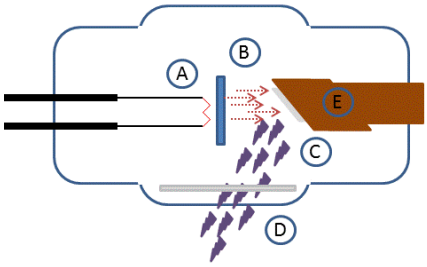

Figure 2.5 Schematic of X-Ray source, X-rays generated by electron impact on a metal (based on X-ray fluorescence process) A) heated filament emits electrons by thermionic emission, B) electrons are accelerated by a high voltage, C) x-rays are produced by when high speed electrons hit the metal target (Al or Mg) D) x-rays pass through Al window to remove Bremsstrahung radiation

Typically a dual anode design is used to allow either Al Kα and Mg Kα X-rays. The inner orbitals are then refilled with electrons dropping down from outer orbitals producing a characteristic fixed wavelength radiation. Aluminum K-alpha photon energy is 1,486.70 eV, Mg K-alpha photons are 1,253.60 eV [2] (see Figure 2.6).

Given that the binding energy of the elements under analysis is calculated from the difference of the incoming x-ray photons and the work function, the tighter the range of incoming photon energies, the sharper the peaks in the associated spectrum. At the same time, Background x-rays (Bremsstrahung or breaking radiation) as well as stray electrons are filtered out by a second aluminum window producing a narrow bandwidth photon source (figure 2.5).

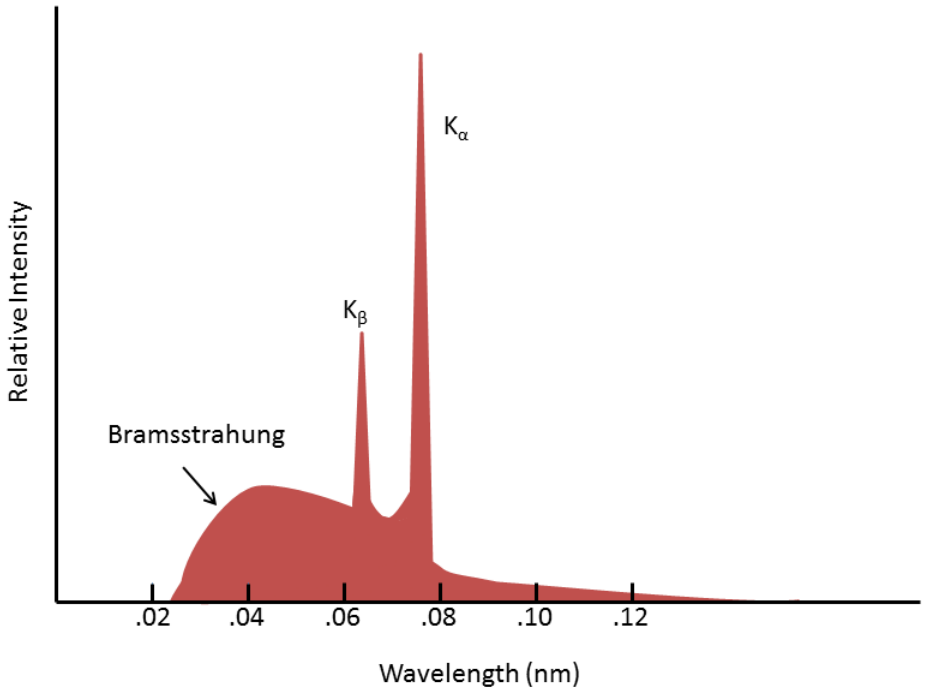

Figure 2.6 Typical Bremsstrahung, K-alpha and K-Beta radiation, Al(Kα) and Mg(Kα) are the most common laboratory sources. Example from molybdenum target at 35 kV[5].

2.6.2 Synchrotron radiation

Accelerating charge results in the emission of electromagnetic radiation. At non-relativistic speeds the radiation is emitted in all directions equally. If however the charge is already moving at speed near that of the speed of light when it is accelerated we see an interesting effect Figure 2.7.

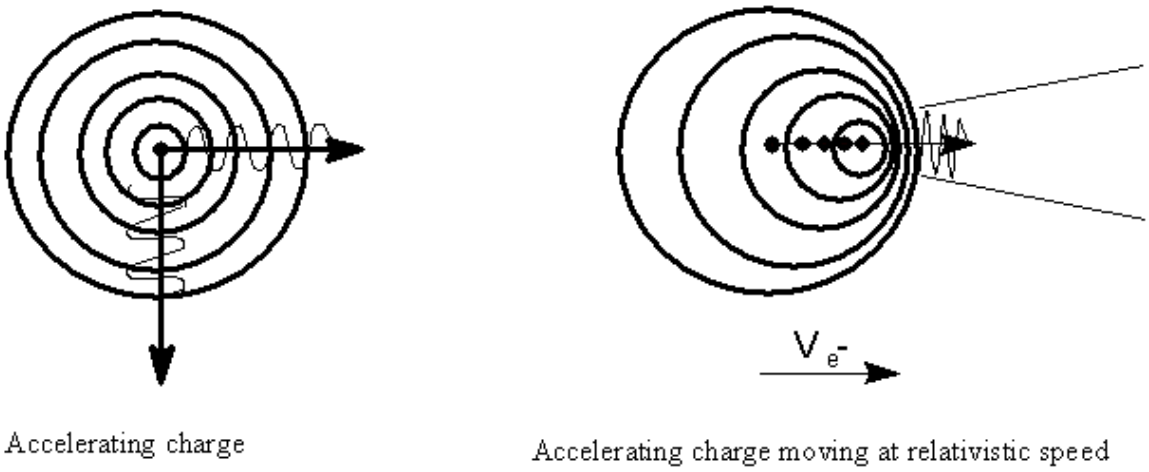

Figure 6.7 Accelerating charge emits electromagnetic radiation, accelerating charge moving at close to the speed of light emits electromagnetic radiation in cone in-line with the direction of travel of charge. In a synchrotron strong magnets create centripetal acceleration of electron beam.

When electrons travel at speeds close to the speed of light (relativistic speeds) they emit radiation in the same direction as they are traveling. In a sense the electromagnetic wave front cannot escape the charge in all directions due to the speed of the electron. As a result the electromagnetic wave front is tightly concentrated into cone shaped area in-line with the charges direction of travel. The Doppler Effect causes the electromagnetic radiation to move to shorter wavelengths as the speed of the electron stream is increased. If the electron stream then undergoes centrifugal acceleration (that is, it bends) the electromagnetic radiation will continuously be emitted outward like mud from a spinning tire. Through this process, modern synchrotrons emit a broad range of photon energies from microwaves to hard x-rays.

The Advanced Light Source in Berkley California is a research centre that uses a series of very strong magnets to bend a hair like beam of electrons into a curved trajectory around

a 200m ring producing intense synchrotron radiation. Beamlines tap into this light source directing finely tuned and focused source of x-rays for experimental use.

Source	Light intensity photons/sec/mm2
Synchrotron (ALS)	10^{16}-10^{19}
Sun	10^{10}
x-ray tube	10^{9}
Candle	10^{5}

Table 2.2 Light intensity of x-ray source [1]

As mentioned previously, hard x-rays (>10^3 eV) cover the range of binding energies associated with core electrons. The intensely high flux of hard x-rays results in a more intense stream of emitted electrons which in turn allows for experiments at higher pressures or greater sensitivities. A comparison of light intensity that is photon emission rates is given in Table 2.2.

2.7 Analytical considerations

2.7.1 Peak Shape

Excited electrons can be ejected directly with their peak kinetic energy equal to the incoming photons energy less the work function of the material. The ideal peak shape is therefore sharp and symmetrical. In reality, peaks are often broader and less symmetrical than the ideal. This is due to a stepped background signal (see 2.7.2) and small changes in surface environments for individual atoms that create a broadening to the range of their binding energies. For this reason, peaks for gas phase photo emission electrons are often much sharper. One descriptor of a peaks' shape is the peak width. The peak width, often

recorded as a full width half maximum (FWHM), is a function of the instrument, the intensity of the x-ray source and the tuning of XPS scan parameters (see paragraph 2.7.9).

2.7.2 Background signal

Not all electrons reach the detector unimpeded. Naturally electrons losing some of their kinetic energy through interaction with other electrons or atoms along the path to the detector will result in a background signal of lesser kinetic energy electrons. Therefore the shape of XPS peaks tends to be sharp on the higher kinetic energy side and smeared to the lower kinetic energy. Often the background takes the form of a step down in binding energy at each peak.

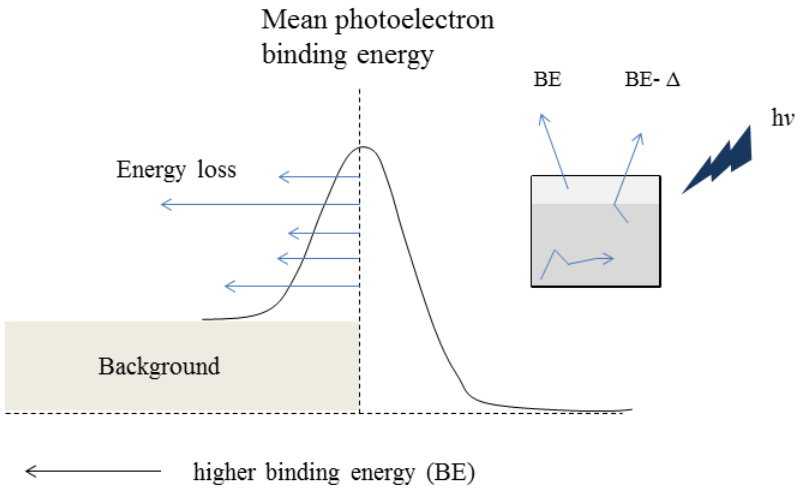

Figure 2.8 Stepped XPS background. Electron energy loss due to inelastic collisions results in a characteristic stepped background. Electrons with energy loss have les kinetic energy which is interpreted as a higher binding energy.

In the diagram above (Figure 2.8) the effect of electron energy loss of electrons escaping the surface layers of a material illustrates the principle cause of the XPS background. The energy loss can range from no energy loss, in which case the electron has the maximum kinetic energy, to so much that the electron never escapes from the bulk. At energy loss between those two extremes, the electron will be detected with a kinetic energy of less than (or conversely as a higher binding energy) that the peak maximum. The greater the energy loss of the emitted electron, the greater the apparent binding energy of that electron. Emitted electrons with partial energy loss will form a background artificially raising the detected counts for all higher binding energies.

For quantitave analysis it is imperative that the background be subtracted from the electron counts associated with the true unimpeded electrons. One of the more common calculations of the background is known as a Shirley curve. The calculation of the Shirley curve and its subtraction is typically done by an analysis package such as CASAXPS. For more detail, the initial mathematical work was documented in a paper by Shirley[6].

2.7.3 Singlets and doublets

Photoelectron peaks can split to form doublets if coupling between the magnetic fields of the spin and the angular momentum occurs (see Figure 2.9). The magnetic field of the

spin adds to the angular momentum to form one peak and the spin is subtracted from the angular momentum to form the other peak. S orbitals are not spin-orbital split whereas p, d & f orbitals will form doublets.

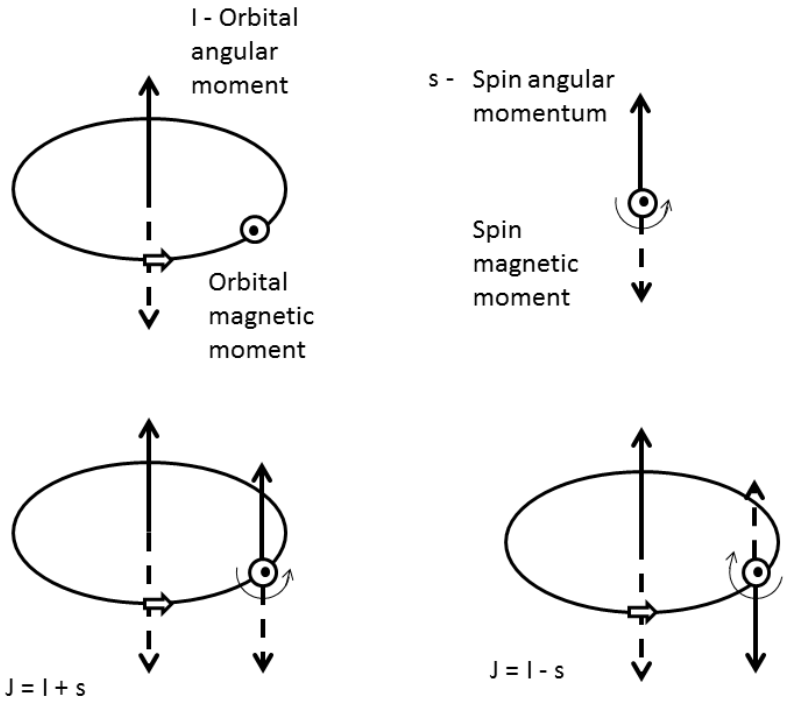

Figure 2.9 Coupling to create doublets, for any electron in orbitals with orbital angular momentum, coupling between magnetic fields of spin and angular momentum occurs in either additive or subtractive manner thereby splitting the peak.

2.7.4 Charging

The removal of electrons from the surface of a sample can result in a charge forming on the surface. This is typically not a problem with conductive materials such as metallic elements but will almost certainly happen for insulating materials. As a material loses electrons it develops a positive charge increasing the binding energy of the remaining

electrons. In practice this results in a shift to higher binding energies for all peaks. If the charging is uniform, that is to say all peaks have been shifted uniformly; one can simply locate a reference peak and shift the entire graph sufficiently so that the reference peak is correctly located. The assumption is that all other peaks will also now be correctly situated. If the charging is not uniform, that is to say the amount of charging increases or decreases during the scanning period or the surface is not homogenously charged, then it becomes increasingly difficult to analyse the spectra. Charging can be mitigated by bathing the surface with low energy electrons or by heating the sample to facilitate conductivity of semi-conductors.

2.7.5 Peak position / chemical shift

There are catalogs of well documented reference spectra for each element, however there are a number of effects that can alter the spectra that make interpretation more challenging. The art of interpreting XPS spectra involves the matching of a sample's physical attributes with its spectra by taking into account the various effects that can modify the reference spectra. Most easily one can think of chemical shift in the following manner. If an atom loses an electron, the remaining electrons can "feel" the effect of positive nucleus more strongly and therefore become bound more tightly. Therefore an oxidizing environment will result in a shift to higher binding energies. A reducing environment adds electrons resulting in more shielding and lower binding energies. Chemical shift help describe the chemical environment of the atom, specifically the oxidation state. As a material is reduced the electrons are held less tightly and therefore have a lower binding energy, oxidizing the same material will result in the

remaining electrons being more tightly bound and hence a higher binding energy. Interestingly much of chemistry views oxidation states as whole numbers whereas this technique shows that oxidation states are perhaps better viewed as real numbers. Additionally the specific nature of the bond affects the nominal oxidation state as shown in Table 2.1.

2.7.6 Auger electron peaks

As mentioned earlier, unlike photo emission electrons, the kinetic energy of Auger electrons in not dependent on the incoming photon wavelength. Auger peaks can be separated from photo emission peaks by changing the incoming photon energy (wavelength). Photo emission peaks will shift and Auger peaks will not. Electrons that reach the detector can be from a number of physical sources. Photoemission and Auger peaks can easily be distinguished by switching between sources, Al vs. Mg in the laboratory or using different wavelengths at the ALS. The photoemission electrons kinetic energy will change with a changing energy of the incoming photon whereas electron emitted through the Auger process will not change.

2.7.7 Relative Sensitivity Factor:

The Relative Sensitivity Factor (RSF) of an element is an element and photon energy specific correction factor that reflects the specific probability that an incident photon with be absorbed by an atom in the material. To make a meaningful quantitative analysis of the XPS spectrum one must use the RSF to adjust the area under each peak to produce comparable areas for quantitative analysis. For example, following multiplication by the elements RSF, a ratio of 2:1 between peaks can be interpreted as a ratio of 2:1 for

element quantities. The RSF allows correlation of the area under a XPS peak with other elements XPS peaks thereby allowing calculation of the relative concentrations.

2.7.8 Quantitative analysis

XPS can also be used to determine the ratio of the various elements on or near the surface of the sample by comparing the area under the peak associated with each element. To use XPS for qualitative analysis one must do two things, remove the background from all analysed peaks and normalize the peak counts for each element based on their Relative sensitivity factor. Once this is done, the area under the peak is indicative of the quantity of the element at the surface. Analytical tools such as CasaXPS have simplified quantitative analysis by automating the calculation and subtraction of a spectra background and tabulating standard RSF values.

2.7.9 The art of XPS

We have discussed the analysis of XPS spectra but there is also much skill required to creating a good XPS. There are a number of parameters and trade-offs associated with their use.

Exposure to X-rays can damage or alter surface chemistry of the sample, increasing the time or intensity increases the likelihood of surface modification by the x-rays. Ideally one would keep the exposure to x-rays to a minimum to minimize surface damage. However increasing the intensity and exposure to x-rays increases the sensitivity of the analysis. Ideally one would like the maximum signal to noise ratio, separating real peak signals above the background signals. One would also like the narrowest peaks as defined by the smallest full width half maximum (FWHM) value. Dwell times and

sample binding energy step size are also important. Increasing dwell times increases electron counts and hence improving signal to noise ratios at a cost of increased time the sample is exposed to x-rays. Similarly too small a step size increases scan time whereas too large a step size reduces the techniques sensitivity to distinguishing narrowly separated peaks.

The pass energy is the narrow window of electron kinetic energies that are allowed to strike the electron detector. Too narrow and electron counts are reduced decreasing the signal to noise ratio. Two broad and the peak width will be artificially increased thereby removing the ability to separate adjacent peaks.

All of these factors must be carefully balanced to achieve successful XPS spectra while minimizing machine time and sample damage.

2.7.10 Analysis procedure

Skill is also required for the analysis of XPS spectra. Peaks must be interpreted with an eye to their shape, width as well as the samples history and the instruments capabilities. Electrons from S orbitals will produce singlets whereas p and d orbitals will produce doublets. A twin peaks where a single peak is expected could indicate different coordination environments, a second peak or even a machine fault. Normally the peak should be symmetrical (taking into account background), asymmetry can indicate one or more additional peaks merging to form one. In interpreting the peaks width, one used the full width half maximum value with an eye to the instruments resolution and the elements natural peak width. If a peak is broader than expected, one must ask why. Finally one must assign peaks based on what could realistically be present based on the sample composition, the environment and preparation history.

2.8 Quadrupole Mass Spectrometry

Throughout the sequence of experiments associated with this thesis, mass spectrometry has been an invaluable tool to track the residual gas composition for direct evidence of formic acid decomposition. Individual molecules are broken apart, ionized, accelerated to several eV and then filtered using an RF field according to mass/charge ratio. The fragment size and ratios of fragment sizes form a diagnostic signature that can be used to identify the original molecule.

Quadrupole mass filters are small, relatively inexpensive and therefore common forms of mass spectrometers. A quadrupole mass filter is also known as a quadrupole mass spec (QMS) a quadruple ion trap, a quadrupole ion store or a Paul trap. Wolfgang Paul shared the 1989 Nobel Prize in physics for describing its principles of operation. Although the mathematics that describe the motion of ions through the quadrupole field is complex and beyond the scope of this document, the principle of operation is relatively simple. A simple diagram of the key components of a QMS is found below (Figure 2.10). A hot filament generates a stream of electrons accelerated to 70 eV, sufficient energy to fragment the sample molecules. The charged molecular fragments are then accelerated as they pass through an electrically charged grid towards an ion detector. Prior to reaching the detector, the ion must pass the length of the quadrupole mass filter. The quadrupole mass filter consists of 4 rods that experience an alternating radio frequency potential. The alternating potential causes the fragments to swirl as they move towards the detector. Excessive or insufficient kinetic energy (determined by the mass and charge of the ion) will cause the fragment to collide with the wall of the mass filter and neutralize the ion.

In a QMS it is the fragments kinetic energy that is key to surviving the journey to the detector.

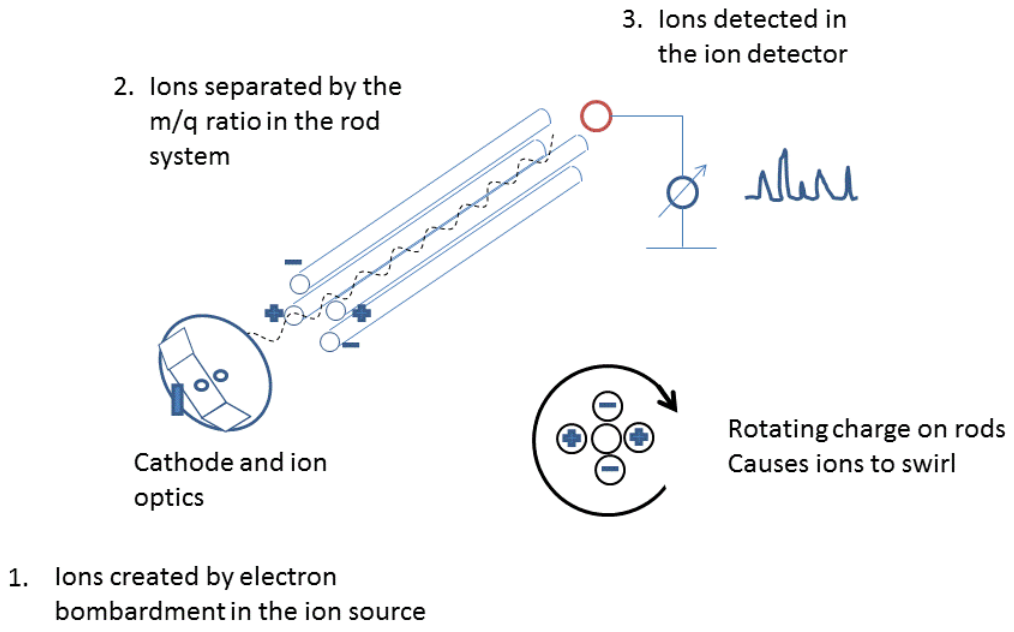

Figure 2.10 Schematic of a simple QMS like the one used in the catalysis experiments[7]

By changing the frequency of the electric fields growth and decay one can alter the ion traps target "pass kinetic energy". By scanning the range of kinetic energies (mass charge combinations), one can create a spectrum of fragments that can then be analysed.

As it is a combination of mass and charge, both a single charge of a given mass and a double charge on twice the mass will both register on the detector for one charge-mass ratio.

Relative sensitivities to ionization for each component must be taken into account when interpreting the QMS results. In addition fragmentation patterns and ratios of subsequent atomic mass unit (AMU) fragments must also be taken into account when attempting qualitative analysis. Some care must be taken in interpreting the resulting spectra as many molecules can be responsible for a given fragment or set of fragments.

References for chapter 2

[1] R. F. Feuerbacher, B. Fitton, B. Willis, Ed., *Photoemission and the electronic properties of surfaces*. Toronto: John Wiley & sons, 1978.

[2] Y.wah Chung, *Practical guide to surface science and spectroscopy*. Academic press, 2001.

[3] C. Attard, Gary Barnes, *Surfaces*. Oxford science publications, 1998.

[4] M. Butt, Hans-Jurgen Graf, Karlheinz Kappl, *Physics and Chemistry of interfaces*. Whiley, 2006.

[5] N. Fairley and A. Carrick, *The Casa Cookbook*. Cheshire: Acolyte Science, 2005.

[6] D. A. Shirley, "High Resolution X-Ray photoemission spectrum of the valence bonds of gold," *Spectrum*, vol. 6, no. 12, 1972.

[7] J. Todd, *Quadrupole ion trap mass spectrometry*. Hoboken: Wiley interscience, 2005.

Chapter Three: Metal oxide catalysts

3.1 Catalytic materials in nature

In nature, catalytic activity often is based around a single metal atom or a cluster of metal atoms sequestered at the heart of a large molecular complex. A good example of this is found in chloroplasts associated with photosynthesis. Here it is the redox capabilities of manganese atoms surrounded by complex organic antenna complexes that accomplish the first and critical step of water splitting.

There are three important factors in the catalytic molecule design that facilitate the water splitting. The first is that the molecule's structure coordinates the water molecule orientation to the catalytic centre. The second is the ability of the manganese atoms to adopt a wide range of oxidation states with great ease and finally the last feature is the catalytic complexes ability to transfer charge from the antenna complexes to the catalytic centre.

3.2 Three key aspects of a catalytic material

Learning from nature, to understand a material's catalytic behaviour, one must look at its redox capabilities, its ability to coordinate reactive materials and finally its ability to transfer charge. Barteau highlights three key concepts applicable to the surface chemistry of metal oxides that closely mirror the key aspects found in some of nature's catalysts:

1) "Coordination environment of surface atoms;

2) Redox properties of the oxide; and

3) oxidation state of the surface"[1].

3.3 Metal oxides

Metals have been well characterized and understood with regards to their catalytic abilities. The knowledge of the capabilities of metal oxides has lagged that of metals due to their complexities and the difficulty in applying standard surface science techniques. Metals are conductive whereas metal oxides are insulators or semi-conductors. The lack of conductivity with their subsequent difficulty to heat & tendency to charge make metal oxides more challenging to apply normal surface science techniques. The lack of conductivity however is also an asset in that it allows for the isolation of individual atoms which allows for the rapid and easy changing of the surface cations oxidation state. The same characteristics that inhibit their study offer an interesting and potentially rewarding area of study for catalysis. In bulk metals the individual atoms are in the zero valent state whereas in metal oxides not only are they oxidized, but especially at their surfaces, they are easily oxidized or reduced.

In addition to the isolation of the metal atoms, for reactions involving oxidation or reduction, the mobility of oxygen ions through the oxide lattice provides a mechanism for stabilization of intermediates.

3.3.1 Coordination

In metal oxides the metal atoms are separated from each other by oxygen anions. Apart from altering the electrical conductivity, this allows metal oxides to exhibit more complex structures with changing coordination sites. This is perhaps the aspect of metal oxides that leads to the belief that they offer significant potential as catalysts. By having a matrix of oxygen atoms and metal atoms, metal oxides surfaces provide a natural anion/cation target for polar molecules. These sites can also be described as acid base

pairs. The oxygen anions act as Lewis bases attracting hydrogen atoms and the metal cations act as Lewis acids. When dealing with formic acid, it is expected that the acid dissociates to form a large formate anion attracted to the metal and a highly mobile proton associates with the oxygen.

3.3.2 Steric factors

Metal oxides do not just create a charge pattern on the surface, steric factors also come into play that will affect which molecules can be stabilized on the surface based on size and orientation. The oxygen anion with an atomic radius of 150 pm is typically much larger than the metal cation resulting in steric hindrance for ions attempting to approach the metal on some surfaces. The size disparity can also trigger surface polarity and surface reconstruction.

3.3.3 Surface stability and polarity

As oxides are not made up of only a single element, their surfaces present more complex and potentially reactive character than a "pure" substance. Surface cations and oxygen may be more acidic or basic than the bulk material depending on how they are oriented and terminated. The surfaces may also reconstruct to stabilize a surface which in turn creates additional chemical reaction sites.

For MgO the (100) surface is the most stable non-polar interface and the (111) surface is a polar orientation that is less stable (has a higher surface energy)[2]. Surfaces will seek to minimize their surface energy by compensating for the charge in some manner. Charge compensation of the polar surfaces is reported to be common. Charge compensation can take the form of a reconstruction becoming steps of a (100) surface on the (111) plane. Three reconstructions have been reported for MgO, $(\sqrt{3} \times \sqrt{3})R30^{\circ}$, (2 X

2) and ($2\sqrt{3}$ X $2\sqrt{3}$)R30°[2]. When a smooth face such as the (111) face of MgO is reconstructed into a series of steps and terraces, the surface area is increased but the overall surface energy is decreased by incorporating low energy surfaces.

The surface may also stabilize by having its dangling bonds terminated with complementary ions. MgO is regarded as a very basic material due to its strong affinity for protons to stabilize its surface.

3.4 MgO

MgO is known for its strong basic character in that it has a strong affinity for protons to stabilise the surface dangling bonds by forming hydroxyl groups.

Because of its reactivity[3], MgO is currently used as a catalyst for bio-diesel production,[4] for catalytic decomposition of ammonium perchlorate[5], and it has been used as a catalyst for the dehydrogenation of formic acid and methanol as well as being used as a support for metal catalysts.[6]

The crystal structure of MgO possesses a fluorite structure, which is cubic, similar to common salt (NaCl). The most stable (100) surface is shown in Figure 3.1, with alternating anions and cations in the same plane. In contrast, the polar (111) surface is shown in Figure 3.2.

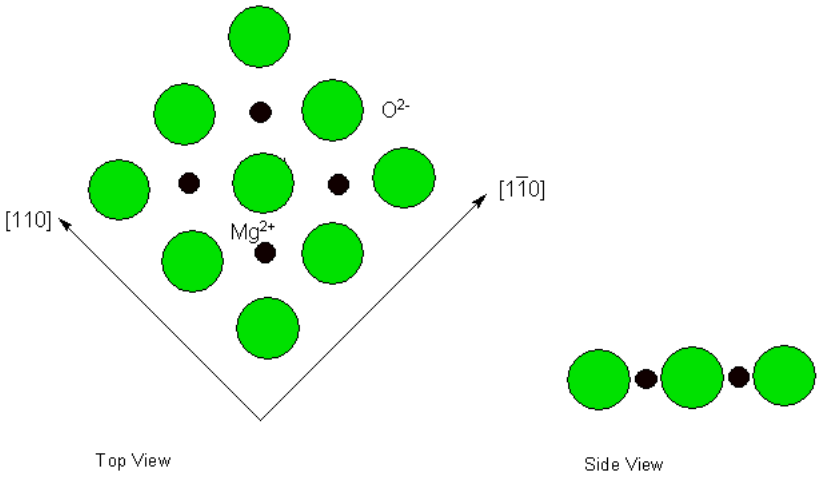

Figure 3.1 top & side view of MgO (100) surface. Side view illustrates lack of polarity.

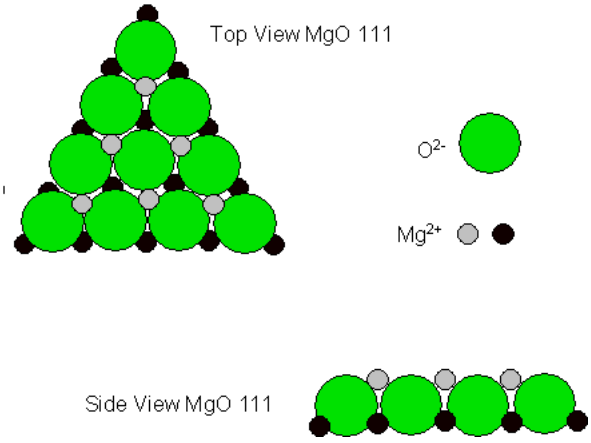

Figure 3.2 MgO (111) Side view illustrates polar layering of charged ions.

The oxygen anion has an ionic radius 2.5 times that of the magnesium cation (150pm vs 60pm) leading to steric factors inhibiting larger molecules from coordinating with the oxygen although this would not be a factor for something as small as a proton (25 pm atomic radius) (see Figure). Depending on the orientation of the crystal structure to the surface different atoms will be exposed. MgO surfaces can be well ordered (MgO(100)) or rich in surface defects (MgO(111) after reconstruction). It is been shown that unlike

methanol, formic acid will adsorb and react with equal likelihood on both the (100) and (111) surface of MgO. [7].

In recent years nano sized crystallites of MgO have become commercially available. Nano sized particles greatly affect the ratio of bulk to surface atoms, increase the surface area and can also affect the electronic properties of the material. In addition, while nominally the surface of nanoparticles is the same as that of larger crystals, there is a further relaxation factor associated with the small size which can produce further reconstructions. Polycrystalline materials usually expose several crystal faces in random orientation. In addition to increased surface area, nano sized crystallites also have a greater density of surface defects[8]

3.5 Yttria stabilized zirconia

Yttria stabilized zirconia (YSZ) is a strong ionic conductor and when paired with Ni or other metals creates a junction enabling the flow of electrons, oxygen anions and protons. Zirconia can exist in different crystalline structures, monoclinic at low temperature and cubic at higher temperatures. Yttria is added to zirconia to stabilise it in the face centred cubic structure also known as the Fluorite crystal structure (see Figure 3.3). The layering of alternating oppositely charged ions (O^{2-}, Zr^{4+}, O^{2-}…) in the (100) orientation results in a very polar surface when cleaved. The fresh polar (100) surface is unstable and will reconstruct if possible. Unlike MgO, it is the YSZ(100) face that is the most reactive and least stable whereas the (111) surface is more stable. Again viewing Figure 3.3 one can see that the (111) surface would have the most even balance of anions and cations and hence be the least polar. The oxidation state of the Zirconium in Zirconia is +4, replacing some of these ions with +3 Yttria ions results in oxygen vacancies in the crystal

structure (see Figure 3.3). The oxygen vacancies allow the migration of oxygen ions from one hole to the next and on a macro scale oxygen conductivity for the crystal.

YSZ alone is not expected to act as a significant catalyst for the reactions in question however it may well act as a promoter enhancing the activity. Nickel and copper are well established as catalysts for diverse areas such as hydrogenation, water splitting[9], hydrocarbon reforming[10], and water gas shift[11]. YSZ can act as a physical support for the metal, reducing the tendency of the metal to lose surface area through agglomeration. Given its ionic conductivity, YSZ could also act as a source or sink for a reactions electrons, anions or protons.

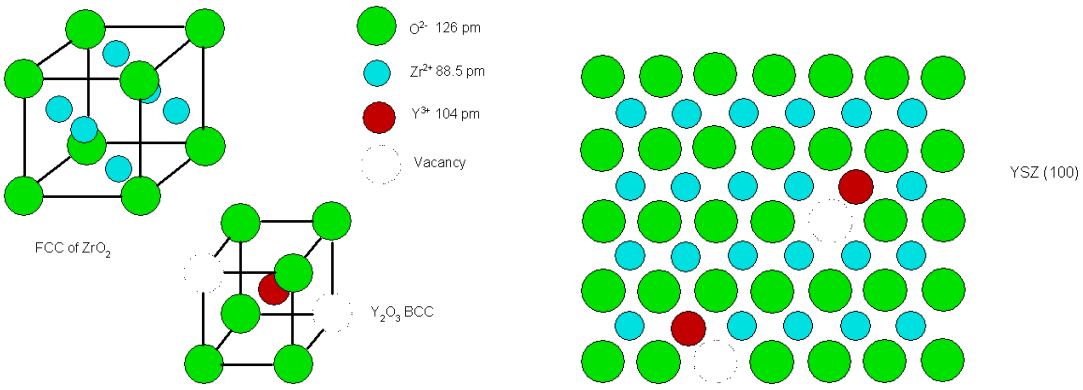

Figure 3.3 YSZ (100). Face centred cubic structure found in YSZ create a polar surface when cleaved on the (100) due to the layering of positive and negative ions. Inclusion of the 3^+ yttria ion forces oxygen vacancies to balance charge.

Given that all three ions have similar ionic radius (yttria 180 pm, zirconia 160 pm and oxygen 150 pm) one would not expect to see steric restrictions associated with the YSZ.

3.6 References for Chapter 3

[1] M. A. Barteau, "Organic Reactions at Well-Defined Oxide Surfaces II .," *Society*, pp. 4-6, 1996.

[2] J. Goniakowski, F. Finocchi, and C. Noguera, "Polarity of oxide surfaces and nanostructures," *Reports on Progress in Physics*, vol. 71, no. 1, p. 016501, Jan. 2008.

[3] P. Mars, P Scholten, J Zwietering, "The Catalytic decomposition of formic acid," *Advances in Catalysis*, vol. 14, no. I, pp. 35-113, 1963.

[4] A. R. Yacob, M. Khairul, A. Amat, and N. S. Samadi, "Calcination Temperature of Nano MgO Effect on Base Transesterification of Palm Oil," *Engineering and Technology*, pp. 408-412, 2009.

[5] G. Duan, X. Yang, J. Chen, G. Huang, L. Lu, and X. Wang, "The catalytic effect of nanosized MgO on the decomposition of ammonium perchlorate," *Powder Technology*, vol. 172, no. 1, pp. 27-29, Mar. 2007.

[6] H. Onishi, C. Egawa, T. Aruga, and Y. Iwasawa, "Adsorption of Na atoms and oxygen-containing molecules on MgO(100) and (111) surfaces," *Surface Science*, vol. 191, no. 3, pp. 479-491, Nov. 1987.

[7] H. Onishi, C. Egawa, T. Aruga, and Y. Iwasawa, "Adsorption of Na atoms and oxygen-containing molecules on MgO(100) and (111) surfaces," *Surface Science*, vol. 191, no. 3, pp. 479-491, Nov. 1987.

[8] M. M. Natile, A. Glisenti, C. Inorganica, and M. Analitica, "Surface Reactivity of NiO : Interaction with Methanol," *Chem Mat.*, no. 18, pp. 4895-4903, 2002.

[9] Z. Zou, J. Ye, K. Sayama, and H. Arakawa, "Direct splitting of water under visible light irradiation with an oxide semiconductor photocatalyst.," *Nature*, vol. 414, no. 6864, pp. 625-7, Dec. 2001.

[10] B. H. J. H. Rostrup-Nielen J.R., "Reforming of Methane over transition metals.pdf," *Journal of Catalysis1*, vol. 144, pp. 38-49, 1993.

[11] S. A. C. C. R. G. Mellor J.R., Coville N.J., "Raney copper catalysts for the water-gas shift reaction II. Initial catalyst optimisation ," *Science*, vol. 164, pp. 185-195, 1997.

Chapter Four: A study of catalysts with high activity for formic acid decomposition

4.1 Introduction

Formic acid has two principal decomposition pathways

1. $HCOOH \rightleftharpoons CO + H_2O$ (dehydration)

2. $HCOOH \rightleftharpoons CO_2 + H_2$ (dehydrogenation)

Plus a third potential reaction between the two product groups.

3. $CO + H_2O \rightleftharpoons CO_2 + H_2$ (water gas shift)

As carbon monoxide can poison many downstream reactions, much value is placed on a catalyst having high selectivity favouring reaction 2 over reaction 1. In addition one must be sensitive to the potential of any catalysts to facilitate the water gas shift reaction in effect reducing the selectivity of the catalyst.

The first stage of our experiment involved the testing of a range of potential catalysts with a simplified apparatus to narrow the field for further research. Copper based catalysts have been reported as active for the selective oxidation of methanol to formate, formaldehyde and formic acid as have rare transition metals belonging to the platinum group such as ruthenium[1][2]. In this chapter we will focus on a range of easily available catalysts, either previously synthesised in house or commercially available. For the most part these are YSZ supported metal oxides or perovskites see Table 4.1.

Catalyst	Characteristics	Source
Background (empty vessel)		
5% Co (cat AB)	$Sm_{0.95}Ce_{0.05}Fe_{0.97}Co_{0.03}O_3$	Synthesized in-house
5% Ce (cat X)		Synthesized in-house
5% Cr (cat BX)		Synthesized in-house
SDC 15 nano	Surface area 195 m2/g Lot # 217-76	Fuelcellmaterials.com
perovskite		Synthesized in-house
Tungsten powder		
Metallic copper powder	Electrolytic grade	Fisher scientific company (C434)
Metallic copper powder reduced	Electrolytic grade	Fisher scientific company (C434)
Commercial CuOYSZ	CuO/(8 mol %) YSZ	MicroCoating technologies
Commercial NiOYSZ	NiO/(8 mol %) YSZ	MicroCoating technologies
NiCoYSZ	4%Ni, 1% Co, 95% YSZ	
NiYSZ07	5% Ni, 95% YSZ	Synthesized in-house
NiYSZ09	5% Ni, 95% YSZ	Synthesized in-house

Table 4.3 Catalysts tested for formic acid decomposition activity as interpreted from light-off curves created using mass spectrometry. Formic acid pressures of 5 Torr and temperatures ranging from room temperature to 473K.

4.2 Experimental:

A range of catalysts were tested for their reactivity with respect to the decomposition of formic acid by using mass spectrometry derived creating light-off curves for temperatures ranging from room temperature to 473K at formic acid pressures of 5 Torr.

4.2.1 Testing catalysts for formic acid synthesis.

We used a catalysis cell (Kratos) for all reactivity experiments. The basic features of the cell are a sample cup surrounded by a mini oven which can be operated between 10^{-8} Torr and 1 atm. A manifold for gas flow and monitoring was designed to fulfill the needs of the experiment. The setup is schematically shown in Figure 4.1. The sample was held in a transparent quartz puck approximately 1cm in diameter.

Using the catalytic cell approximately 1 gram of a candidate material was placed on the sample holder and it was inserted into the cat cell. The initial gas mixture was created by evacuating a stainless steel bottle and then filled it initially with 20 PSI of CO_2 and then increasing the pressure to 40 PSI with H_2 creating a 50:50 mixture of the reactant gases. The cell was evacuated to 1 x 10^{-8} Torr and then the reactant gases were added to a pressure of 5 Torr. An attached Pfeiffer Quadrupole Mass Spectrometer (QMS) was then used to monitor the gas composition as the cell temperature was ramped from room temperature to 473K.

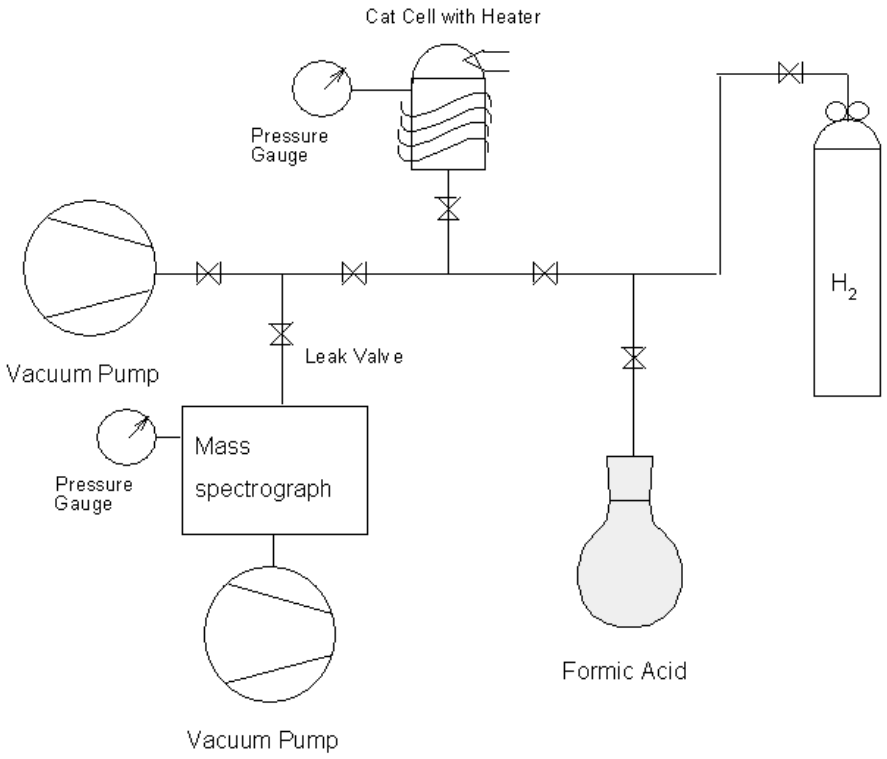

Figure 4.1 Schematic of test setup

4.2.2 Testing of catalysts with potential to decompose formic acid.

Using the same catalytic cell/mass spectrometer setup the initial gas mixture of hydrogen and carbon dioxide was replaced with formic acid under the same starting pressure of 5 Torr. The temperature of the catalytic cell was ramped from room temperature to 673K with a ramp rate of 10 K per minute. Again the cat cell gases were monitored with the attached Pfeiffer QMS and later plotted as a function of temperature.

Where available, commercially produced catalytic materials were tested alongside those synthesised in our lab. Where synthesis was necessary the procedure outlined below was used.

4.3 Synthesis of 5% Ni YSZ catalyst

Using a previously outlined synthesis method[3], approximately 2g of $NiCl_2 \cdot 6H_2O$(Strem lot# B5814020), 1.3g of Y_2O_3 (Aldrich) and 15g of $ZrCl_4$ (Strem lot# A1811077) was dissolved in 10mL of HCL mixed with 165 mL distilled water. To the resulting acidic solution, sodium hydroxide (Aldrich) was added until a pH of 13 was achieved. A milky green precipitate formed. The precipitate was filtered and washed with successive 500mL lots of distilled water until the wash tested to a pH of less than 8. The precipitate was then dried at 393 K for eighteen hours, crushed and ground to a fine powder in a mortar and pestle. The powder was then calcined at 1023 K for four hours.

4.4 Results

4.4.1 Effect on reverse reaction

All of the catalysts tested showed no effect regarding the synthesis of formic acid from the hydrogen and carbon dioxide reactants at the pressures and temperatures tested. The

initial QMS readings for hydrogen and carbon dioxide rose with temperature as would be expected with the rising pressure in the closed catalysis cell. Atomic mass readings associated with the presence of formic acid remained at background levels throughout the temperature range. These results were expected as the ΔG for the reaction at these pressures and temperatures was slightly positive however the tests were performed for completeness.

4.4.2 Formic acid decomposition activity

Various materials were tested and a plot of the atomic mass of the molecular fragments against temperature provided light off temperatures for the decomposition of formic acid on the various catalysts. As the temperature was ramped at a constant rate of 5 degrees per minute, it was possible to observe both the change in products and reactants over time and temperature.

The most obvious change was a deviation in the slope of some products indicating the onset of a reaction. Although by not following the reaction to its completion, we did not see the full S-shaped curve of a traditional light-off curve, we interpret this inflection point as the light-off temperature.

4.4.2.1 Chart interpretation.

Pressure in the reaction vessel rose during the course of the reaction, due both the temperature rise (simple gas law relationship) and reaction stoichiometry. Pressure within the QMS chamber was kept constant through adjustment of a leak valve. At temperatures greater than the light-off temperature, increases in decomposition products were often accompanied by a decline in QMS values for all other AMU. This is not

thought to be due to an actual reduction in spectator gases but simply a change in the ratio of their partial pressure to the total pressure.

If the products of dehydrogenation (H_2 & CO_2) rise in parallel and the products of dehydration and formic acid fall in parallel we deemed the reaction to be dehydrogenation.

If the products of dehydrogenation climb, formic acid falls and the products of dehydration deviate from the formic acid pattern, either falling less slowly or staying steady we interpreted this as both decomposition reaction occurring with the faster rising products dominating.

All atomic masses were recorded during the tests but for clarity I have only plotted five masses. Two masses associated with dehydrogenation (2 AMU & 44 AMU), two masses associated with dehydration (18 AMU & 28 AMU) and the mass associated with formic acid (46 AMU)

4.4.2.2 Decomposition in empty chamber (gas phase reaction)

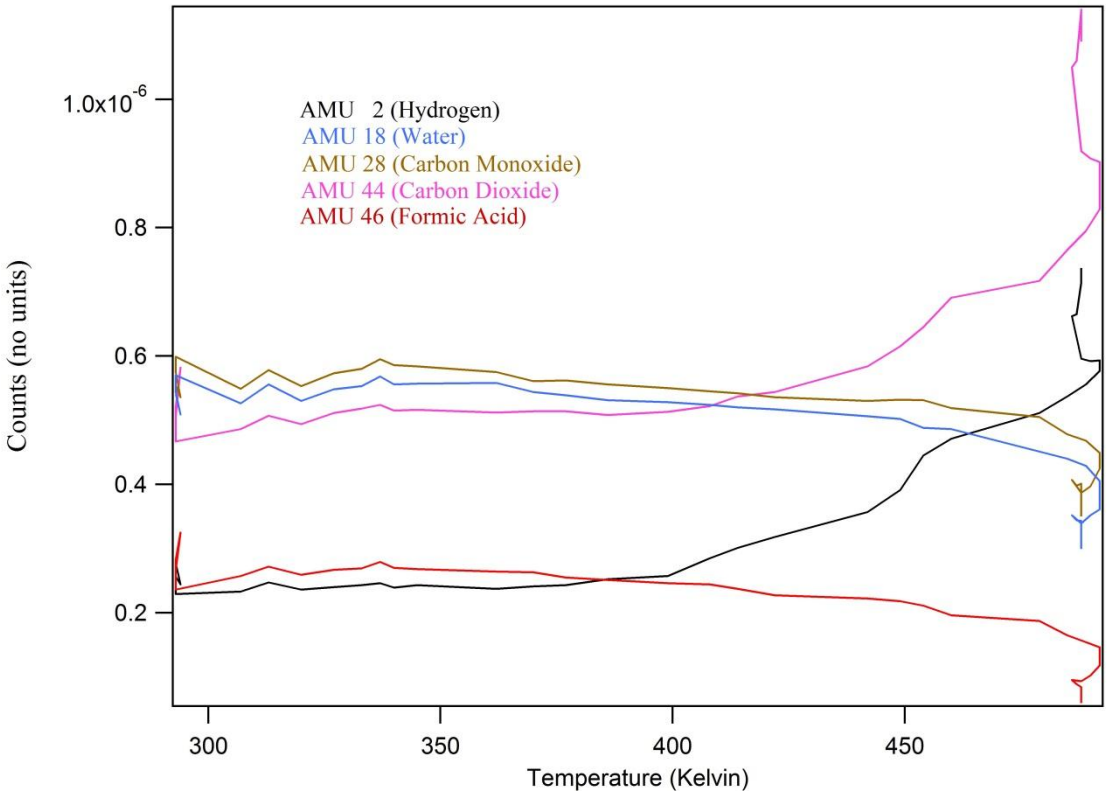

Figure 4.2 Decomposition in empty chamber. Initial chamber pressure was $1x10^{-8}$ Torr. The chamber was flooded with formic acid at between 3 and 5 Torr. Temperature ramp speed 5K per minute.

A background test was run multiple times to establish the pattern for decomposition of formic acid in an empty chamber (Figure 4.2). As the chamber and lines feeding the gases to the QMS were made of a steel alloy, it is reasonable to assume that they might play a small role in the decomposition, although the surface area is small enough to consider the background reaction as occurring in the gas phase. As can be seen from the chart below (Figure 4.3), when formic acid does decompose at temperatures in the range tested, it does so mostly via the dehydrogenation reaction. Starting at ca. 393 K, the

formic acid, water and carbon monoxide all start to decline and the hydrogen and carbon dioxide counts start to rise. That is dehydrogenation (equation 1) is favoured over dehydration (equation 2).

$$HCOOH \rightleftharpoons H_2 + CO_{2(g)}$$

Equation 15 Dehydrogenation of formic acid

$$HCOOH \rightleftharpoons CO_{(g)} + H_2O_{(v)}$$

Equation 16 Dehydration of formic acid

The resulting graph is known as a conversion temperature plot (or light-off plot) of a catalyzed reaction. I have attempted to identify the inflection point transitioning from background reactivity to rapidly increasing reaction. I will refer to this inflection point as the light off temperature.

At first thought it seemed reasonable that a decline in formic acid is observed concurrent to the rise in hydrogen and carbon dioxide however closer examination reveals a parallel decline in the carbon monoxide and water signals. An alternative and more likely reason for the decline of the three gases signals is the rise in chamber temperature resulting in a rise in background pressure. The leak valve was closed accordingly to ensure constant pressure at the QMS with the corresponding loss of signal for the water, carbon monoxide and formic acid vapour.

4.4.2.3 Copper powder and reduced copper powder

Unreduced copper powder (not shown) had little effect on the decomposition of formic acid however when the copper powder was reduced under hydrogen gas at 433 K for 16 hours it clearly had a catalytic effect (Figure 4.3). A pattern of rising hydrogen and carbon dioxide signals was paired with a matching decline in the water, carbon dioxide and formic acid.

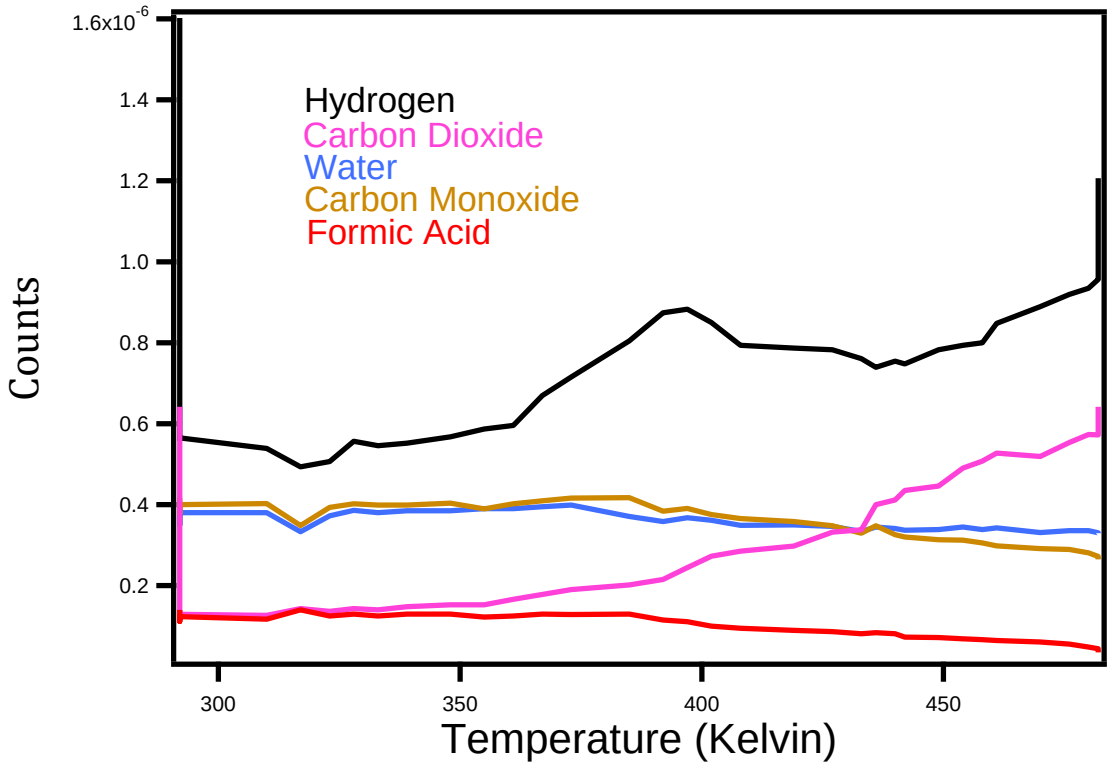

Figure 4.3 Formic acid over reduced copper powder, reduced by exposure to 10 PSI H_2 for 240 min at 673K. sample had a bright copper colour on completion of reduction. Exposed to formic acid at between 3 and 5 Torr. Temperature ramp speed 5K per minute.

We see the inflection point for the hydrogen and carbon dioxide gases occurs at ca. 363 K and the rates of both generation of hydrogen and carbon dioxide and loss of formic acid

are increased as compared to the un-catalysed reaction. This was not surprising as both Ni and Cu have been reported as being catalytically active with respect to formic acid decomposition[4][5]. The results, however did confirm the effectiveness of the test apparatus.

Bowker reported that the formate should be stable on Cu(110) up until 450 K[5] whereas these results clearly show a rise in products at a much lower temperature. Finely powdered copper would be expected to expose many crystal faces and that may account for the lower "light-off" temperature observed.

4.4.2.4 Reduced copper on YSZ support (CuYSZ08)

With catalytic reactions often supported catalysts are more effective than pure unsupported catalysts. The added activity may be due to an increase in the dispersion of catalytic material or because the pure catalyst tends to agglomerate and lose surface area over time. The support may also play an active role in the catalysis. With formic acid decomposition, we find evidence of an increased activity when using commercially provided CuYSZ08 (see Table 4.3). The temperature at the inflection in the slope for the partial pressure of carbon dioxide and hydrogen is essentially the same as for powdered copper but the rate of decomposition of formic acid seems to have increased (see Figure 4.4). As evidenced by the significantly greater degassing time, it is likely that the commercial sample has a greater surface area with a commensurate increase in active sites and that this is the drives the increased rate.

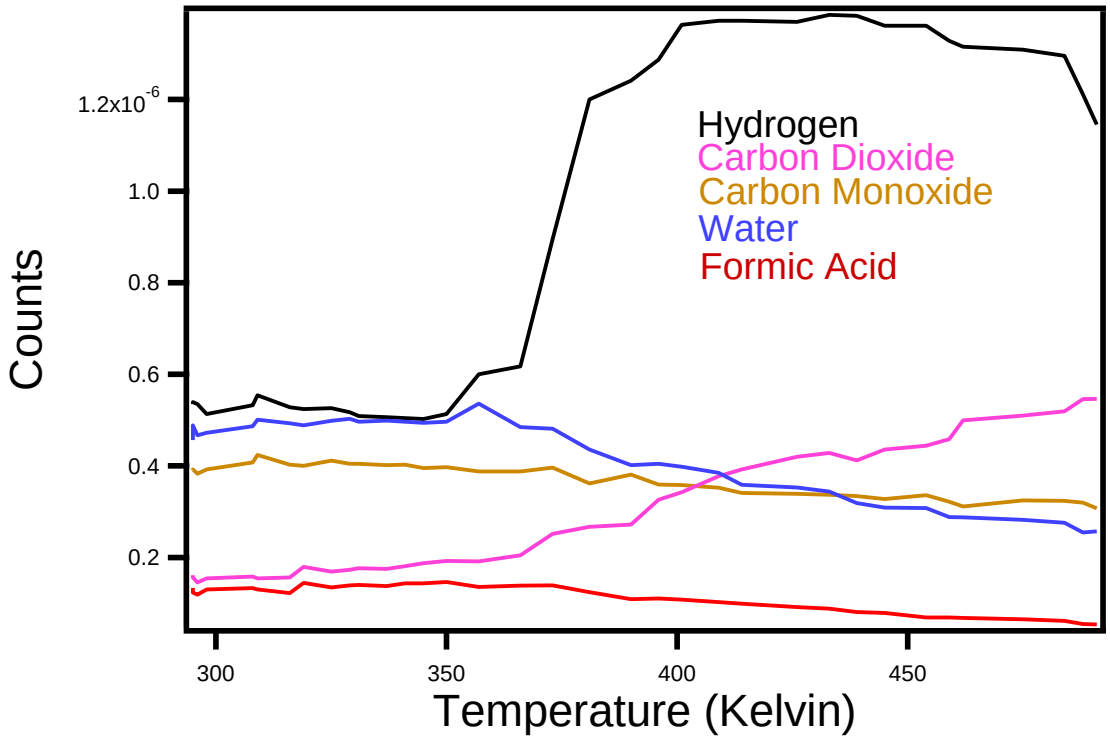

Figure 4.4 Formic acid decomposition over commercial CuYSZ (CuYSZ08), sample off gassed for 24 hr under 10^{-6} Torr followed by reduction at 10 PSI H_2 for 600 min at 673K. Exposed to formic acid at between 3 and 5 Torr. Temperature ramp speed 5K per minute.

4.4.3 Reduced Nickel on YSZ support (NiYSZ06)

Commercial metal oxide catalysts on YSZ supports were found to be very gassy requiring extended pumping periods to achieve UHV conditions. I would suggest that this is a side effect of the greater surface area of the commercial supported catalysts. In all cases the NiYSZ samples were active at catalyzing the dehydrogenation reaction starting at the lowest temperature of any material tested (see Figure 4.5).

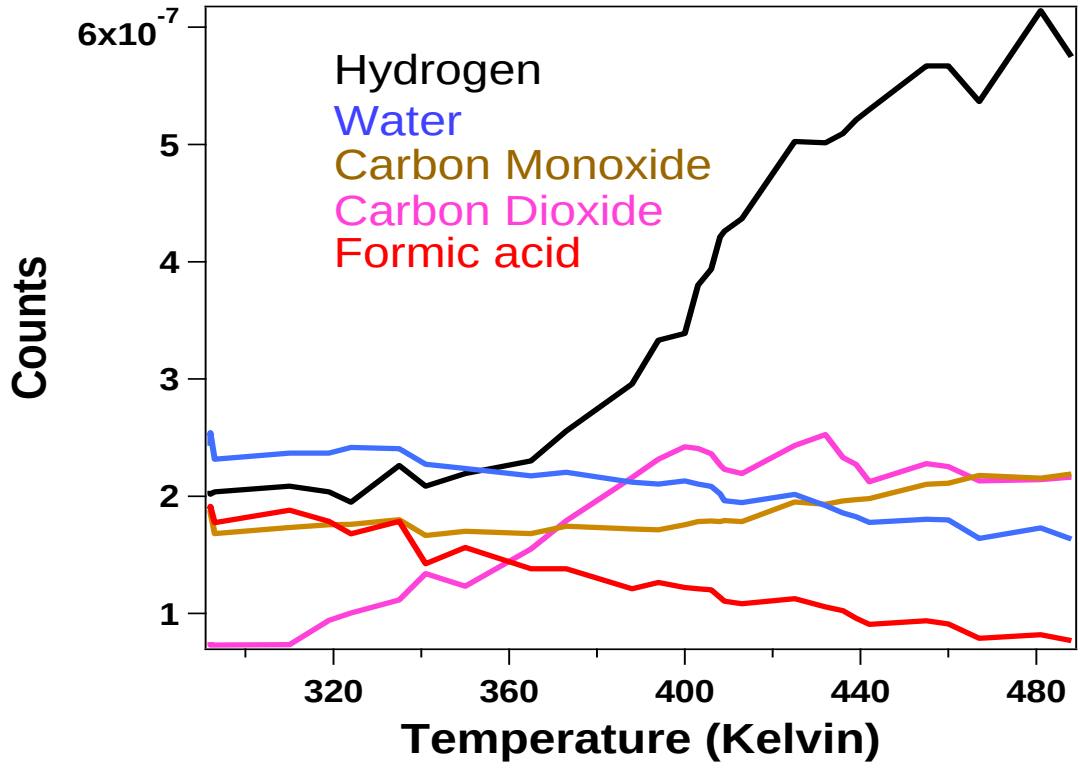

Figure 4.5 Formic acid decomposition over commercial NiYSZ (NiYSZ06), sample off gassed for 24 hr under 10-6 Torr followed by reduction at 10PSI H2 for 240 min at 673K. Exposed to formic acid at between 3 and 5 Torr. Temperature ramp speed 5K per minute.

Analysis of residual gas raises some questions about the selectivity of nickel as a catalyst. It is clear in all results that hydrogen and carbon dioxide are produced beginning at a very low temperature of ca. 323 K. Water and formic acid levels decline but with the commercial sample, carbon monoxide begins to rise at temperatures over 423 K. (see Figure 4.5). In the lab synthesised samples we also see that unlike with copper catalyst, water, carbon monoxide and formic acid do not all decline in tandem, instead in Figure 4.6 and Figure 4.7 we see the formic acid decline but the water and carbon

monoxide generally stay constant. Although not conclusive, this data may indicate that nickel also activates the dehydration reaction. If so then this would be evidence that nickel would be more effective at reducing the activation energy for the reaction but would be less selective than copper.

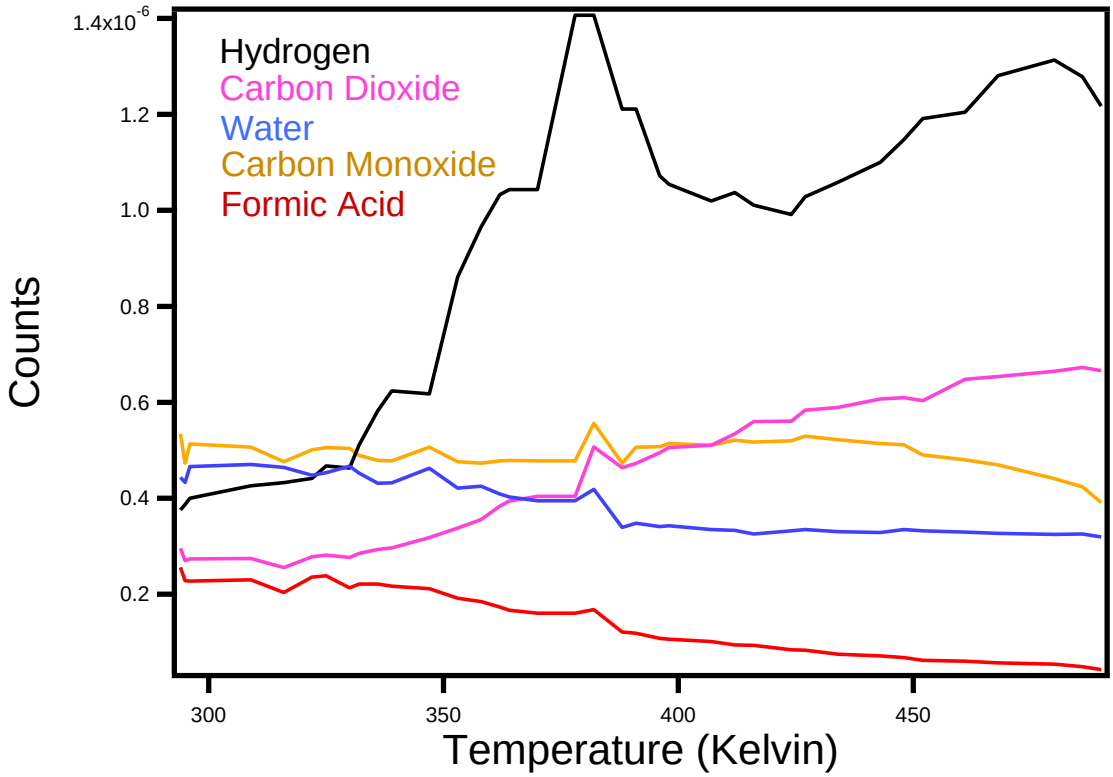

Figure 4.6 Formic acid decomposition over lab synthesised NiYSZ-07 sample off gassed for 12 hr to reach under 10^{-6} Torr followed by reduction at 10PSI H_2 for 240 min at 673K. Exposed to formic acid at between 3 and 5 Torr. Temperature ramp speed 5K per minute. the spike at just over 373 K as evidenced by the concurrent spike in all gases, was due to a rise in pressure within QMS and is not significant for the analysis.

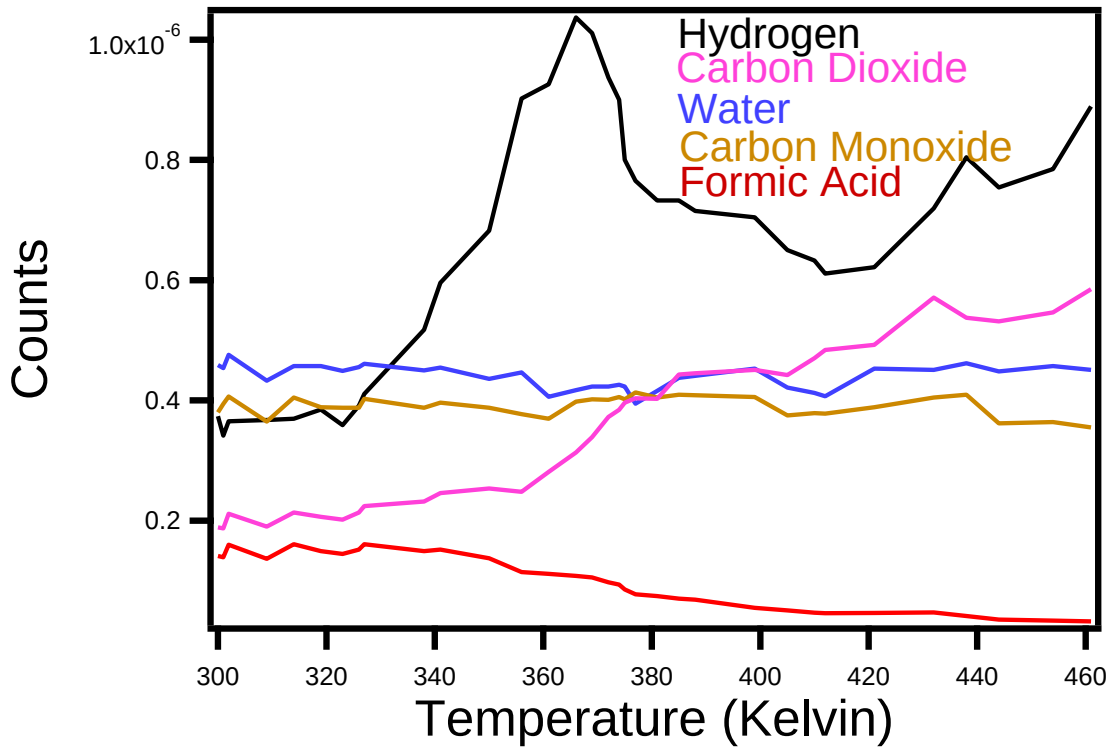

Figure 4.7 Formic acid decomposition over lab synthesised NiYSZ-09. Sample was allowed to de-gas for 12 hr reaching under 10^{-6} Torr followed by reduction at 10PSI H_2 for 240 min at 673K. Exposed to formic acid at between 3 and 5 Torr. Temperature ramp speed 5K per minute.

The results are highlighted in Table 4.4. Of course this is a far from complete survey of potential catalysts but it did highlight the interesting behaviour of some materials.

Catalyst	Light off temperature (Celsius)	AMU declining	AMU ascending
Background (empty vessel)	120	18, 28, 46	2, 44
5% Co (cat AB)	140	18,28,46	2,44
5% Ce (cat X)	150	18,28,46	2,44
5% Cr (cat BX)	> 200	constant	constant
SDC 15 nano	120	Constant	constant
perovskite	140	18,28,46	2,44
Tungsten powder	> 200	constant	constant
Metallic copper powder	130	constant	2, 44
Metallic copper powder reduced	90	18, 28, 46	2, 44
Commercial CuOYSZ	90	18, 28, 46	2, 44
Commercial NiOYSZ	65	18, 46	44,2 then 28
NiCoYSZ	100	18, 28, 46	2, 44
NiYSZ07	65	18, 46	2, 44 then 28
NiYSZ09	65	46	2, 44 then 28, 18

Table 4.4 Catalyst activity with respect to formic acid as interpreted from the mass spectrometry derived light-off curves at formic acid pressures of 5 Torr.

4.5 Conclusion

It is not surprising that heterogeneous catalysis would aid the decomposition of formic acid. Many species adsorb and dissociate on a surface thereby creating intermediate ions that lower the activation energy required to complete the reaction. A basic surface that encourages the loss of a hydrogen atom from the formic acid to form a free hydrogen ion and a formate ion which can then dissociate further to liberate CO_2 and H_2 would fulfill this role.

Most of the materials tested were found to be not or minimally catalytically active for formic acid decomposition. The light off curves for reduced copper powder and reduced commercial CuOYSZ both display a similar light-off temperature although the CuOYSZ produced a more rapid rise in dehydrogenation products. It would be expected that a supported catalyst would benefit from an enlarged surface area over pure metal powder. This finding also suggests that the YSZ does not play more than a support role in this case.

Although the experimental resolution was not sufficient to make a definitive claim, it does suggest that copper has a higher selectivity than Ni. The lower light off temperature of Ni suggests that it is the more catalytically active.

4.6 References for Chapter 4

[1] W. L. Guo, L. Li, L. L. Li, S. Tian, S. L. Liu, and Y. P. Wu, "Hydrogen production via electrolysis of aqueous formic acid solutions," *International Journal of Hydrogen Energy*, vol. 36, no. 16, pp. 9415-9419, Aug. 2011.

[2] J. Goniakowski, F. Finocchi, and C. Noguera, "Polarity of oxide surfaces and nanostructures," *Reports on Progress in Physics*, vol. 71, no. 1, p. 016501, Jan. 2008.

[3] C. M. Grgicak, M. M. Pakulska, J. S. O'Brien, and J. B. Giorgi, "Synergistic effects of Ni1−xCox-YSZ and Ni1−xCux-YSZ alloyed cermet SOFC anodes for oxidation of hydrogen and methane fuels containing H_2S," *Journal of Power Sources*, vol. 183, no. 1, pp. 26-33, Aug. 2008.

[4] R. . Bowker, I. Madix, "XPS, UPS and Thermal Desorption studies of alcohol adsorption on Cu(110) I. Methanol," *Surface Science*, vol. 95, pp. 190-206, 1980.

[5] S. Bowker, M. Rowbotham, E. Leibsle, F.M. Haq, "The adsorption and decomposition of formic acid on Cu(110)," *Surface science*, vol. 349, pp. 97-110, 1996.

Chapter Five: XPS of NiYSZ at ALS

5.1 Introduction

An opportunity became available to use beamline 9.3.2 on the Advanced Light Source (ALS) in Berkeley California for XPS studies of YSZ type materials. The extreme intensity of the X-rays and the ability to tune the wavelength of the X-ray radiation allow researchers both the sensitivity to detect very small quantities of surface species and to distinguish between very narrowly separated peaks. This is ideal for distinguishing between different carbon species and their orientation on the surface of the catalysts.

For our beam time on the ALS we chose to use a NiYSZ material synthesized in our lab. (see synthesis earlier in report).

5.2 Experimental

5.2.1 ALS Beamline 9.3.2

The XPS spectra were taken using beamline 9.3.2. at the advanced light source (ALS) in Berkeley. Beamline 9.3.2 is an ambient pressure x-ray photoelectron spectroscope that has been designed to support energy research on surfaces, interfaces, catalytic processes and fuel cells. Beamline 9.3.2 provides an energy range of 30-850 eV and a photon flux of up to 1.5 X 10^{11} photons/sec[1]. Endstation 2 is setup with a Scienta 4000R-Hipp electron analyser using a spot sample size of ~1mm x 1mm. The sample environment allows for pressures from UHV up to 1 Torr and heating to 1100K.

5.2.2 Sample preparation

Following insertion of the sample into the chamber, the NiYSZ was reduced at $6X10^{-5}$ Torr H_2 at 1123K for 260 minutes. This procedure was also very effective at removing all signs of adventitious carbon (Figure 5.1).

Following the reduction procedure the sample was allowed to return to room temperature (300K). Initial surveys showed significant shift of photo emission electron peaks indicating charging.

5.2.3 Charge dissipation

To reduce the charging, 200 mTorr of argon was added to the chamber and the sample was heated to 423K using a button heater. Adding argon also had the advantage of allowing all peaks to be calibrated against the distinctive and sharply defined AES peaks associated with argon(Figure 5.1)[2]. Unless otherwise stated all spectra for the NiYSZ were referenced to the argon Auger peak $L_2M_{23}M_{23}(S_0)$ at kinetic energy of 201.09 eV.

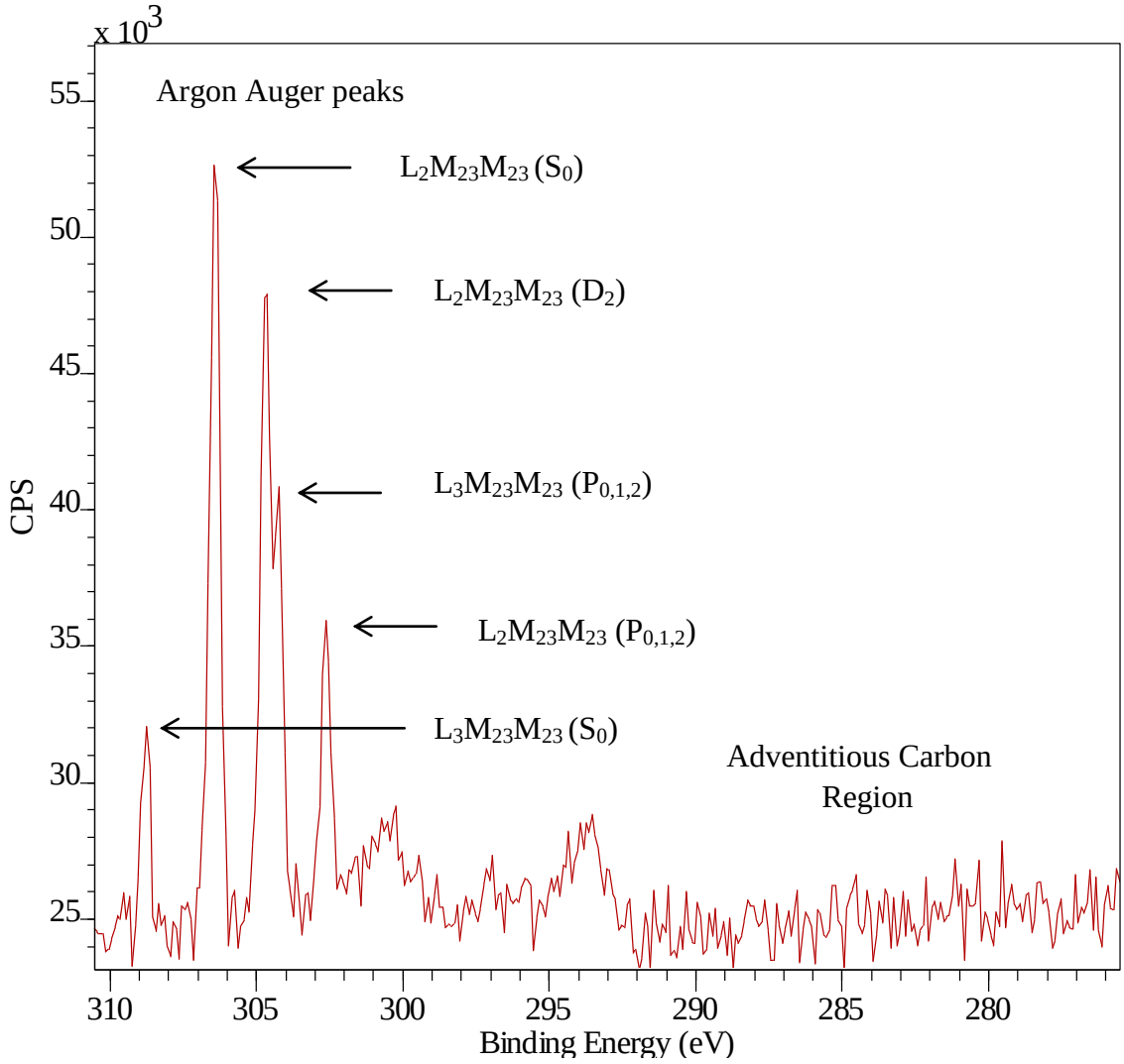

Figure 5.1 C 1s XPS spectra of NiYSZ following anneal under H_2, (#167, C1s region, λ 510 eV, pass 20 eV, step 0.1 eV, dwell 200 ms, 197 mTorr Ar, 150°C)

5.2.4 Formic acid exposure

200 mTorr of formic acid vapour was introduced to the chamber and the attached RGA was used to monitor for formic acid and its decomposition products. (CO_2, CO, H_2, H_2O, HCOOH, HCOO, H_2CO). XPS surveys and high resolution spectra were obtained for each spectrum area of interest – that is Ni 3p, Y 3d, Zr 3d, C 1s, O 1s, O KLL, Ar AES

and the valence band. Once complete, the dose of the formic acid was increased to 463 mTorr and then 582 mTorr, each time completing the same range of XPS spectra.

5.3 Results

5.3.1 Ni 3p XPS Spectra

The Ni 3p peak is found in reference tables at 66.0 eV for metallic nickel and 66.1 eV for nickel oxide[3]. Figure 5.2 is an overlay of the NiO 3p region for NiOx/YSZ samples as recorded at varying concentrations of formic acid. The peak centre was found consistently at 66.1 eV for all exposures. Nominally a value of 66.1 eV would suggest only oxidized nickel being present however because of the peak breadth (FWHM of 3.9) and the close binding energies, suggest that the metal exists in multiple oxidation states and is partially reduced.

The successively lower photo emission electron counts with increasing doses of formic acid are due to the shielding of the emitted electrons by an increasingly thick layer of formic acid and attenuation from gas phase molecules. This identical shape and positioning of the reduced Ni peak and that with an initial dose of formic acid would suggest that while the nickel may be playing a role in the decomposition, it is not playing that role through a change in oxidation state.

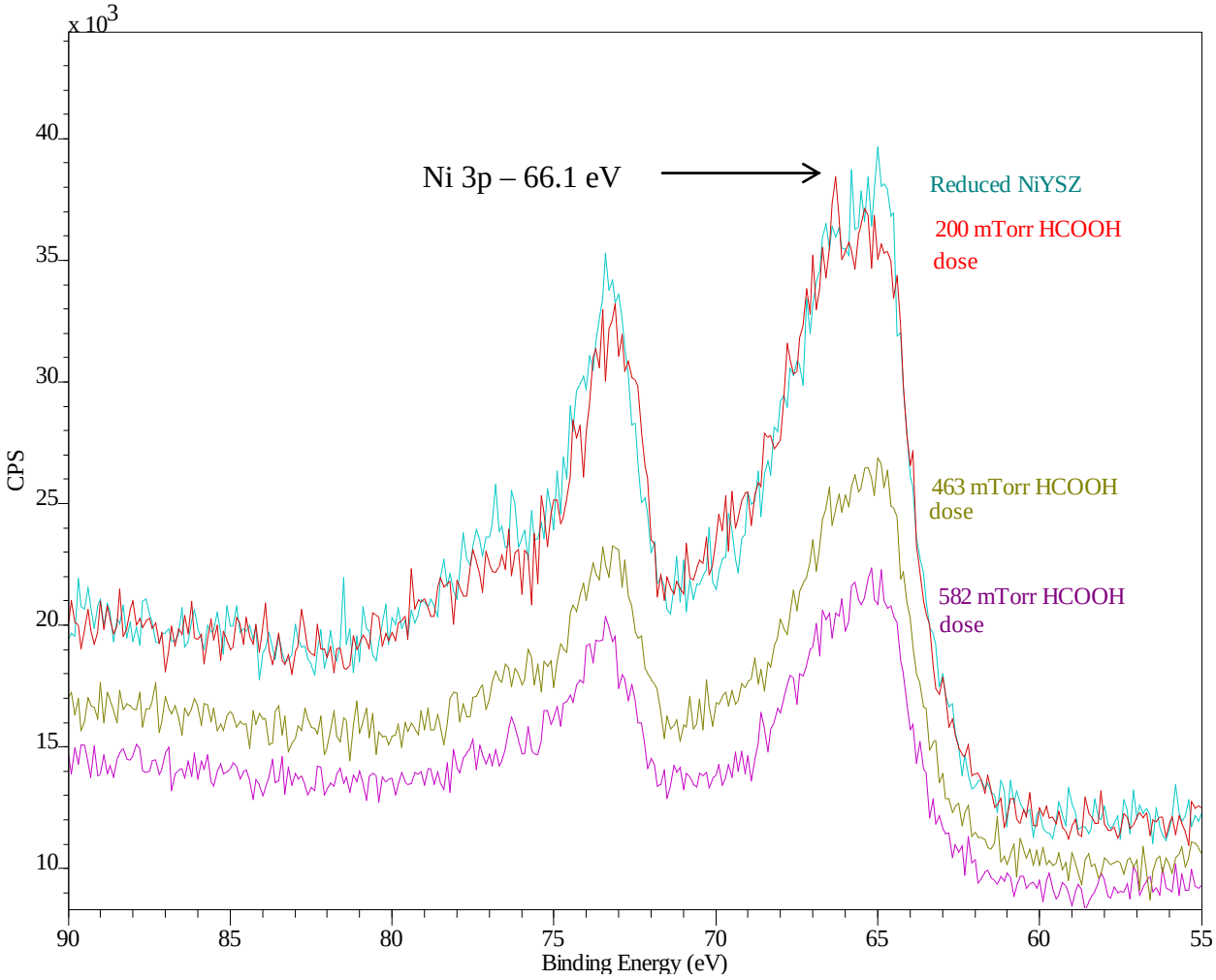

Figure 5.2 Ni 3p XPS spectra at various doses of formic acid (#174,189,215,230, Ni 3p region, λ 490 eV, pass 20 eV, step 0.1 eV, dwell 200 ms, 197 mTorr Ar, 150°C)

5.4 Zr 3d & Y 3d XPS Spectra

Metallic yttrium is expected to display a 3d peak at 155.7 eV, metallic zirconium at 178.7 eV[3]. Analysis of the peaks in Figure 5.3 reveal a yttrium 3d peak at 158.4 eV along with a zirconium 3d peak at 182.4 eV. This is in agreement with the published values for YO and ZrO of 158.4 eV and 182,4 eV respectively[3]. No change of binding energy was observed between the reduced sample and the sample dosed with various concentrations of formic acid although, as expected, the photoelectron counts were

reduced as greater concentrations of formic acid were added to the environment. The narrow aspect of the peaks (FWHM of 1.2 and 1.9 for Zr and Y respectively) suggests that only one oxidation state is present, therefore one can conclude that the yttrium and zirconium are not being oxidized or reduced during the creation of surface layers of formate and other intermediates.

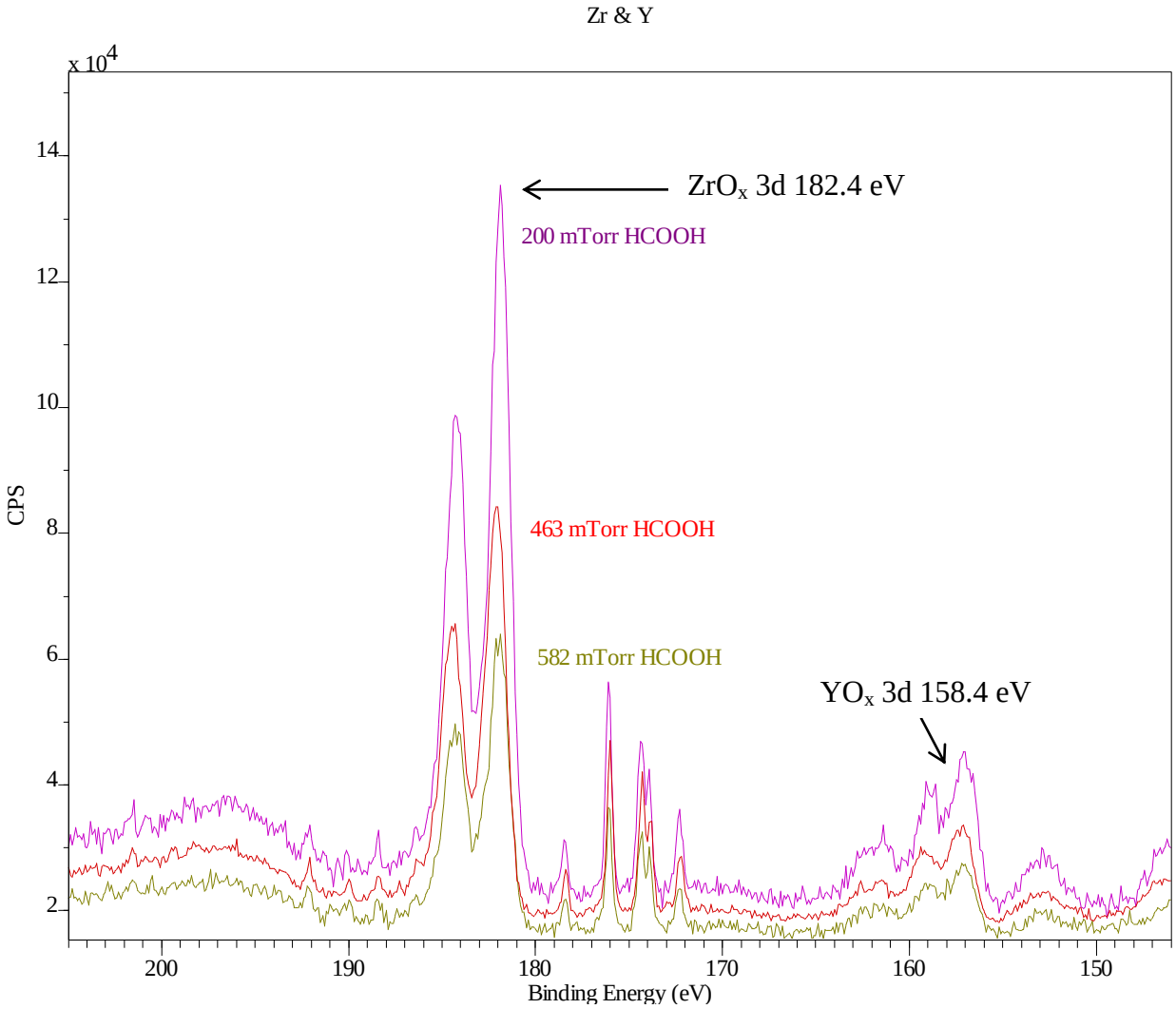

Figure 5.3 Zr 3d and Y 3d XPS spectra (#169,205,224,234, Zr 3p and Y 3p regions, λ 380 eV, pass 20 eV, step 0.1 eV, dwell 200 ms, 197 mTorr Ar, 150°C)

5.5 C 1s XPS Spectra

Following dosing with 200 mTorr HCOOH four peaks appear in the C 1s region, two sharp peaks at, 292.2 eV, 290.3 eV and one broad peak which has been identified as containing two contributions at 288.5 and 289.2 eV(see Figure 5.4). Assignment of four peaks to our experimental data is based on the full width half maxima of the peaks and can be readily compared to previous work. We assign the four peaks based on their binding energy to the following species:

292.2 eV: CO_2 on Ni [4]

290.3 eV, carbonate [5]

289.2 eV Formate mono-dentate [5]

288.5 eV, Formate bi-dentate [5]

Previous work concerning XPS of the carbon species produced by adsorption/reaction of formic acid on nickel was at a much lower resolution. For example Barteau's published spectra for formic acid on MgO were at a lower resolution and displayed a significantly broader peak centred at 290.3eV although covering binding energies from 289 eV to 292eV. Therefore it is quite possible that the four peaks that we now report were all buried within Barteau's spectra[6]. It is interesting to note that regarding formic acid to date Barteau's work is considered the state of the art and reference sources like NIST reports HCOOH peaks all based on Barteau's work.

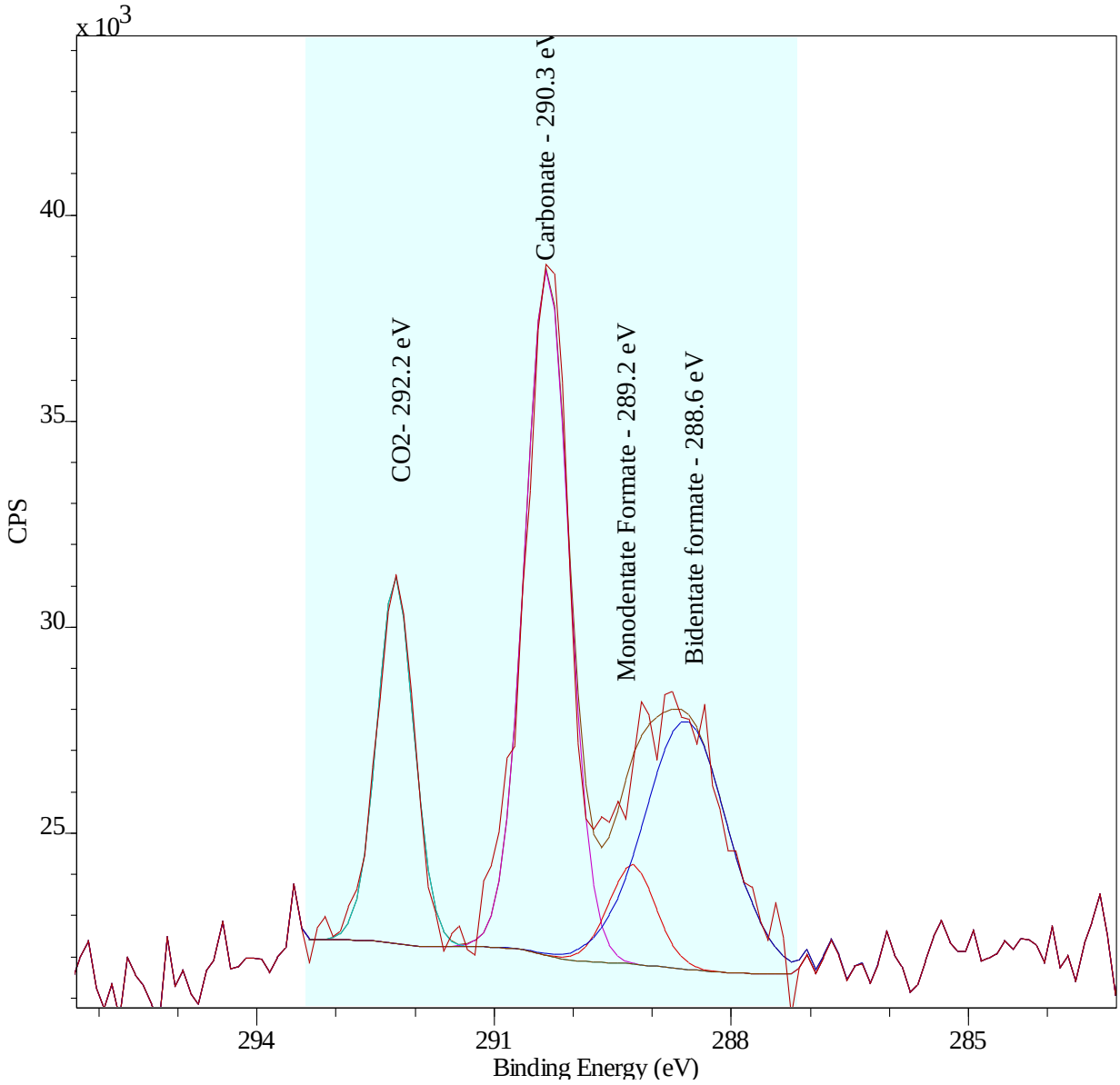

Figure 5.4 NiYSZ C1s dosed with 200 mTorr HCOOH (#184, C 1s region , λ 510 eV, pass 20 eV, step 0.1 eV, dwell 200 ms, 197 mTorr Ar, 150°C)

5.5.1 Formate peaks

Senanayake reported results associated with formate formation on Au with a peak centred at 288.8 eV[5] and attributed to a C-O species, likely either carbonate or formate. A second paper by Senanayake documents peaks for carbonates (CO_3^{2-}), carbonyl(CO) and formate at 290.5, 287.9 and 288.7 eV respectively[7]. The density functional theory (DFT) calculations predict that the bidentate configuration is more stable than the monodentate by a Δ0.65 eV[7].

Our results with two peaks at 288.5 and 289.2 eV are in agreement with Senanayake attribution of formate peaks centred at 288.7 eV. Analysis of our results shows a smaller peak at 289.2 eV separated by 0.68 eV from a larger peak and we attribute these to mono & bidentate formate respectively. Of the two peaks we calculate that the ratio of monodentate to bidentate is approximately 1:4 under these pressure conditions.

5.5.2 Carbonate Peak

Senanayake attributed a peak at 290.3 eV to adsorbed formic acid however it was only visible at temperatures below 200K[5]. Although carbonate has been found to decompose at temperatures over 320K, complete decomposition occurs at 560K. Our experiments were performed at 423K and therefore a peak associated with carbonate is not unexpected. The C1s XPS peak for carbonate has been reported at 290 ± 0.1 eV for $MgCO_3$[8]. No carbonate peak was seen in the reduced sample although following dosing with HCOOH a very strong peak does appear at 290.3 eV.

The observation of a carbonate species may be used as an indicator for temperature dependent reaction mechanism [9][5].

5.5.3 CO_2 on Ni

This leaves the last peak at 292.2 eV unaccounted for. Possible species include either gaseous CO_2 (291.9 eV) or CO_2/Ni (291.2 eV). Although initially considered unlikely, no other species seem to account for such high binding energies. It is therefore likely that the signal is caused by CO_2.

High binding energy electrons for C 1s have been previously observed for CO_2 on Ni at 150K[4]. A TPD study by Illing under UHV conditions reveals that CO_2 on Ni peak desorbs or decomposes by 300K leaving only peaks associated with CO[4]. However, the breadth of the peak suggests a surface not gaseous species and at the higher pressures associated with our experimental conditions (2×10^{-6} mbar) it seems reasonable that attributing the peak to adsorbed CO_2 is valid.

5.5.4 Other species

To help piece together the reaction pathways it is also instructive to highlight the potential intermediate peaks that are not observed. Carbonyl (CO) and formyl species (HCO), if present were expected to present peaks at 287.9 eV and 287.7 eV respectively. In both cases no signal could be distinguished above the background. Any peak associated with carbide on Ni (282 eV) was also not detectable above the background signal.

5.6 O1s XPS spectra

Following the reduction process, one would expect the O1s spectra to be comprised of contributions from the lattice oxygen associated principally with zirconium along with smaller peaks associated with yttrium and possibly nickel oxide (Figure 5.5).

Lattice oxygen associated with the YSZ should appear at 530.2 eV[10] and 531.3 eV-529.9 eV[11][12] for yttrium oxide and zirconium oxide respectively. The nickel oxide (NiO) and nickel trioxide (Ni_2O_3) also has been reported with a peaks at 529.9 eV and 531.7 eV[13].

Typical laboratory spectra cannot distinguish between these contributions, but with the high resolution of the synchrotron source we had hoped to be able to distinguish between the peaks.

Our analysis however shows only one broad (FWHM of 3) and symmetrical peak at 531.6 eV in which we were unable to differentiate individual components with confidence.

The similar binding energies for O 1s on all three metal oxides, nickel, yttrium or zirconium and the fact that when synthesised it is likely that oxygen coordination among the three metals would result in a smearing of pure oxide peaks into one broad metallic oxide peak.

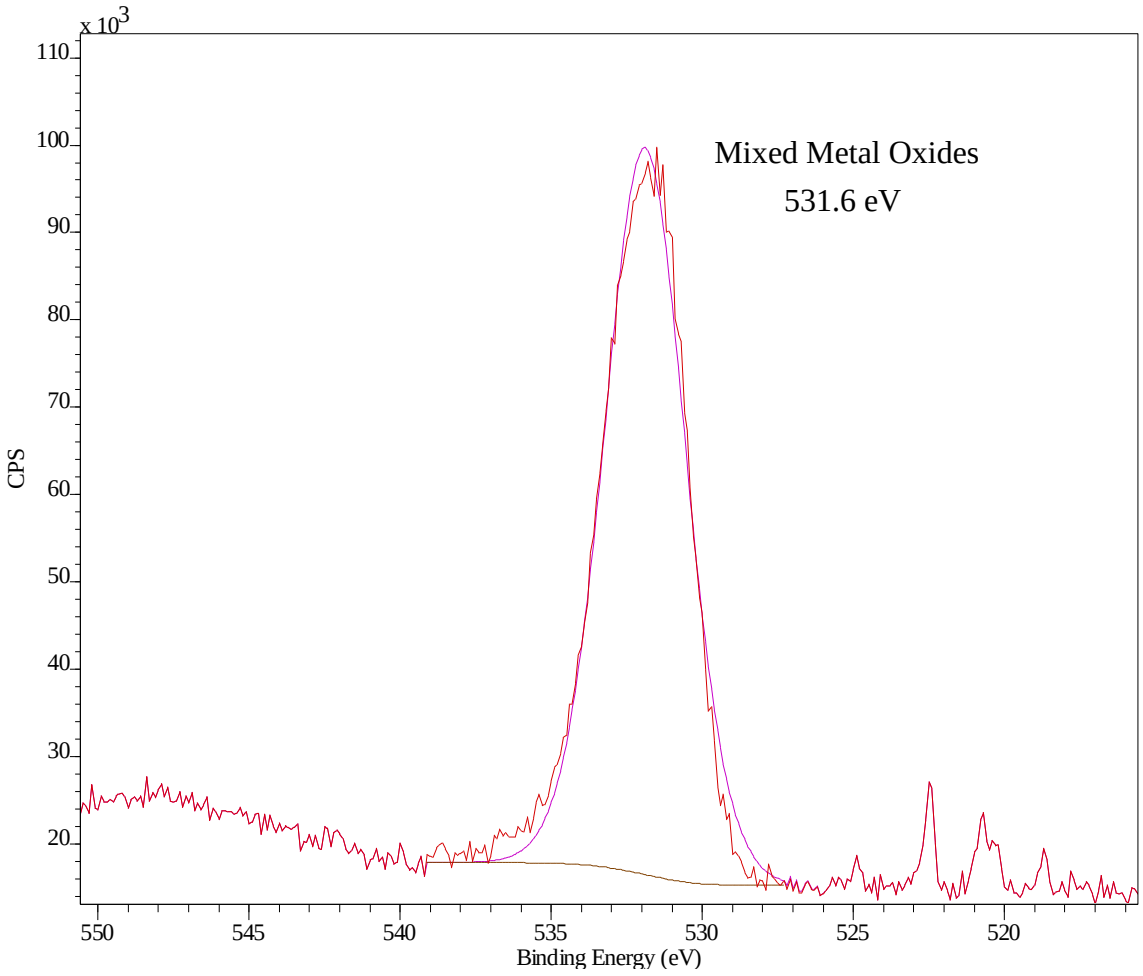

Figure 5.5 Oxygen 1s NiYSZ reduced under H_2 (#170, O 1s region associated with Ni, Y, Zr ,λ 726 eV, pass 20 eV, step 0.1 eV, dwell 200 ms, 197 mTorr Ar, 150°C)

When formic acid is added to the system we can see the suppression of the surface peaks associated with the metals and the immediate growth of two peaks with higher binding energy and one at a lower binding energy see Figure 5.6. An enlargement of the area of the new peaks allows us to see more clearly the new peaks (Figure 5.7). As these species are at the surface they are not suppressed and show more strongly in the spectra. We have identified the 530.0 eV peak as an hydroxyl group.

When formic acid is added to the system, the O1s peak centred at 531.6 eV is joined by growing shoulders at 532.5 eV and 534.5 eV. The previously identified metal oxide peak found at 531.6 eV is still visible although it has been attenuated by the over-layer of formic acid.

A broad peak at 534.5 eV is generally associated with formate [14] species in laboratory experiments.

The fitting procedure used here shows two contributions at 532.5 eV and 534.5 eV are attributed to carbonate and formate bound to the surface. A third contribution at 530.0eV is attributed to a hydroxyl group bonded to the Ni[15]. The reaction of H_2O with Ni surface should form OH groups which in turn could react with carbon monoxide to form the previously documented intermediate groups (HCOO, HOCO and CO_3).

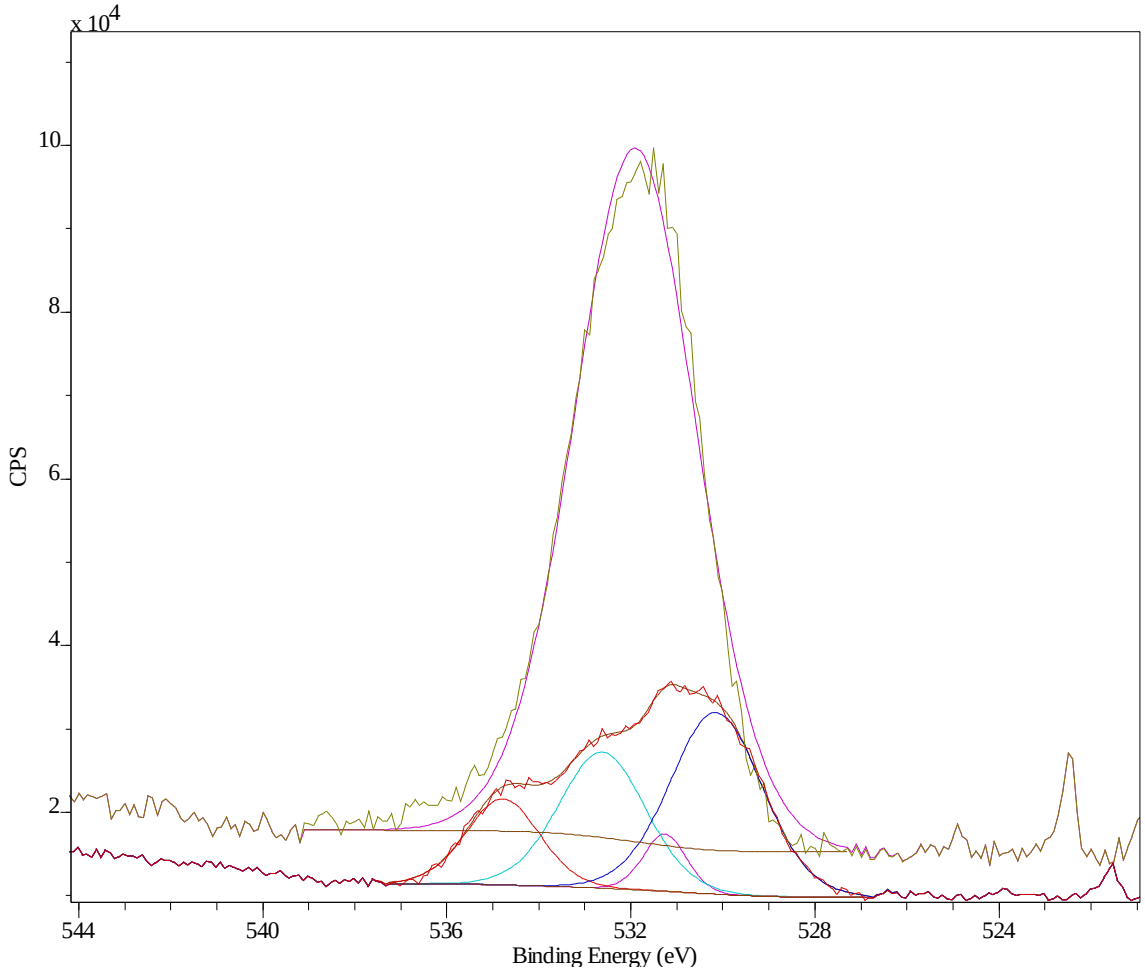

Figure 5.6 Oxygen 1s NiYSZ O1s pre & post formic acid (#170 & #227, O 1s region associated with Ni, Y, Zr ,λ 726 eV, pass 20 eV, step 0.1 eV, dwell 200 ms, 197 mTorr Ar, 150°C)

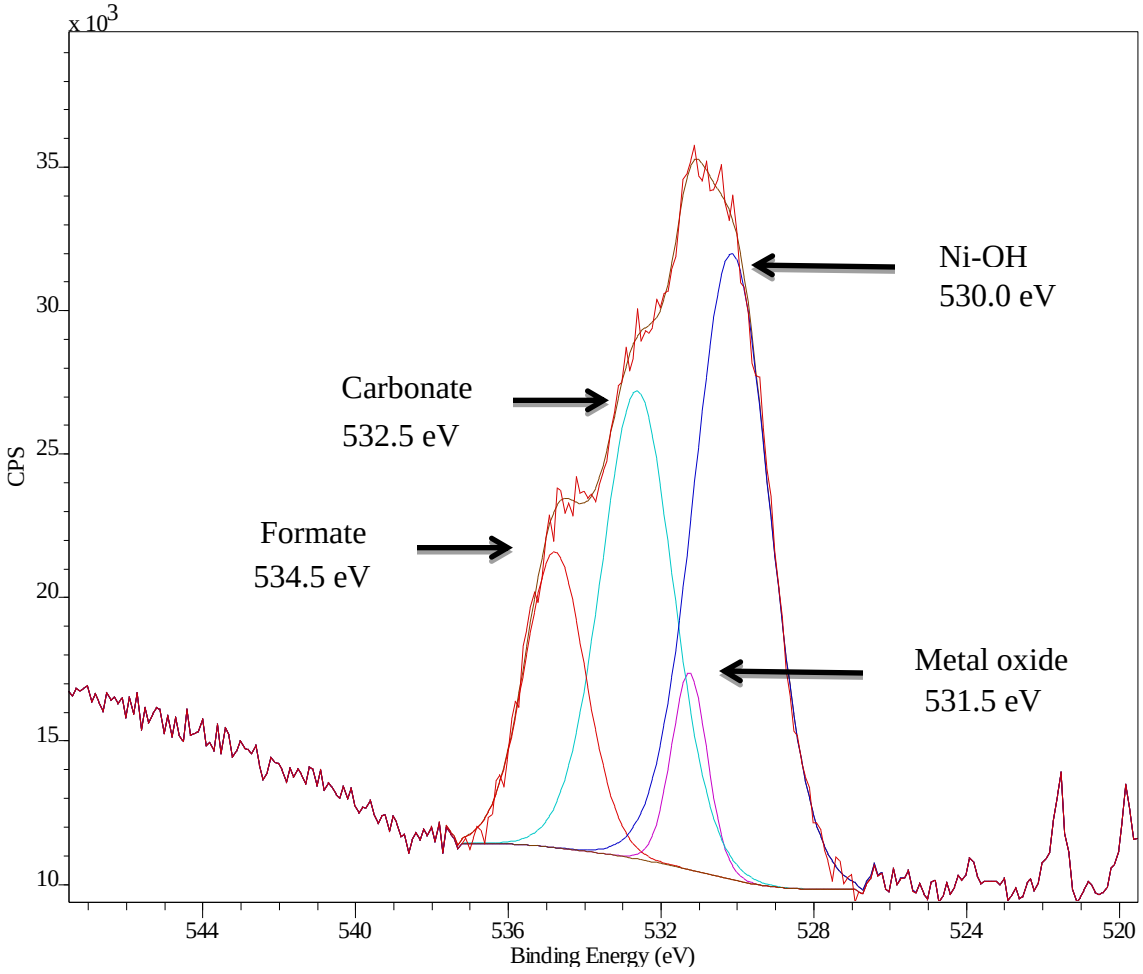

Figure 5.7 Oxygen 1s NiYSZ following exposure to formic acid (#227, O 1s region associated with Ni, Y, Zr ,λ 726 eV, pass 20 eV, step 0.1 eV, dwell 200 ms, 197 mTorr Ar, 150°C)

5.7 Results

5.7.1 Reaction mechanisms

In previous chapters we have discussed the decomposition of formic acid via either de-hydration or de-hydrogenation. The rising levels of both reaction products in our mass spec study (Chapter 4) of NiYSZ is indicative that both reactions are present. Due to the experiment's design, it is difficult to determine an accurate ratio of the two reactions

however it is clear that NiYSZ favours the de-hydrogenation reaction. A simple analysis based on the rate of increase of the product gases would suggest that the de-hydrogenation reaction is favoured over the de-hydration reaction by a ratio of between 10:1 and 5:1. This value generally agrees with Mars reported a ratio of CO : CO_2 for the decomposition of formic acid over nickel to be 0.138 at 431K for passive atmosphere and 0.228 at 419K for a rapidly flowing formic acid gas [16]. Walton and Verhoek also published CO2 : CO ratio of between 2.5 and 4 for formic acid decomposition over nickel at a temperature of 461K [17]

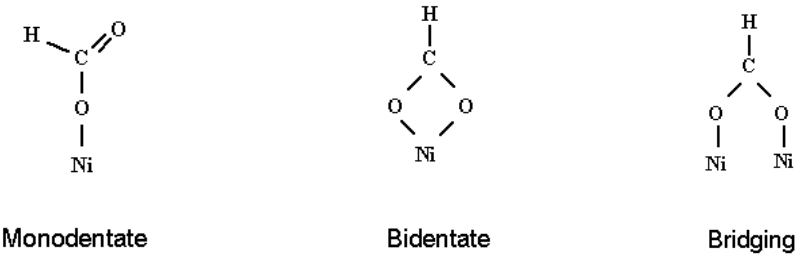

Figure 5.8 Orientation of formate anion on surface

The deprotonation of the formic acid to create a free proton and a formate ion is also well documented. The formate can coordinate with the surface in as either monodentate, bidentate or bridging configurations (Figure 5.8) [4]

The XPS study of the NiYSZ identified a peak at 289.2 eV associated with mono-dentate formate and a second at 288.6 eV associated with bidentate formate. Of the formate peaks, 19% is associated with mono-dentate and 81% is bidentate. Although no references could be found for the binding energy of bridged formate it is expected that it would be similar in binding energy to bidentate [5].

Carbonate and CO_2 on Ni peaks were also identified leading to the conjecture that the surface coordination site is on Ni. Confidence in this would be improved if a reference for CO_2 on Zr and Y could be found.

5.7.2 Dehydration reaction

It is proposed that the dehydration reaction proceeds through the monodentate coordinated formate ion (Figure 5.8). Hydroxyls groups are expected to be present terminating the dangling bonds on the surface of the oxides. In the dehydration reaction it is expected that hydrogen on the formate ion will coordinate with a hydroxyl group to create a water molecule.

The formate molecule is firmly attached to the surface through the Ni-O bond, the proton on the hydroxyl group is thought to be mobile across the oxide surface, in effect proton hopping [18] is the equivalent of a mobile hydroxyl group. When the hydroxyl group approaches the hydrogen on the formate molecule it forms a coordination complex allowing for the decomposition of the formate into water and carbon monoxide. This action restores the surface to its original oxide configuration allowing for the deprotonation of another formic acid molecule (Figure 5.9).

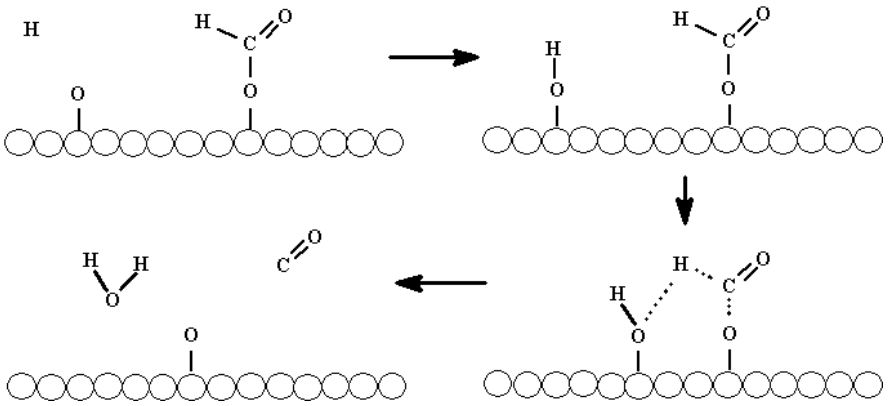

Figure 5.9 Proposed dehydration pathway, balls represent the catalyst surface, Ni or YSZ

The monodentate coordination allows the lone formate proton to dip close enough to the surface to coordinate with the oxygen associated with a hydroxyl, whereas the bidentate and bridged configurations hold the proton further from the surface allowing only highly mobile protons to get close enough to form dihydrogen. Based on the expected bond lengths, the bidentate or bridge configuration would hold the proton in the order of 5 angstroms from surface(Ni), with monodentate coordination the proton is in the order of 3-4 angstroms from surface(Ni), and perhaps less due to inherent bending of the monodentate structure. For the hydroxyl complex, the proton is held close to 2.5 angstroms from surface (Ni). Therefore in monodentate coordinated formate the proton is approximately the right distance from the oxygen in hydroxyl to allow water to form. A hydroxyl approaching the monodentate formate would weakly bond to the lone proton in a favourable orientation. Next the formate would decompose to create a water molecule and a monodentate carbon dioxide molecule. Finally the monodentate carbon dioxide may desorb or cleave leaving an oxygen attached to the surface and a molecule of carbon monoxide (Figure 5.9).

5.7.3 Dehydrogenation reaction

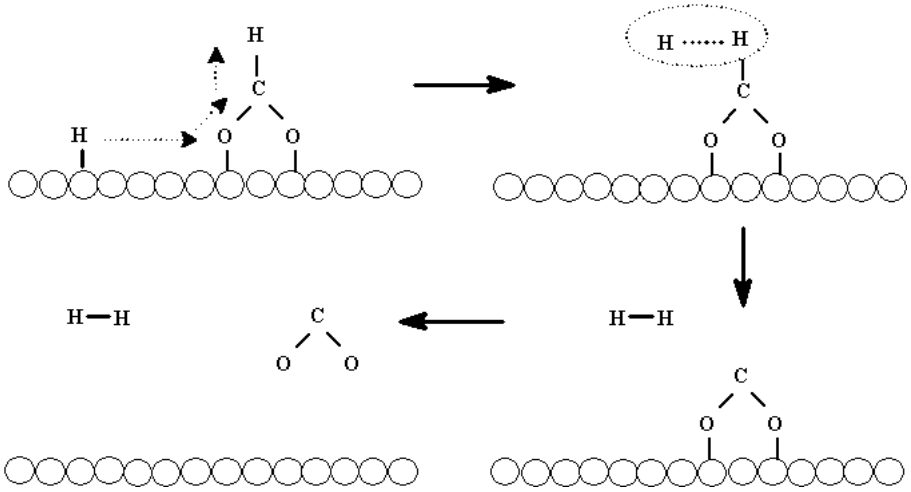

Figure 5.10 Proposed dehydrogenation pathway (Bridging), balls represent the catalyst surface, Ni or YSZ

For dehydrogenation, formate coordinated to the surface by two oxygen atoms forms either a bidentate or bridged configuration. In either of these configurations the lone hydrogen is left dangling above the surface. In the dehydrogenation reaction (Figure 5.10 and Figure 5.11) it is a proton that will coordinate with the formate's hydrogen to create a dihydrogen molecule. Unlike in the dehydration reaction where the proton on the hydroxyl group is maintained at a fixed distance from the surface, in dehydrogenation, the proton is more mobile.

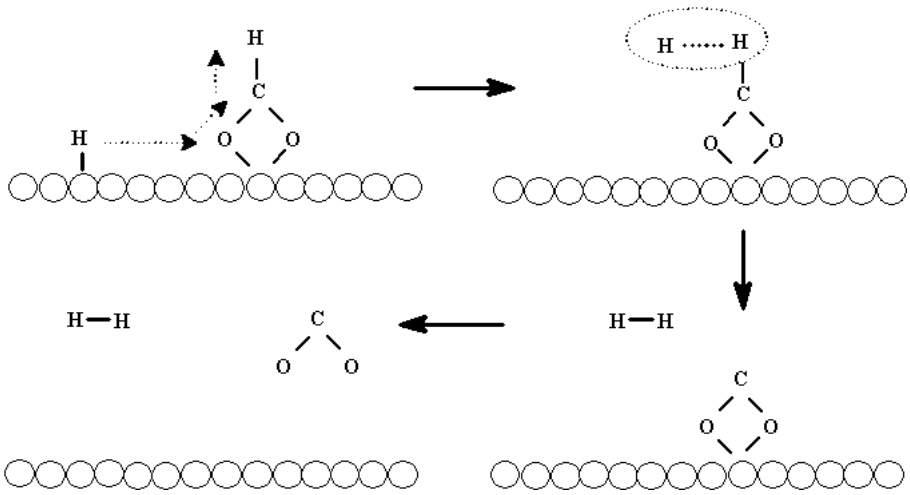

Figure 5.11 Proposed dehydrogenation pathway (Bidentate), balls represent the catalyst surface, Ni or YSZ

5.7.4 CO_2 XPS peak

In both of the reaction pathways, it is possible to explain the appearance of the CO_2 peak. In the dehydration reaction, mondentate CO_2 on the surface could be observed either as a long lived transient between the H_2O release and the CO generation or due to a substantial steady state concentration.

In dehydrogenation one would expect to find either bridged or bidentate CO_2 on the surface. This agrees with the XPS specta of the NiYSZ although it does not distinguish between mono, bridged and bidentate bonding. In the case of the dehydration it is expected that the monodentate carbon dioxide will lose an oxygen atom to the surface releasing carbon monoxide.

5.7.5 Light off temperature

At the reaction temperatures, the bidentate and bridged carbon dioxide associated with the dehydrogenation will most likely simply leave the surface due to thermal agitation. This may help to explain the light off temperature required for the catalyst to become active. If sufficient thermal agitation is not present, the surface would quickly become

fully populated with CO_2 and block any further reactivity. Published temperature programmed desorption studies document CO_2 desorption from $Ni/CeZrO_2$ at 423K [19]. This would agree with our later results involving MgO (Chapter 6) where at 300K the formate peak initially grows on exposure to formic acid only to reach a static level that is interpreted as full coverage.

5.8 Conclusion

Cleaning the sample by annealing under 6 x 10^{-5} Torr H_2 at 1123K for 270 minutes was successful in removing all carbon species and OH groups from the catalyst surface.

After the surface was exposed to formic acid at a pressure of 200 mTorr we observed peaks associated with hydroxyl, carbon dioxide, carbonate and formate. The formate was further resolved into both monodentate and bidentate coordinations at a ratio of 1:4. It was observed that both dehydration and dehydrogenation were occurring at a similar ratio. This may indicate that monodentate formate is an intermediate for dehydration and bidentate formate is an intermediate for dehydrogenation. In keeping with the observed CO_2 peak assignment, reaction mechanisms were proposed that have CO_2 as an intermediate for both reactions. It was further proposed that the surface adsorbed CO_2 limits the reaction until a sufficient temperature is reached to free the surface from CO_2[19].

Senanayake reports that the peak associate with HCOOH shifts to higher BE with temperature and this is attributed to a shift in populations from bi-dentate at low temperatures (<150K) to predominately monodentate at higher temperatures (>500K) As we changed HCOOH coverage but not temperature we did not observe this shift in BE

for the C1s spectra. Given the hypothesis that the monodentate formate is associated with dehydration, changing the surface temperature would change the selectivity of the catalyst.

5.9 References for Chapter 5

[1] "Advanced light sourse Beamline 9.3.2." [Online]. Available: http://www-als.lbl.gov/index.php/news-and-publications/alsnews/123-932.html.

[2] D. Zehner, "Gas Phase Argon AES.pdf," *Journal of vacuum technologies*, vol. 16, no. 2, pp. 562-565, 1979.

[3] V. Crist, *Handboook of Monochromatic XPS spectra, the elements and Native Oxides*. John Wiley & sons, 2000.

[4] H. J. Illing, G. Heskett, D. Plummer, E. W. Freund, "adsorption and reaction of CO_2 on Ni: XPS, Near-edge x-ray absorption fine structure and diffuse leed studies," *Surface Science*, vol. 206, pp. 1-19, 1988.

[5] S. D. Senanayake, D. Stacchiola, P. Liu, C. B. Mullins, J. Hrbek, and J. a. Rodriguez, "Interaction of CO with OH on Au(111): HCOO, CO_3 , and HOCO as Key Intermediates in the Water-Gas Shift Reaction," *The Journal of Physical Chemistry C*, vol. 113, no. 45, pp. 19536-19544, Nov. 2009.

[6] M. A. Peng, X. D. BARTEAU, "Dehydration of carboxylic acids on the MgO(100) surface," *Catalysis Letters*, vol. 7, pp. 395-402, 1990.

[7] S. D. Senanayake and D. R. Mullins, "Redox Pathways for HCOOH Decomposition over CeO 2 Surfaces," pp. 9744-9752, 2008.

[8] L. Wang, T. Shinohara, and B.-P. Zhang, "XPS study of the surface chemistry on AZ31 and AZ91 magnesium alloys in dilute NaCl solution," *Applied Surface Science*, vol. 256, no. 20, pp. 5807-5812, Aug. 2010.

[9] G. Jacobs, P. Patterson, U. Graham, a Crawford, and B. Davis, "Low temperature water gas shift: the link between the catalysis of WGS and formic acid decomposition over Pt/ceria," *International Journal of Hydrogen Energy*, vol. 30, no. 11, pp. 1265-1276, Sep. 2005.

[10] R. Phenomena, E. S. P. B. V, Y. Uwamino, T. Ishizuka, and H. Yamatera, "X-ray photoelectron compounds spectroscopy of rare-earth," *Journal of electron spectroscopy and related phenomena*, vol. 34, pp. 67-78, 1984.

[11] C. D. Wagner, D. a. Zatko, and R. H. Raymond, "Use of the oxygen KLL Auger lines in identification of surface chemical states by electron spectroscopy for chemical analysis," *Analytical Chemistry*, vol. 52, no. 9, pp. 1445-1451, Aug. 1980.

[12] C. N. R. Sarma, D. Rao, "Xpes studies of oxides of second- and third-row transition metals including rare earths*," *Journal of electron spectroscopy and related phenomena*, vol. 20, no. 1, p. 25, 1980.

[13] K. S. Kim, “x-ray photoelectron spectroscopic studies of nickel-oxygen surfaces using oxygen and argon ion bombardment,” *Surface science*, vol. 43, pp. 625-643, 1974.

[14] M. A. Barteau, “Organic Reactions at Well-Defined Oxide Surfaces II .,” *Chem. Rev.*, pp. 4-6, 1996.

[15] M. M. Natile, A. Glisenti, C. Inorganica, and M. Analitica, “Surface Reactivity of NiO : Interaction with Methanol,” *Society*, no. 18, pp. 4895-4903, 2002.

[16] P. Mars, P Scholten, J Zwietering, “The Catalytic decomposition of formic acid,” *Advances in Catalysis*, vol. 14, no. I, pp. 35-113, 1963.

[17] F. H. Walton, D.K Verhoek, “The decomposition of formic acid vapor on evaporated nickel films,” *Advances in Catalysis*, vol. 9, pp. 682-698, 1957.

[18] S. Raz, K. Sasaki, J. Maier, and I. Riess, “Characterization of adsorbed water layers on Y_2O_3 -doped ZrO_2,” *Solid State Ionics*, 2001.

[19] H. Eltejaei et al., “Methane dry reforming on $Ni/Ce_{0.75}Zr_{0.25}O_2$–$MgAl_2O_4$ and $Ni/Ce_{0.75}Zr_{0.25}O_2$–γ-alumina: Effects of support composition and water addition,” *International Journal of Hydrogen Energy*, vol. 37, no. 5, pp. 4107-4118, Mar. 2012.

Chapter Six: Formic acid on MgO

6.1 Motivation

In considering the possible mechanisms for formic acid decomposition and the two competing reactions, it became evident that oxides (and in particular defective oxides) could be tuneable catalysts for these reactions. Following the research on NiYSZ, internal discussions suggested that the availability of labile oxygen atoms should affect the ratio of reaction pathways. Similarly, one could take advantage of size effects in different oxides to fine tune the available binding sites for formic acid and subsequent reactivity. With these thoughts in mind, a collaboration was initiated with Dr. Matthew Brown at Eidgenossische Technische Hochschule (ETH) Zurich to study the reactivity of nano-sized MgO toward formic acid. In preliminary work, Dr Brown obtained IR spectra (Figure 6.1) of formic acid species on the surface of nano sized crystals of MgO as a function of coverage at room temperature.

IR is particularly well suited for identification of organic intermediates, but because of peak overlap, some of the species were not reliably identified. We expect to find formate coordinating with the MgO surface in three modes, monodentate, bidentate and bridged[1][2].

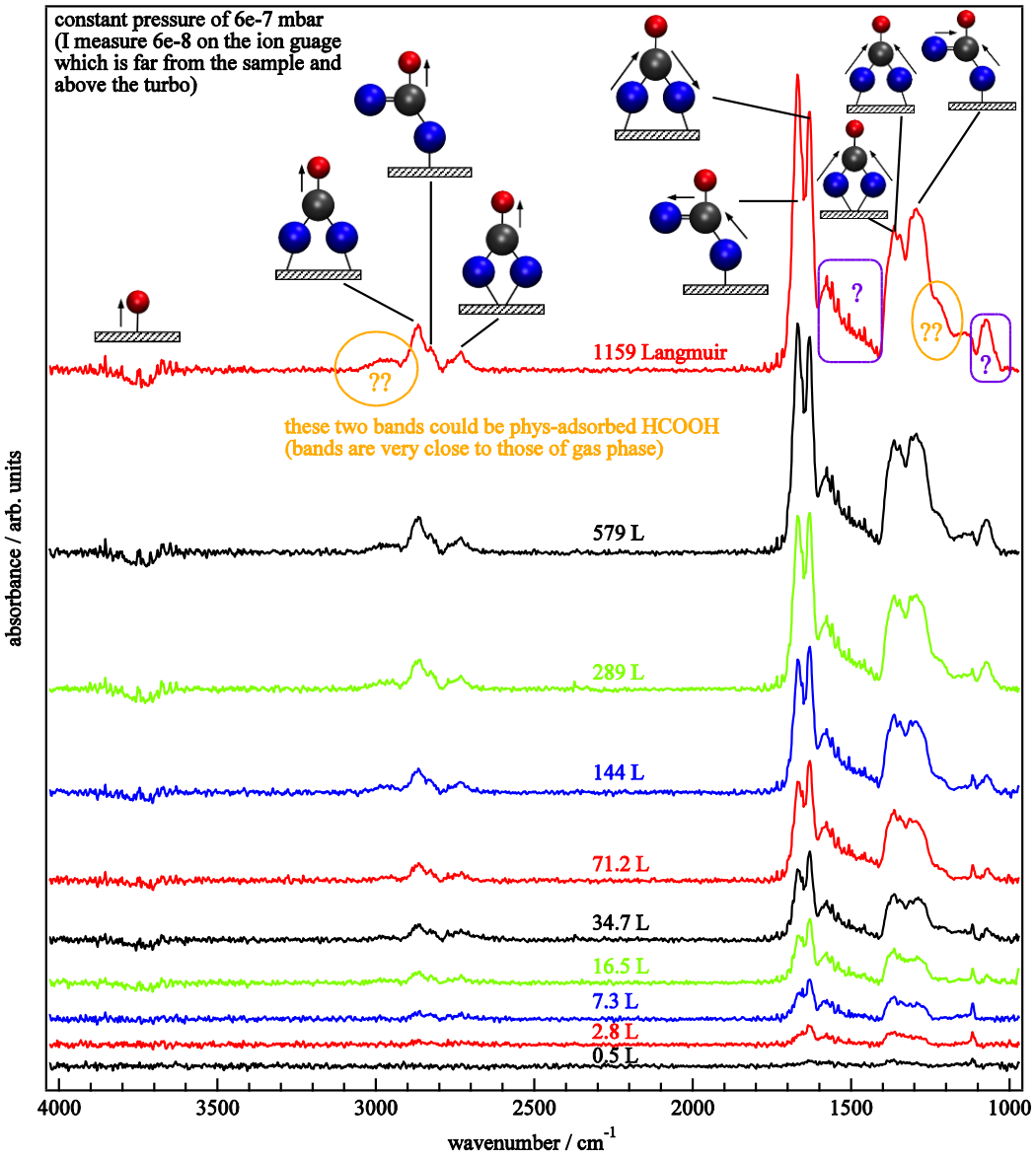

Figure 6.1 Infra-red evidence of formate species on MgO. These are preliminary results and peak assignments are tentative.

Given the success in the previous section in using XPS to distinguish between monodentate and bidentate formate on NiYSZ, it was hoped that the same success could be achieved with MgO. In addition, the IR setup provided limited sample preparation capabilities and it was hoped to better understand and document the sample preparation

and cleaning procedure to provide a consistent basis for future studies. In particular, carbon containing samples may provide additional sites for reaction.

6.2 Experimental

6.2.1 Experimental setup

The XPS examination of formic acid on Nano powder MgO was performed on the Giorgi lab large UHV chamber (Specs Gmbh). The chamber was designed for multiple operations under UHV conditions. A series of roughing, turbo and ion pumps maintain pressures in the 10^{-10} Torr range. Samples are mounted on a sample puck sandwiched between washers of sapphire to allow the electrical isolation of the sample. Thermocouples provide temperature monitoring and the ability to drain charge through to ground. Heating is provided through thermionic emission from a charged filament and cooling through liquid nitrogen. The sample puck can be shuttled from one technique station to another allowing for different tests without exposing the sample to the atmosphere see Figure 6.2.

As an x-ray source for x-ray photoemission spectroscopy a Specs XR50 provided a high intensity twin anode (Mg/Al) design operating at 300W/400W. For electron detection a Specs Phobos 150 hemispherical energy analyser was used.

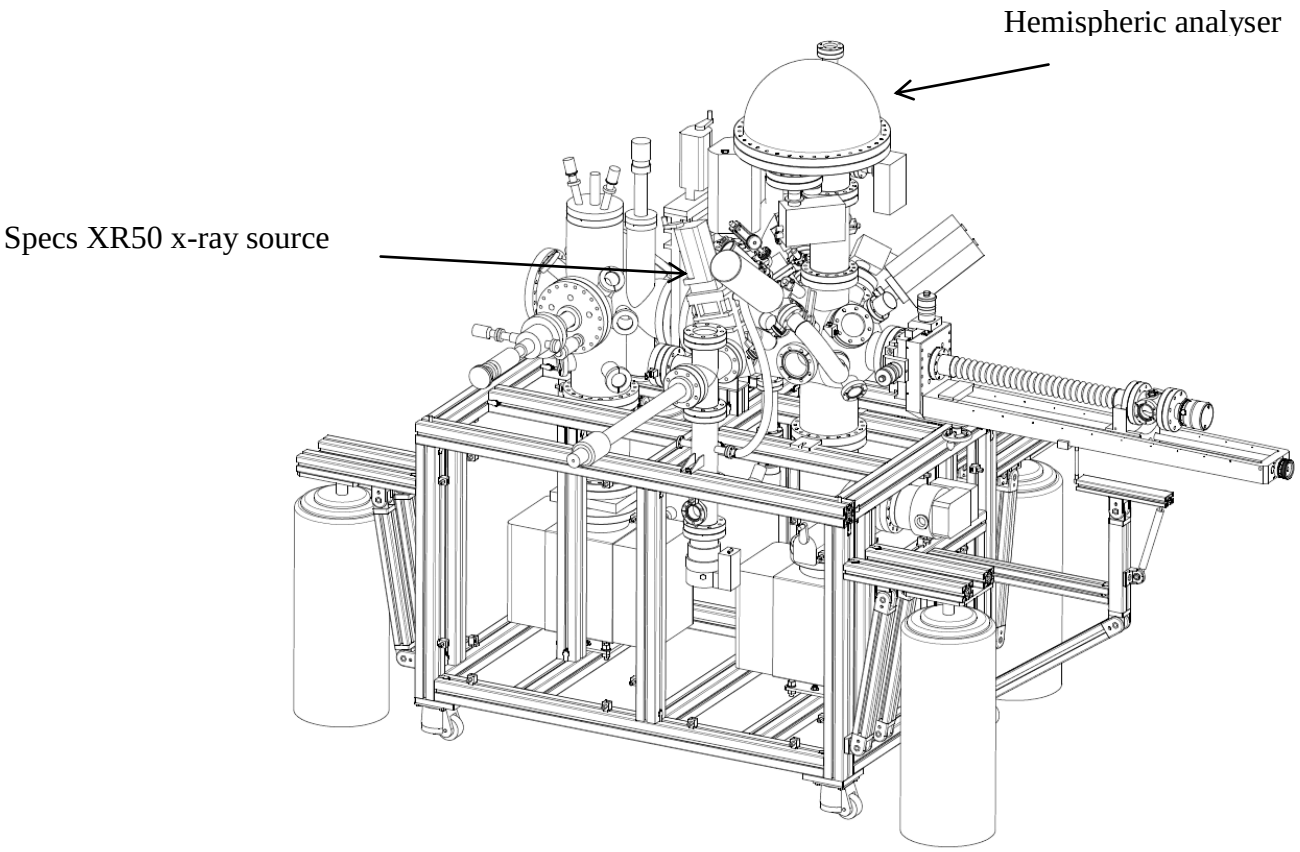

Figure 6.2 SPECs UHV chamber housing XPS system (source: SPECs documentation)

6.2.2 Sample preparation

Pellets were prepared placing 0.15g of MgO Nanopowder (Strem chemicals, MgO Nano powder lot #A2592020) in an 8mm steel die and pressed to 3.5T for 5 minutes. Using a calliper, the resulting pellet was found to have a thickness in the range of 500µm and seemed relatively robust. The pellet was mounted on a puck with a thermocouple on the surface held in place with a sapphire ring and molybdenum clips (Figure 6.3).

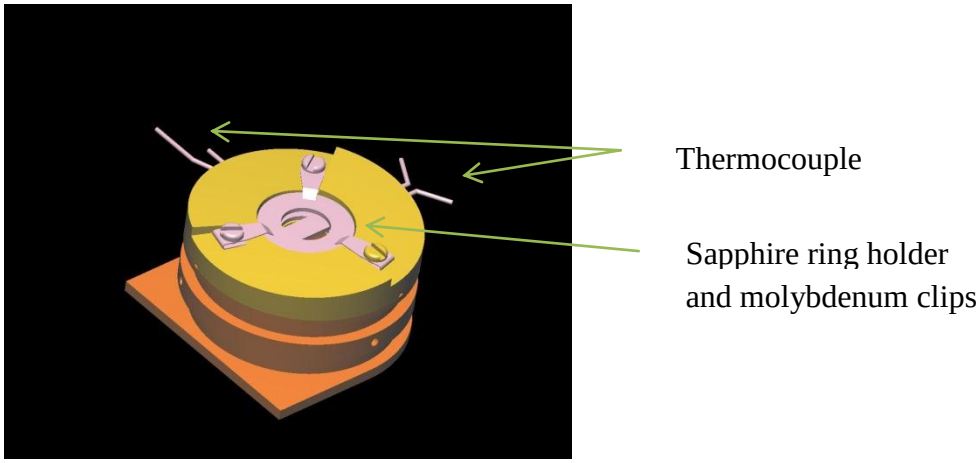

Figure 6.3 Sample puck holder (RHK design used in the Specs UHV system).

6.2.3 Sample cleaning procedure

Upon entering the UHV chamber the MgO pellet was allowed to degas at room temperature for 24 hours. The puck was then chilled by flowing liquid N_2 until the sample temperature, as registered by a thermocouple, was less than 113K (approximately 1 hour). Cooling is necessary for the safety of internal components during subsequent high temperature annealing steps for the sample. Oxygen was leaked into the chamber until the chamber pressure rose to 1×10^{-6} Torr. An accelerating voltage of 800V was used between the heating filament and the sample. The MgO sample was then heated through radiant and thermionic emission with a ramp rate of approximately 5K per minute until the sample reached 773 K. The sample was maintained at 773 K for 5 minutes before its temperature was ramped back down at a rate of 50K per minute. Following this process an initially observed slight brownish discolouration of the sample was lost and a white surface was observed indicative of the removal of surface carbon species. Fine grained cracks were also observed but the sample maintained its physical integrity (Figure 6.4).

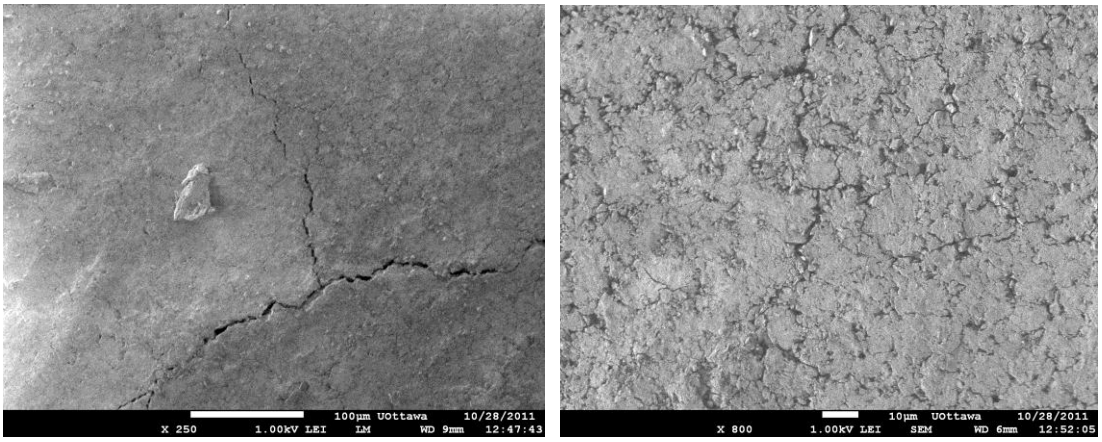

Figure 6.4 SEM images MgO post anneal at two different magnifications

6.2.4 Fixed dose procedure

The background pressure of the chamber was $1x10^{-9}$ Torr before and after the sample cleaning. The sample was cleaned by annealing under $1x\ 10^{-6}$ Torr at 773K for one hour. The main chamber was maintained at less than $2\ x\ 10^{-9}$ Torr. A round bottom glass reservoir was partially filled with 30ml of Fluka analytical 98% purity formic acid (lot # szba2240v). The reservoir atmosphere was purified by three repeated freeze-evacuate-thaw cycles. The pressure in the reservoir was maintained at less than 1 Torr using a roughing pump. The atmosphere over the formic acid liquid was then used as a source to dose the sample. A Labview program monitored the pressure and time providing a running total of the dose in Langmuir. A leak valve was gently opened until the chamber pressure increased to $1\ x\ 10^{-6}$ Torr until the targeted dosage was achieved at which point the leak valve was closed and the chamber returned to its original pressure. XPS spectra of the MgO pellet were recorded over all regions of interest before and after dosing with

formic acid (50 Langmuir 100 Langmuir , 150 Langmuir & 200 Langmuir of formic acid).

6.2.5 Continuous dosing procedure

In a manner similar to the fixed dose procedure above, following sample cleaning, the leak valve was opened until the chamber pressure registered 1.1 x 10^{-7} Torr. As the Labview program monitored the ongoing formic acid exposure high resolution XPS spectra of the carbon 1s and the oxygen 1s regions were taken continuously. The dose was recorded at the start of each scan.

6.3 Results

6.3.1 Green MgO

The sample was loaded into the UHV chamber and allowed to rest under vacuum for 24 hours. During that period the sample was flashed several times to 773K to test the heating procedure and to aid in the degassing process. The first XPS spectra was then taken on the green sample as received (prior to the cleaning procedure), and the cleanliness of the sample was assessed by monitoring the carbon peaks (see Figure 6.5).

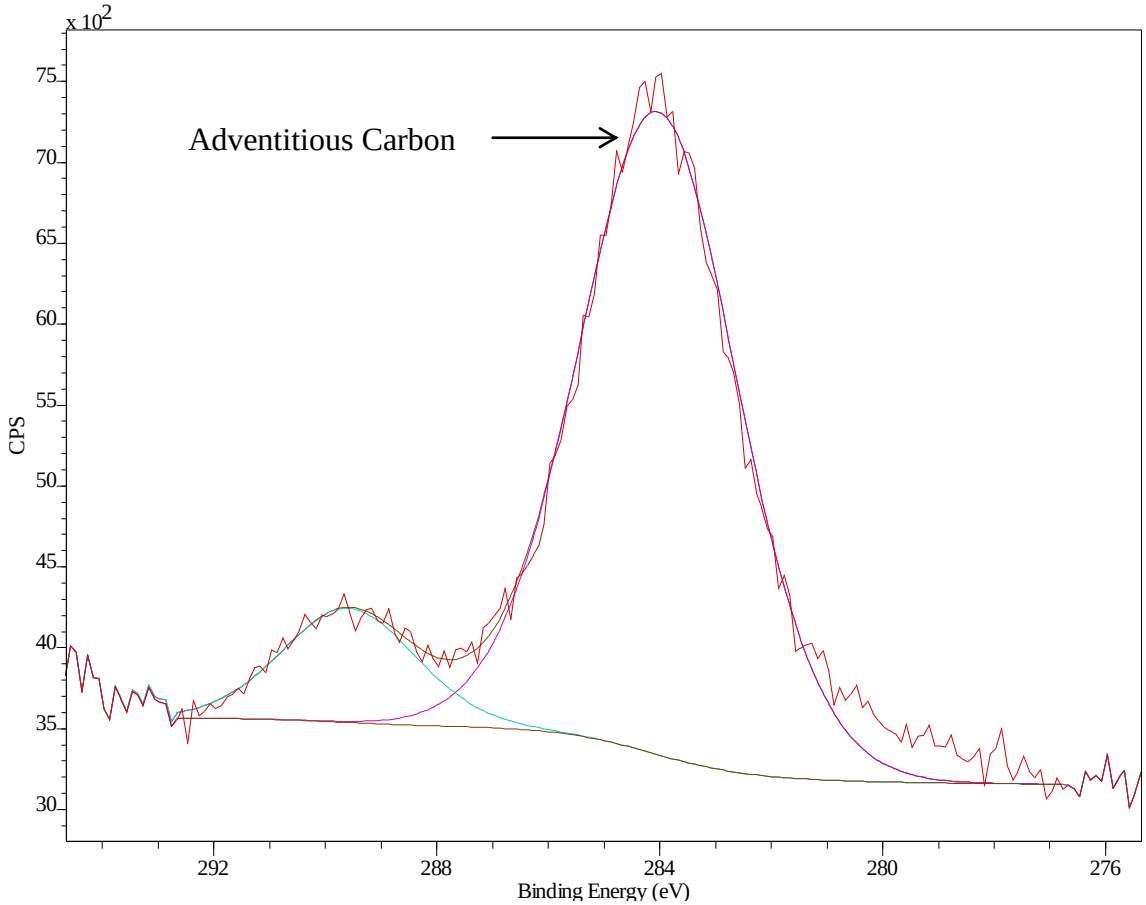

Figure 6.5 XPS of the carbon 1s region for an as received MgO pellet. Fitted peaks correspond to adventitious carbon and other higher binding energy species. Parameters: Al source, energy 1486.7 eV, dwell 800 msec, pass energy 10 step 0.2 eV

All XPS spectra were referenced to the Mg 2p peak with a binding energy of 50.8 eV. As can be seen in Figure 6.5, the green sample has a large and broad peak (FWHM 3.4) centred around 285 eV along with a second broad peak (FWHM 2.8) centred at 290 eV. The width of the peaks suggests that, as you would expect, there are many carbon species on the surface prior to cleaning. Following cleaning of MgO, a significant reduction in the C1s peaks as well as the loss of discolouration is evidence that the cleaning was

effective (Figure 6.6). However the continuing existence of a diminished adventitious and carbidic peak suggests that a more rigorous cleaning procedure is required to completely remove all carbon species. It is likely that a more energetic or harshly oxidizing environment would be required to reduce these peaks. The results of the synchrotron study with NiYSZ suggest that rather than oxidizing the carbon to clean the surface, reduction under H_2 to form CH_4 may be more effective. The reduction under hydrogen of NiYSZ produced a surface clean of all carbon species.

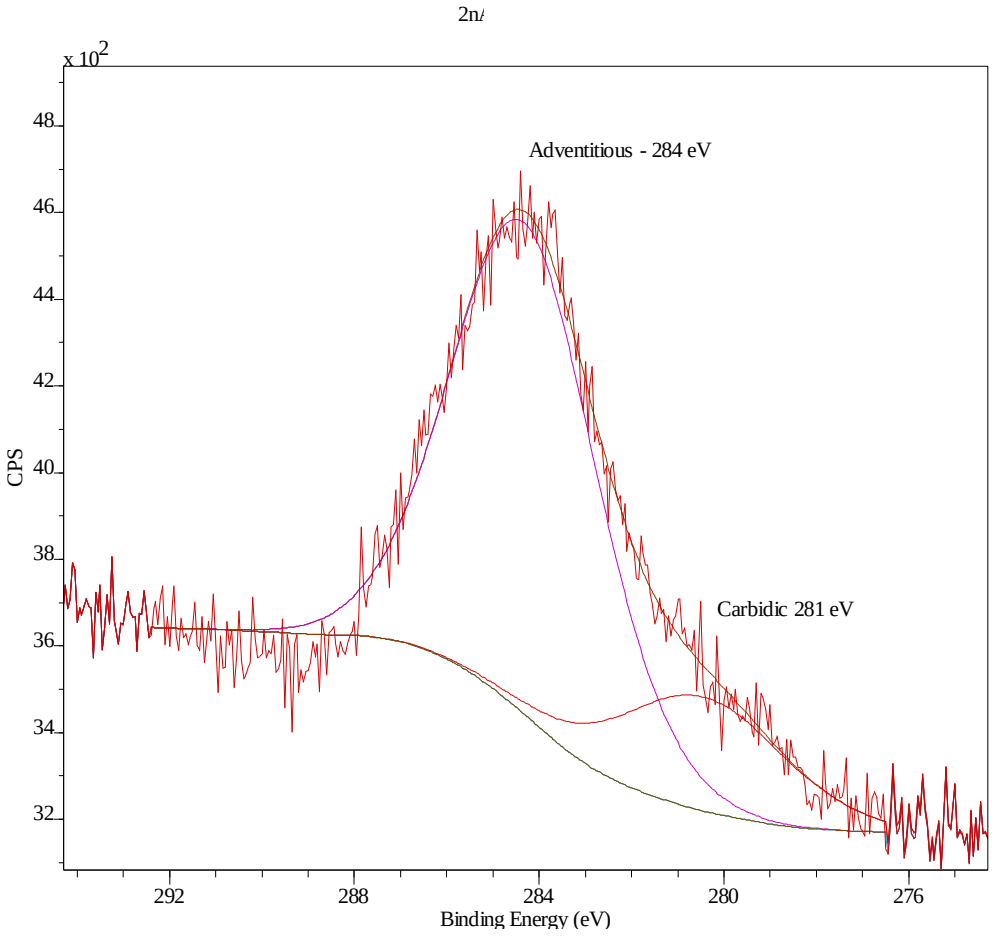

Figure 6.6 Post anneal XPS spectra of the C 1s region for an as received MgO pellet. Fitted peaks correspond to adventitious carbon and carbidic species. Parameters: Al source, energy 1486.7 eV, dwell 800 msec, pass energy 10 step 0.2 eV

Following the annealing procedure the total carbon signal is reduced, as expected. The peak height of the adventitious carbon has shrunk to approximately ½ that of the green sample. Of the two peaks that are apparent, one peak centred at 284 eV that is attributed to adventitious carbon [3], along with a second peak of much lower area centred at a binding energy of 280 eV. This second peak is associated with carbon directly bonded to the magnesium[4] and I will refer to it as carbidic. NIST database provides references to NiC with an XPS peak at 280.5 eV. Magnesium is known to form a carbide with the formula Mg_2C_3 but no XPS references were found.

The carbidic carbon peak, while also reduced has also narrowed to a peak centred at 281eV. The higher peak centred at 290 eV observed in the green sample has now disappeared.

The anneal under vacuum and the anneal under oxygen both resulted in a similar spectra for the O1s (Figure 6.7). The peak centred at 532.9 eV has been attributed to OH and the peak at 531.0 eV to MgO lattice oxygen. MgO is well known for its affinity to forming hydroxyl terminations on its surface[2][5][6]. Clearly the results indicate that the annealing process was not harsh enough to remove the hydroxyl groups.

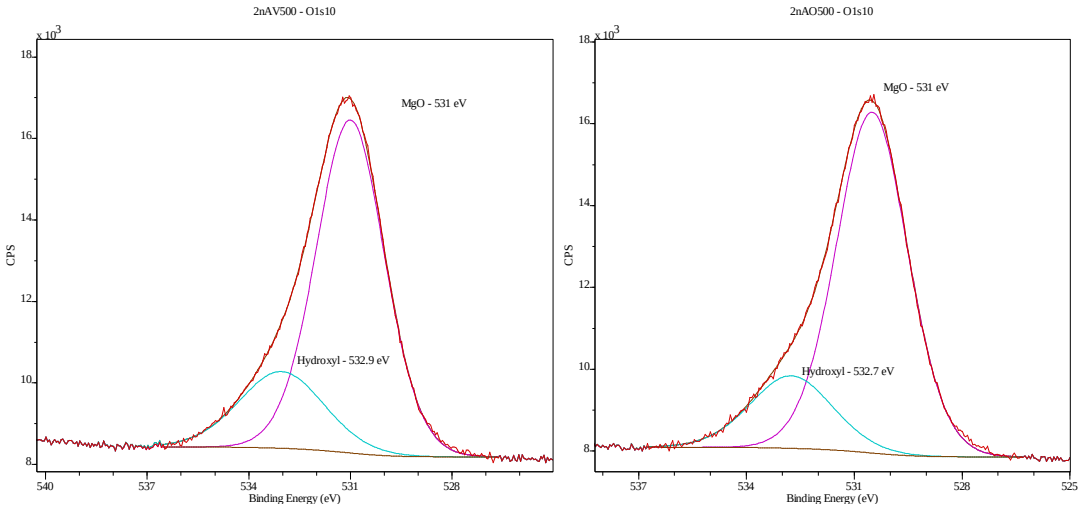

Figure 6.7 XPS spectra of MgO annealed under vacuum ($1x10^{-9}$ Torr) and under oxygen. Fitted peaks correspond to lattice oxygen (531.2 eV) and hydroxyl (532.9 eV). Parameters: Al source, energy 1486.7 eV, dwell 800 msec, pass energy 10 step 0.2 eV, temperature 300K

6.3.2 MgO following fixed exposure to formic acid at 50L, 100L, 150L and 200L

6.3.2.1 Mg 2s region

As the spectra were all referenced to the Mg 2p peak at 50.8 eV, one would expect no significant shift to appear in the Mg 2s peak (Figure 6.8) however the binding energy of the Mg 2s peak is calculated as 89.3 eV not 88.1 eV as referenced in the literature[7]. It may be that we are seeing a shift in the binding energy for the Mg 2p peak due to the very small crystallite size of 3 nm. If this were the case we might expect other peaks to be shifted relative to their literature values.

Although we have some uncertainty in the absolute peak position, we do not detect any shift in Mg 2p or Mg 2s peak shapes or positions as we compare a range of formic acid surface exposures from clean to 200L.

We do see a slight decrease in the signal strength (photo emission electron counts) due to the presumed over layer of formic acid interfering with escaping electrons. The lack of shift would suggest that the magnesium is not being reduced or oxidized during the process of being covered in an over layer of formate ion. That would suggest that either it does not coordinate with the formate ion or it does so through an oxygen ion thereby creating a similar electronic environment to the hydroxyl terminated magnesium.

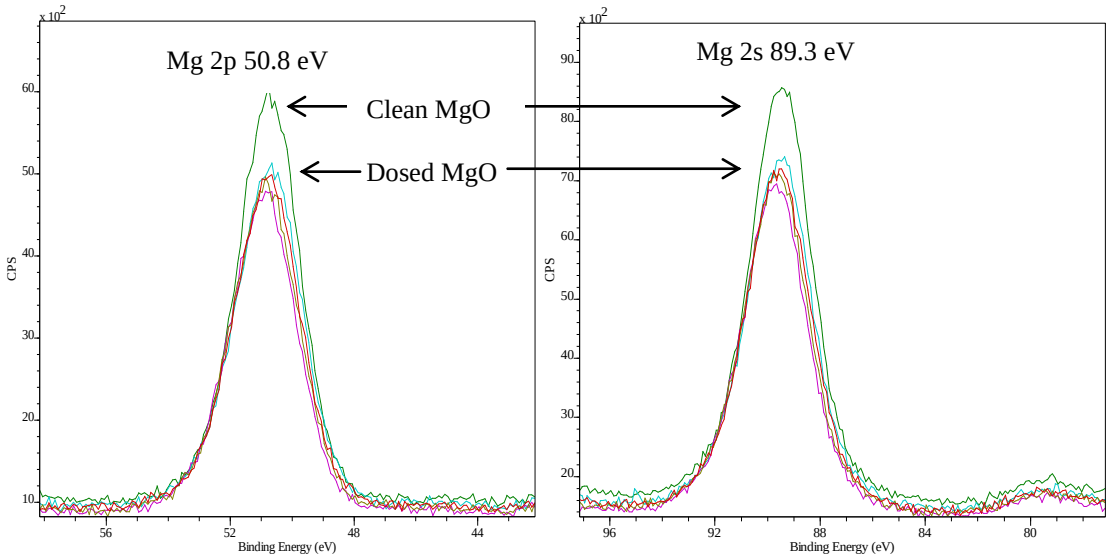

Figure 6.8 Tiled XPS spectra of the Mg 2p and 2s regions for various exposures to formic acid, (clean, 50L, 100L, 150L & 200L). Fitted peaks correspond to Mg 2s peak referenced to Mg 2p at 50.8 eV. Parameters: Al source, energy 1486.7 eV, dwell 800 msec, pass energy 10 step 0.2 eV

6.3.2.2 Carbon 1s region

As per the precedent set by Barteau's work[3] [4][6], I have chosen to reference the spectra to the Mg 2p peak at 50.8 eV however this resulted in the other peaks being shifted to lower binding energies than was expected. The example, adventitious carbon was found at 284 eV, not the expected 284.5 eV.

Upon dosing with formic acid we see that in addition to the adventitious and carbidic peaks, a peak centred at 291 eV is observed (Figure 6.9). It is assigned to the formate anion on MgO [8]. The lower binding energy peak has shifted to slightly lower binding energy although this may be due to the challenge in the analysis application (CASA XPS) accurately analysing the peak shape of a broad low peak. As only carbide species are found at this low a binding energy in the carbon 1s region, it is assigned carbidic although the breadth of the peak may indicate multiple carbidic species[10].

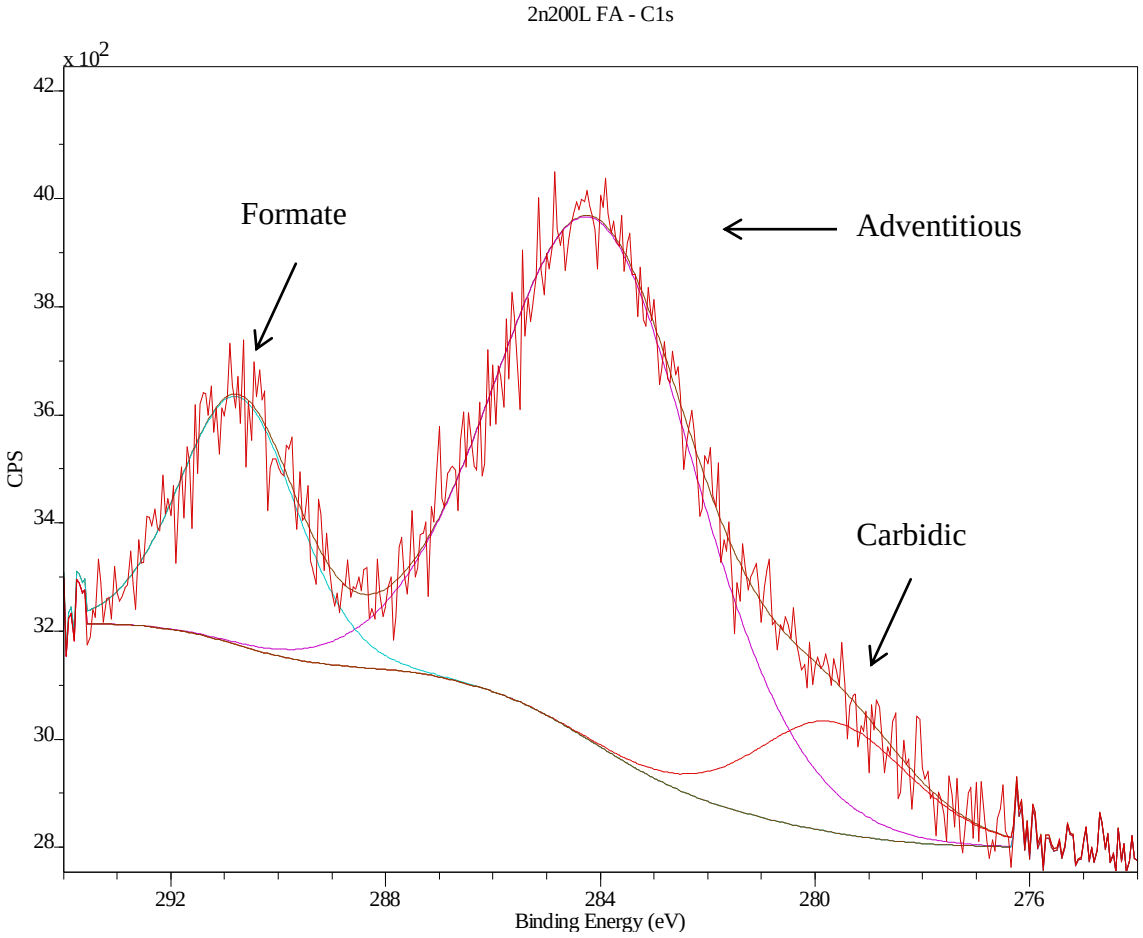

Figure 6.9 MgO XPS spectra of the C 1s region for MgO sample dosed with 200L formic acid. Fitted peaks correspond to formate, adventitious carbon and carbidic species. Parameters: Al source, energy 1486.7 eV, dwell 800 msec, pass energy 10, step 0.2 eV, Temperature 300K

When the XPS spectra of the carbon 1s region for MgO exposed to various concentrations of formic acid are tiled we see that the peaks do not shift in binding energy or shape but the relative area of the formate peak does grow between 50L and 100L after which is maintains its relative area (Figure 6.10).

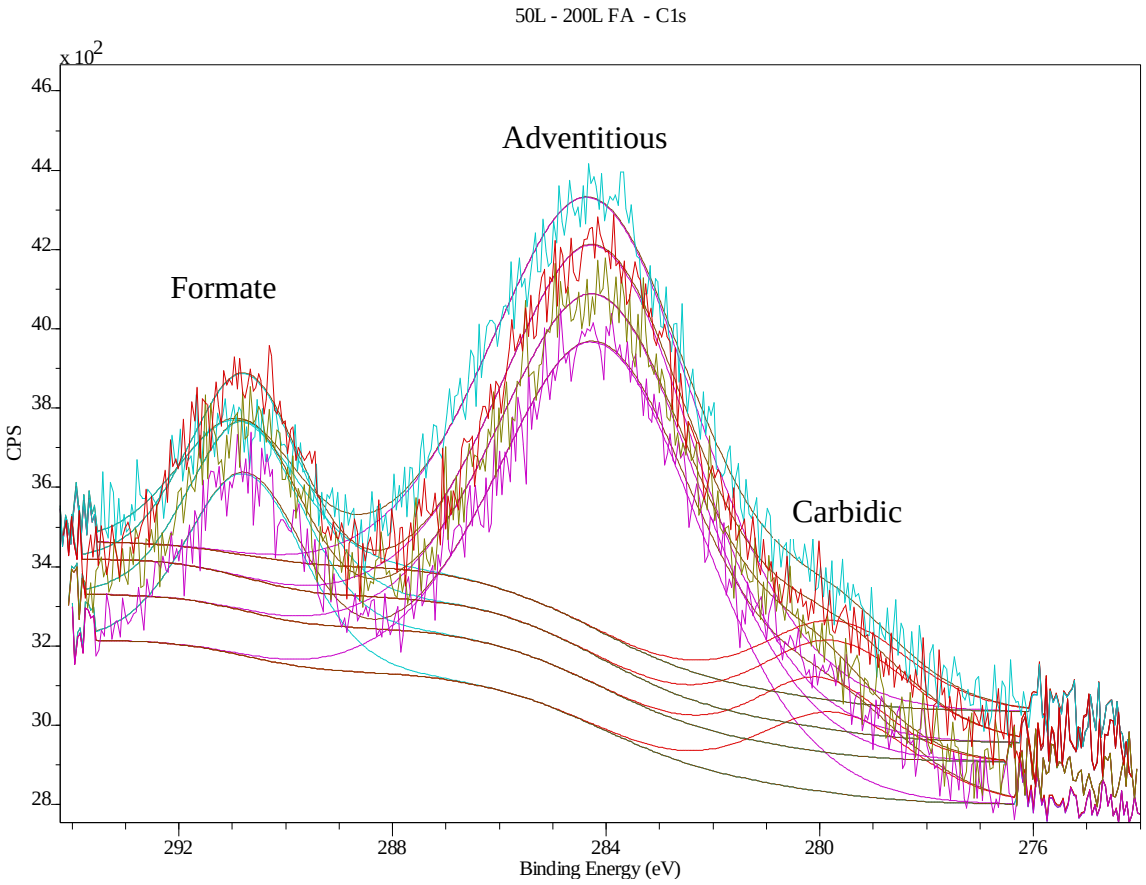

Figure 6.10 Tiled overlay of C1s region for 50L, 100L 150L and 200L (blue, red, green, purple) dose of formic acid on MgO. Fitted peaks correspond to formate, adventitious carbon and carbidic species. Parameters: Al source, energy 1486.7 eV, dwell 800 msec, pass energy 10 step 0.2 eV

No clear trend was discerned between the different doses of formic acid as to the changes to these peaks. No shift of binding energy was observed nor was there an identifiable change in the peak area of the adventitious or carbidic carbon. The ratio areas of the

formate:adventitious:carbidic peaks were 2:11:3 for 50L spectra with formate rising to 3:11:3 for all exposures over 50L.

6.3.2.3 Oxygen 1s region

The binding energies for all three identified peaks are in close agreement with the results published by Peng and Barteau [3]. The formate group (533.4 eV) replacing the hydroxyls (533.2 eV) on the surface of the MgO is rapid (Figure 6.11). The O1s peaks morphology change is complete following the first dose of 50Langmuir of formic acid and although there is a change in the peak heights there is no observed change in peak shape. The reduced peak heights with larger doses of formic acid is thought to be due to shielding of the underlying MgO by successive layers of formic acid.

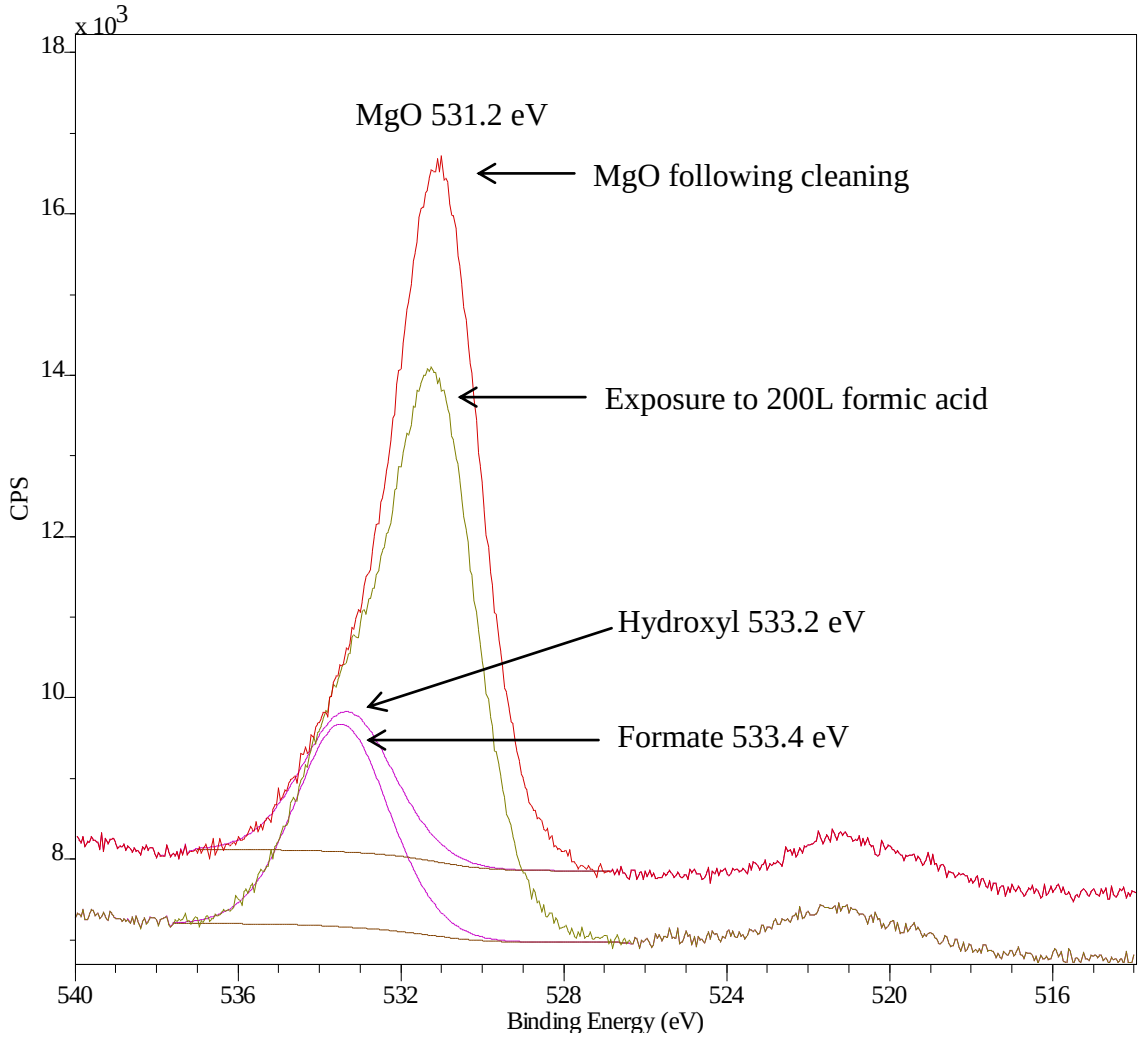

Figure 6.11 XPS Oxygen 1s region for MgO tiled overlay Annealed under O_2 (red curve) and following exposure to 200L formic acid (green curve). Fitted peaks correspond to hydroxyl (533.2 eV) and formate (533.4 eV). Parameters: Al source, energy 1486.7 eV, dwell 800 msec, pass energy 10 step 0.2 eV temperature 300K

6.3.3 Effect of continuous dosing of Formic Acid on MgO

The next experiment in the series was to continuously dose an annealed sample of MgO with formic acid and to simultaneously produce detailed XPS spectra of the C 1s and O 1s spectrum.

6.3.3.1 Carbon 1s

Following exposure to formic acid at 1.1 x 10^{-7} Torr we see the initial carbon species rapidly joined by a third species with a binding energy centred at 291 eV (Figure 6.12). The third peak is interpreted as formate on the MgO surface. The rapid rise of the formate peak to stable peak suggests that the surface sites are rapidly filled and maintained by any ongoing reaction (Figure 6.13). Attempts to force fit a forth peak resulted in only a broad peak of very minor intensity that was interpreted as unlikely. Unfortunately resolution of the instrument was insufficient to resolve different binding energies associated with potential different coordination of the formate to the surface.

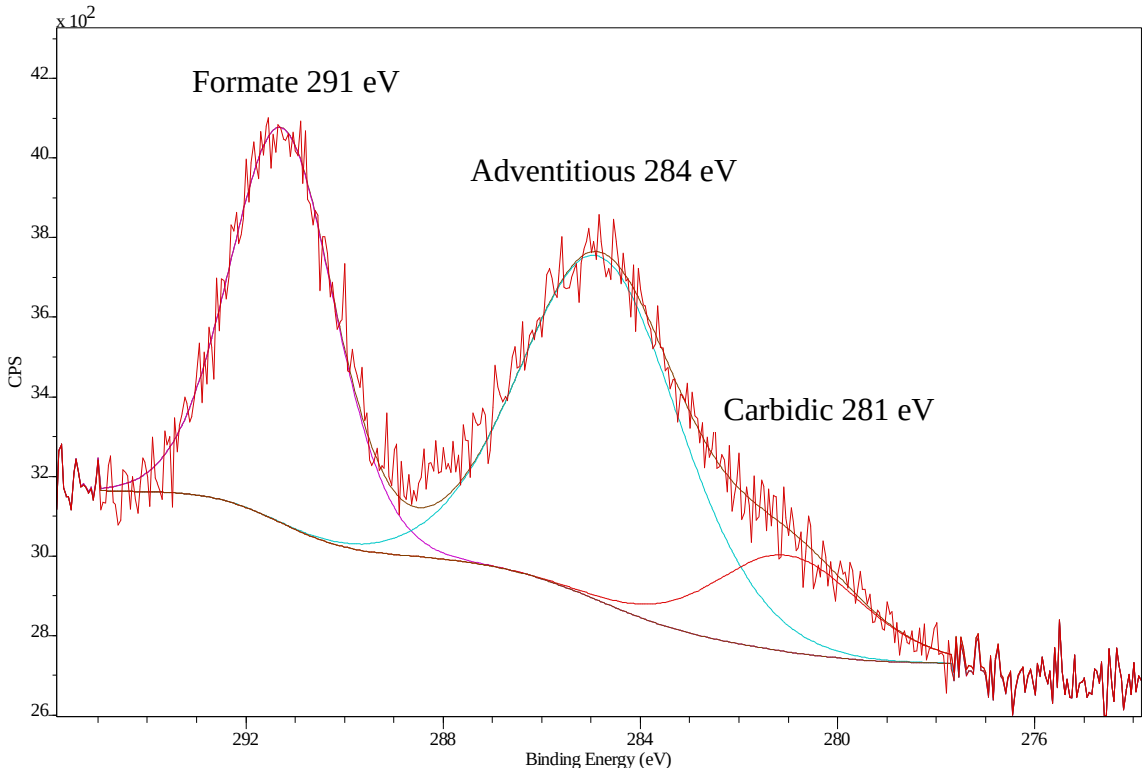

Figure 6.12 XPS Carbon 1s region for MgO following exposure to 70L of formic acid. Fitted peaks correspond to formate, adventitious carbon and carbidic species. Parameters: Al source, energy 1486.7 eV, dwell 800 msec, pass energy 10 step 0.2 eV temperature 300K

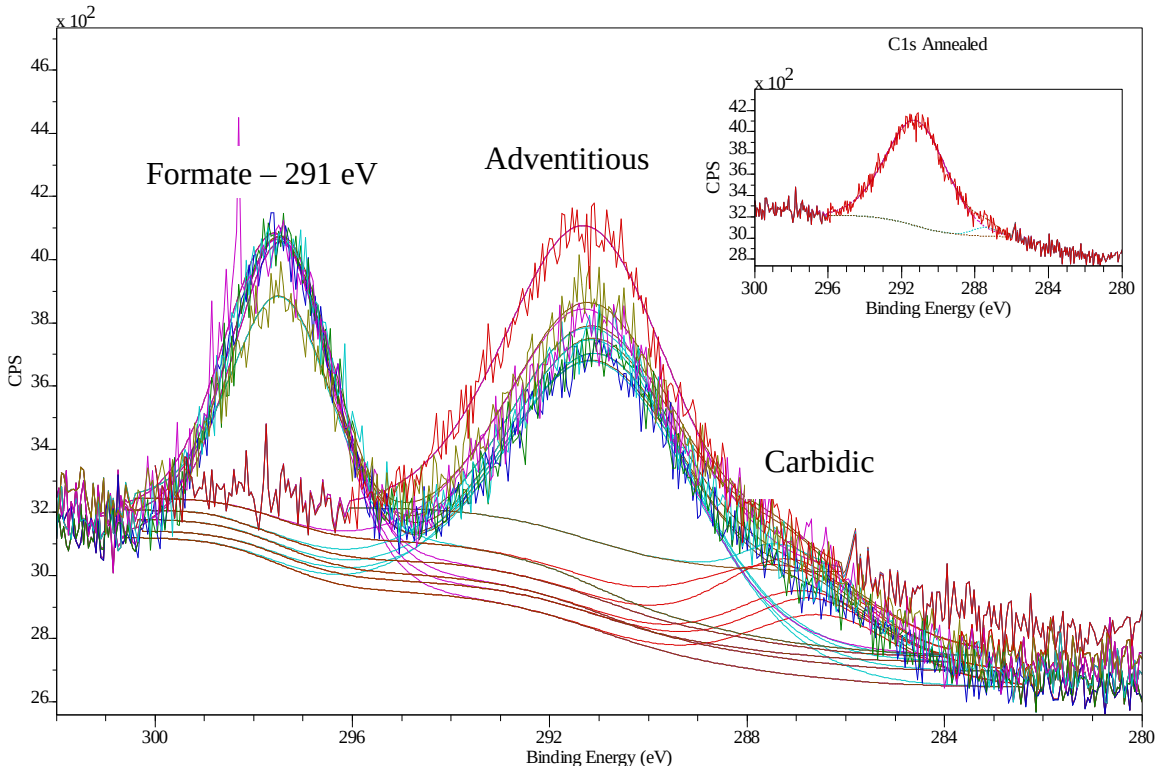

Figure 6.13 Multiple XPS of the Carbon 1s region for MgO following continuous exposure to formic acid at 1.1×10^{-7} Torr. Exposure at the start of each spectra was 20L, 70L, 120L and 170L. Fitted peaks correspond to formate, adventitious carbon and carbidic species. The insert corresponds to the sample following cleaning and prior to exposure to formic acid. Parameters: Al source, energy 1486.7 eV, dwell 800 msec, pass energy 10 step 0.2 eV, temperature 300K

Plotting the area of individual peaks areas allows us to see a different view of the effect of formic acid dosing on the MgO. The appearance of the formate peak rises rapidly with no discernable effect on the carbidic or adventitious carbon peaks. The stability of the ratios of the carbon species would indicate that the surface settles into a fixed pattern of coverage by the different species rather rapidly. In the fixed dose case (Figure 6.14), we observe some change between 50 Langmuir and 100 Langmuir after which no significant change is observed.

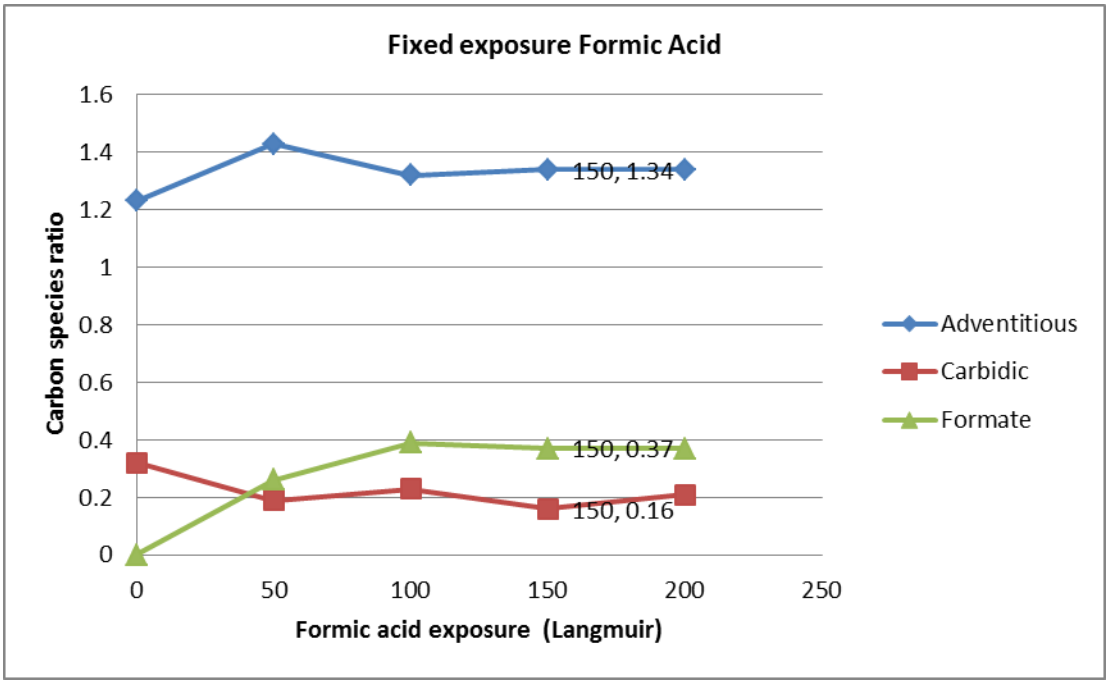

Figure 6.14 Carbon 1s species peak areas - fixed dose

In the continuous dose situation (Figure 6.15) we have better resolution of the growth of the formate peak, rising rapidly to a steady state by exposure to 120 Langmuir of formic acid. As we do not see a corresponding decline in other carbon species with the rise in formate species we interpret this as the annealing process resulted in a surface with some of the coordination sites occupied prior to the introduction of the formic acid. As formic acid was introduced, the remaining sites fill with formate in some as yet unknown coordination. Peng and Barteau suggest that formate will desorb at 550K but will not at 260K [3] As the experiment was done at room temperature, the formate was unlikely to desorb and so we effectively painted the surface with formate until all coordination sites were filled.

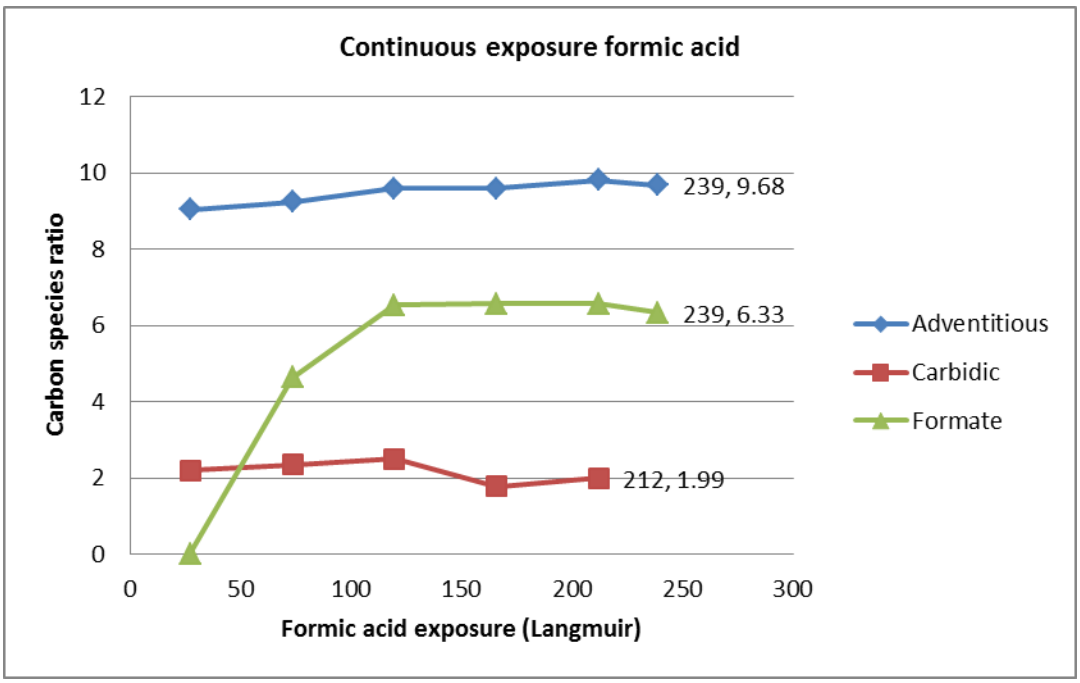

Figure 6.15 Carbon 1s species peak areas - continuous dosing

6.3.3.2 Oxygen 1s

Earlier spectra (6.7) suggest the annealed MgO with O 1s peaks at 532.9 eV and 531.0 eV associated respectively with OH and MgO oxygen components showing no shift over the range of doses. As the experiment scanned only the O 1s and C1s regions, O 1s peaks were normalized using adventitious carbon at 285 eV. This may explain the small observed shift from earlier spectra. Over the course of the exposure to formic acid we see the growth of a high binding energy shoulder on the main peak. The clean MgO peak was already asymmetrical with a small high BE shoulder due to hydroxyl. During exposure to formic acid the hydroxyl is replaced along with additional coverage by slightly higher BE formate (Figure 6.16).

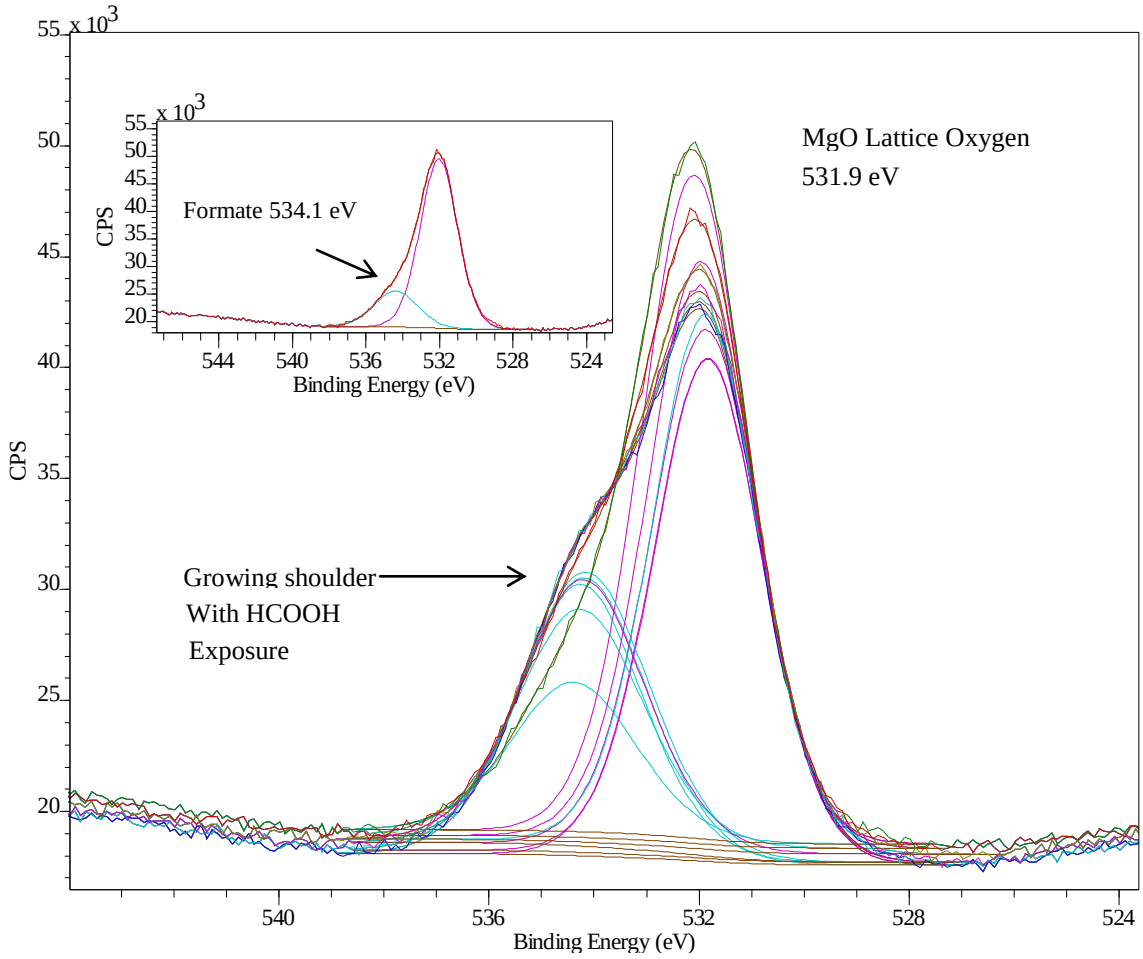

Figure 6.16 Multiple XPS Oxygen 1s region spectra for MgO following continuous exposure to formic acid at 1.1×10^{-7} Torr. Exposure at the start of each spectra was 20L, 70L, 120L and 170L. Fitted peaks correspond to lattice oxygen and formate. The insert corresponds to the sample following cleaning and prior to exposure to formic acid. Parameters: Al source, energy 1486.61 eV, dwell 800 msec, pass energy 10 step 0.2 eV, temperature 300K

Tiled overlap of the O 1s peaks formed during continuous dosing of MgO with formic acid ranging from 0 to 220 Langmuir formic acid are shown in Figure 6.16. The inset

spectrum is of the annealed MgO prior to dosing. Given the binding energies involved, it is likely that the higher binding energy peak is associated with some residual formate and not hydroxyl.

6.4 Reaction pathways

We have previously discussed that the formic acid can decompose via either de-hydration or de-hydrogenation. However given that the experimental conditions were selected to observe formate on the surface, the temperature was too low to allow either decomposition reaction to proceed.

6.5 Conclusion

Ramping the temperature of MgO under vacuum to 773K and then holding the temperature for 5 minutes prior to cooling was found to reduce but not eliminate surface carbon. Following the same cleaning procedure under 5×10^{-6} Torr oxygen was judged equally effective.

We have observed the replacement of OH groups on the surface of MgO with formate anions. At too temperature the surface saturates with no visible sign of reaction. We require a higher resolution instrument (as in the previous chapter) to contribute further in the identification of binding sites.

6.6 References for Chapter 6

[1] C. Nakatsuji, Hiroshi Yoshimoto, Masami Hada, Masahiko Domen, Kazunari Hirose, "Theoretical study on the chemisorption and the surface reaction of HCOOH on a MgO(001) surface," *Surface Science*, vol. 336, pp. 232-244, 1995.

[2] E. Carrasco et al., "Thickness-Dependent Hydroxylation of MgO(001) Thin Films," *The Journal of Physical Chemistry C*, vol. 114, no. 42, pp. 18207-18214, Oct. 2010.

[3] M. A. Peng, X D and Barteau, "spectroscopic characterization of surface species derived from HCOOH, CH_3COOH, CH_3OH, C_2H_5OH, $HCOOCH_3$ and C_2H_2 on MGO thin film surfaces," *Surface Science*, vol. 224, pp. 327-347, 1989.

[4] D. Starr, E. Pazhetnov, a Stadnichenko, a Boronin, and S. Shaikhutdinov, "Carbon films grown on Pt(111) as supports for model gold catalysts," *Surface Science*, vol. 600, no. 13, pp. 2688-2695, Jul. 2006.

[5] G. Jacobs, P. Patterson, U. Graham, a Crawford, and B. Davis, "Low temperature water gas shift: the link between the catalysis of WGS and formic acid decomposition over Pt/ceria," *International Journal of Hydrogen Energy*, vol. 30, no. 11, pp. 1265-1276, Sep. 2005.

[6] H. Eltejaei et al., "Methane dry reforming on $Ni/Ce_{0.75}Zr_{0.25}O2–MgAl_2O_4$ and $Ni/Ce_{0.75}Zr_{0.25}O_2$–γ-alumina: Effects of support composition and water addition," *International Journal of Hydrogen Energy*, vol. 37, no. 5, pp. 4107-4118, Mar. 2012.

[7] I. S. Nefedov, V.I. Firsov, M.N. Shaplygin, "Electronic structures of $MRhO_2$, MRh_2O_4, RhMO4 nad Rh2MO6 on the basis of x-ray spectroscopy and esca data," *Journal of electron spectroscopy and related phenomena*, vol. 26, pp. 65-78, 1982.

[8] X. D. Peng and M. A. Barteau, "Acid-base reactions on model MgO surfaces," *Catalysis Letters*, vol. 12, pp. 245-253, 1992.

[9] M. A. Peng, X. D. Barteau, "Dehydration of carboxylic acids on the MgO(100) surface," *Catalysis Letters*, vol. 7, pp. 395-402, 1990.

[10] R. W. Waldrop, J.R. Grant, "Formation and schottky barrier height of metal contacts to B-SiC," *Applied Physical Letters*, vol. 56, p. 557, 1990.

Chapter Seven: Conclusion

7.1 Surface cleaning procedures

Of the two cleaning procedures tested, reduction with hydrogen at 1100K was the most effective at removing all forms of carbon as well as hydroxyls although only tested with two substrates. Annealing under vacuum or under oxygen at 773K was less effective at reducing the adventitious and other species of carbon and was not sufficient to completely clean the surface.

7.2 Catalytic decomposition of formic acid

Of the different materials tested, NiYSZ and CuYSZ were both found to be active at catalyzing the decomposition of formic acid. Mass spectrometry results suggest, that for all catalysts tested, both reactions were present although dehydrogenation was the primary reaction path. NiYSZ displayed a lower light off temperature (ca. 323K) although CuYSZ had higher selectivity. Further mass spectrometry results suggest that NiYSZ was found to be active in catalyzing formic acid decomposition via both dehydrogenation and dehydration. The catalyst favoured the dehydrogenation reaction over the dehydration reaction by a ratio of approximately 5:1.

7.3 Surface species

Formate anions were found to bind to the surface of NiYSZ in three different configurations: monodentate, bidentate and bridged. XPS analysis suggest 19% monodentate and 81% bidentate. The close agreement between formate coordination and decomposition path ratios suggests a potential link that could be exploited, that is,

dehydrogenation could be further enhanced by selectively allowing a bridged intermediate.

Formic acid exposure to MgO at temperature less than the decomposition temperature results in formate anions adhering to all empty coordination sites and then reaching a steady state.

7.4 Reaction pathways

Experimental evidence suggests that the decomposition path of either dehydrogenation or dehydration may be influenced by the coordination of the formate ion on the surface. Empirical evidence suggests that the ratio or monodentate coordinated formate to bridged coordination is similar to the ratio of dehydrogenation to dehydration reaction products. A potential reaction mechanism was proposed with the less rigid monodentate configuration enabling bending that could facilitate terminal formate proton interaction with surface species resulting in water formation. A second proposed reaction mechanism see the more rigid bridged configuration holding the terminal formate proton away from the surface restricting its reactivity coordinating with highly mobile surface adsorbed hydrogen. In the second reaction mechanism dihydrogen is evolved as the next step.

7.5 Future

I believe one of the most exciting prospects regarding catalyst research for the reactions studied here, or other similar reactions, is the capability to scientifically tailor new catalysts based on the deeper understanding of factors associated with a catalysts activity, its reactivity and the light-off temperature. Examining the activity of a catalyst separately from its selectivity may allow future design of highly active catalysts that are also very

selective. As an example, the suggested link between coordination and reaction pathway for formic acid on NiYSZ may enable surface modification of the NiYSZ to remove or block unwanted coordination and in turn improve the selectivity of the catalyst. Understanding the surface chemistry changes that occur when light-off temperature is reached may also allow for the tailoring of the surface to meet design needs. If the start of reactivity is being blocked by a surface species such as CO_2 or formate it may be possible to modify the surface to reduce their binding. In the case of MgO we found evidence that at room temperature (presumably a temperature below the light-off temperature) the surface sites became saturated blocking any reactant turnover. Future research into lowering the light-off temperature might attempt to identify the blocking species and determine factors to mitigate the blocking.

Appendix A

Novel Work

For chapter 4 of this thesis I designed experimental apparatus for reducing catalyst samples and then testing the residual gases of formic acid decomposition as the temperature was increased over a fixed range.

For chapter 5, in association with J.B Giorgi, M.A. Brown, R.G. Green at the ALS in Berkley: sample preparation and pellet creation, analysis of spectra. I am indebted to Matthew Brown and Richard green for performing the actual XPS on the synchrotron.

For chapter 6 of this thesis, I prepared the samples, created the pellets, performed the XPS and analysed the spectra.